Centrifugal Microfluidic System for Biochemical Applications

by
Yuting Hou

A thesis submitted in partial fulfillment of the requirements for the degree of

Doctor of Philosophy

Department of Chemistry
University of Alberta

Abstract

The development of life sciences has imposed higher requirements for biochemical analysis, especially for point-of-care analysis. Polymer-made centrifugal CD microfluidic chips could fulfill the needs of biochemical analysis with their low cost, the feasibility of mass production, excellent biocompatibility, miniaturization, and automation. With recent advances, the field of centrifugal microfluidics has become more attractive than ever for the integration of complex laboratory workflows. Therefore, the research and development of centrifugal microfluidic discs are of great significance.

We explored two possible applications of centrifugal microfluidic in the biochemical field. One disc is designed to complete a multiple-step bench-top blood sample clean-up procedure automatically where the output sample could be directly used for downstream instrument analysis. Another disc is an integrated system with an on-disc readout sensor, a compact device for on-site use. All discs are fabricated with transparent PMMA and then laminated together by PSA. Both PMMA and PSA are laser cut using a commercial CO_2 laser cutting machine. Reagent reservoirs are mainly fabricated on PMMA layers, while fluid transportation channels are featured on PSA layers. The thickness and hydrophobicity of PSA enable neatly liquid transfer and siphon valving. The pneumatic valve and siphon valve are two crucial features for realizing automation with the cooperation of centrifugal force. Also, other forces in a rotating reference system play important roles in on-disc operation like mixing.

The first centrifugal microfluidic disc aims to prepare whole blood for small molecule detection automatically. Fresh blood is one of the most critical bio-samples that reflect the stimulant

condition of the human body and is widely used in research and diagnosis. However, the complicated matrix of blood hinder the direct analysis of small molecules and make sample preparation necessary, especially for mass spectrometry detection, which is the golden rule in small molecule studies. Sample preparation procedures such as blood cell separation, protein precipitation, and lipid removal are all integrated on the disc. Although mixing is a challenge in the centrifugal system, the mixing of plasma and organic solvent for protein precipitation is realized by "shaking" mode, which takes advantage of acceleration and deceleration when spinning speed changes. The processed sample is proved to be suitable for both HILIC-MS and MALDI-MS analysis. According to the Agilent HILIC-MS protocol for the analysis of 16 underivatized amino acids, all these 16 amino acids in the disc-processed blood sample are separated and analyzed by positive mode HILIC-MS using HILIC. MALDI-MS is employed during C18 and silica particle usage optimization by observing the crystallization of sample spots on GLAD film and comparing the S/N of several amino acid peaks. Also, quick estimations of specific amino acids are performed by MALDI-MS involving spiked isotopes.

Other than automated sample preparation, developing a miniaturization integration detection system is another direction of the centrifugal microfluidic investigation. In the second work, we first introduce smart polymer-based etalon sensors to the centrifugal microfluidic system with transparency disc material PMMA. The etalon is fabricated with a sandwich structure on a thin glass slide, including two layers of Au and one middle layer of hydrogel. The top Au surface is modified with anti-progesterone(P4) DNA aptamer, which exhibits distinctive reflected color changes with the absence of different concentrations of progesterone in the sample. All required on-disc procedures to enable etalon sensoring, including sample incubation, buffer wash, and salt stimuli, are automated by three pneumatic valves and one siphon valves. Three pneumatic valves

with increased burst spinning speed allow the sequential release of each preloaded reagent, including sample, wash buffer, and salt solution. At the same time, the reusable siphon takes charge of emptying the incubation chamber after each reaction. The color change degree of the etalon is inversely related to the concentration of P4 as the P4 binding DNA aptamer takes reformation that prevents polymer hydrogel collapse caused by stimuli of Na^+ in the salt solution. The color change is readout by image color analysis, avoiding the usage of sophisticated optical devices like reflectance spectrometer, which further simplify the device setting and make the system applicable for on-site use.

Preface

The research outcome in Chapter 2 has been published as Zhao Y, **Hou Y**, Ji J, Khan F, Thundat T, Harrison DJ. "Sample preparation in centrifugal microfluidic discs for human serum metabolite analysis by surface assisted laser desorption/ionization mass spectrometry". Analytical chemistry. 2019 May 15;91(12):7570-7. Yufeng Zhao was in charge of disc design and disc development. The other authors provided some guidance and direction at various stages. This thesis' author took responsibilities for the disc fabrication process, including printing and cutting transparency films as well as disc assembly. The quantification method using HILIC-MS was introduced and performed by the author. The GALD film for SALDI-MS was provided by the author too. Quantification data from SALDI-MS and HILIC-MS was collected and processed by the author.

The work in Chapter 3 will be submitted as **Hou Y**, Mishra R, Ducrée J, Harrison DJ, "An automated centrifugal microfluidic for efficient multistep blood sample preparation and clean-up towards small ion-molecule analysis". The author of this thesis initially developed the project idea, experiment designs, and disc design with Dr. Harrison's supervision. Rohit was in charge of drawing the CAD software design and calculating on-disc operation parameters with Dr. Ducrée's supervision. The author was in charge of all experimental operations and data collection. The optimization and video record of the on-disc procedure were finished by the author in Dr. Ducrée's lab on spinning-stand platform with Rohit's assistance. All data were collected in Dr. Harrison's lab by running the disc in a centrifuge with a proper adaptor. Chapter 3 has already been published as Hou Y, Jing J, Mishra R, Ducrée J, Harrison DJ. "Centrifugal blood sample preparation for metabolite derivatization and analysis by solid matrix laser desorption/ionization mass spectrometry (SMALDI-MS)", Proceedings of MicroTAS 2018, Taiwan, Nov 11-15.

The human blood sample was investigated in Chapter 3. The author has obtained approval from University of Alberta Health Research Ethics Board - Biomedical Panel to handle human blood samples. The approved study ID is Pro00081968, and the study title is "Centrifugal microfluidic device for sample preparation". The approval is valid from July 18, 2018 to May 20, 2020.

The work presented in Chapter 4 collaborates with both Dr. Jens Ducrée's group and Dr. Michael Serpe's group. The author in charge of disc design, experimental operation, and data collection. Rohit was responsible for realized the disc design by CAD software with proper parameters after calculation. The optimization and video record of on-disc liquid control is conducted in Dr. Ducrée's lab with Rohit's mentoring when the author visited DCU. The concept of aptamer-modified etalon sensor is learned from Dr.Serpe's group. Menglian Wei has instructed the author to modify the etalon sensor when she was post-doctoral in Dr. Serpe's group, who later joined another group. Nicholas Balasuriya has facilitated etalon fabrication, especially the microgel coating. Part of chapter 4 has already been published as **Hou Y**, Mishra R, Wei M, Balasuriya N, Serpe MJ, Ducrée J, Harrison J. "An automated centrifugal microfluidic system integrated with etalon sensor films for rapid image analysis detection of hormones in milk", Proceedings of MicroTAS 2019, Basel, Oct 27-31. In the future, the work in Chapter 4 will be submitted as **Hou Y**, Mishra R, Wei M, Balasuriya N, Serpe MJ, Ducrée J, Harrison J. "An automated centrifugal microfluidic system integrated with etalon sensor films for rapid image analysis-based detection of progesterone".

Acknowledgments

This thesis was completed under the careful guidance of my supervisor, Professor Jed Harrison. During my Ph.D. study, I have benefited a lot from Dr. Harrison's rigorous academic attitude and scientific research spirit. When I needed thought-provoking suggestions, I was inspired in every discussion with him due to his profound knowledge and abundant experience. Also, he has provided generous support to help me realize my research ideas and access all resources for collaborations. Besides, he supported group members for international conferences and academic travels, which broadened our knowledge and experience. In life, he gave extensive care to all group members' especially when we international students needed to adapt to a new environment and culture. I would like to express my sincere gratitude to him for his assistance with the completion of this thesis.

I would like to express my gratitude to Professor Jens Ducrée. They accepted me to learn and use centrifugal microfluid systems in Fraunhofer Project Centre for Embedded Bioanalytical Systems at Dublin City University (FPC@DCU). All the group members were very kind to me and were always willing to provide help. I was honored to have worked and studied in his lab with a group of energetic and intelligent people. The postdoc fellow Dr. Rohit Mishra, whom I directly collaborated with in DCU, is a knowledgeable patient mentor. We worked together to revise many versions of centrifugal disc design to make it work efficiently and automatically (video in Appendix). Rohit always could give me instructive advice when I was frustrated. The experience in DCU will become one of the most memorable chapters of my life.

Also, I would like to thank Professor Michael Serpe, who approved the cooperation of the centrifugal system and his group's etalon sensoring system. His group members are so vigorous and enthusiastic. The postdoc fellow Dr. Menglian Wei gave me thorough instruction of etalon modification, while the graduate student Nicholas Balasuriya offered lots of help in etalon preparation. I appreciate the convenience provided by Serpe's group members when I worked in their lab.

I am very grateful for the guidance and suggestions from my supervisory committee, Dr. Julianne Gibbs and Dr. Liang Li. As an expert in metabolomics research, concerns raised by Dr. Li remind me to rethink the drawbacks of my work which lead me to optimize the research plan. Juli educated me to be a rigorous researcher both in her lectures and my candidacy exam, which makes me confident for future challenges. I thank all exam committee members for attending my defense and providing helpful comments on my work.

Staffs in Department of Chemistry and other department provides excellent facilitation and technical assistance to my study. Their excellent work allows me to focus on my research without concern. I'd like to also express my gratitude to previous and current members of our group, especially Yufeng Zhao who lead me into the microfluidic field when I first joined Harrison's group. All group members are so cooperative in the lab. I enjoy their companies in the lab and fruitful discussions with them during meetings.

Lastly, I would like to thank my parents and friends for their support and encouragement. My mother is the one who gives all her warmth and love to me. This thesis is dedicated to her.

Table of Contents

List of Tables

List of Figures

List of Acronyms

3D	Three dimensions
BPA	Bisphenol A
CAD	Computer-aided design
CCD	Charge-coupled device
CE	Capillary electrophoresis
CHCA	Cyano-4- hydroxycinnamic acid
COC	Cyclic olefin copolymer
CTAB	Cetrimonium bromide
DF	Dissolvable film
DHB	5- dihydroxybenzoic acid
DHPT	3,4,5-tetrakis (3', 4' -dihydroxylphenyl) thiophene
DIC	Differential interference contrast
DMF	Digital microfluidic
DNA	Deoxyribonucleic Acid
DNPH	2,4-dinitrophenylhydrazine
EDTA	Ethylenediaminetetraacetic acid
EI	Electron impact
ELISA	Enzyme-linked immunosorbent assay
ESI	Enzyme-linked immunosorbent assay
FE-pNIPAm	Ferrocene-modified poly(N-isopropylacrylamide)-co-acrylic acid microgels
FT-ICR	Fourier transform ion cyclotron resonance
GC	Gas chromatography
GLAD	Glancing angle deposition
HILIC	Hydrophilic interaction liquid chromatography
HMDB	Human metabolites database
HMW	High molecular weight
HPLC	High-performance liquid chromatography
IMAC	Immobilized metal affinity chromatography
LC	Liquid chromatography
LCST	Lower critical solution temperatures
LDI	Laser desorption/ionization

LIFM	Laser-irradiated ferrowax microvalves
LIGA	German abbreviations of Lithograghie, Galvanoformung, Abformung
LMW	Low molecule weight
LMWC	Low molecule weight compound
LOD	Limit of detection
LOD	Lab on a disc
LOQ	Limit of quantification
LSPR	Localized surface plasmon resonance
MALDI	Matrix-assisted laser desorption/ionization
MCH	6-mercapto-1-hexanol
MCP	Multichannel plate
MEMS	Micro-electromechanical system
MRM	Multiple reaction monitoring
MS	Mass Spectrometry
MSE	Matrix suppression effect
P4	Progesterone
PC	Polycarbonate
PCL	Print, cut and laminate
PCR	Polymerase chain reaction
PDMS	Polydimethylsiloxane
PE	Polyethylene
PET	Polyethylene terephthalate
PETG	Polyethylene terephthalate
PLA	Polylactic acid
PMMA	Polymethyl methacrylate
pNIPAm	Poly (N-isopropyl acrylamide)
POC	Point-of-care
PP	Polypropylene
PS	Polystyrene
PSA	Pressure sensitive adhesive
PVC	Polyvinyl Chloride
RGB	Red, Green, Blue
RNA	Ribonucleic acid
RPLC	Reversed-phase liquid chromatography

SALDI	Surface assisted laser desorption/ionization
SERS	Surface-enhanced Raman spectroscopy
TCEP	Tris (2-carboxyethyl) phosphine hydrochloride
TIR	Total internal reflection
TOF	Time-of-flight
μ TAS	Miniaturized total analysis system
UV	Ultraviolet
VPTT	Volume phase transition temperature
XPS	X-ray Photoelectron Spectroscopy

Chapter 1. Introduction

1.1. Centrifugal microfluidic

1.1.1. Overview

Microfluidics is the science and technology of systems that process or manipulate a small amount of fluid or gas, using channels with dimensions of tens to hundreds of micrometers. Extreme miniaturization was a new field that drew many scientists' attention after Dr. Richard P. Feynman's lecture "Plenty of Room at the Bottom", which encouraged the study of miniaturization possibilities.[1] Following the development of the micro-electromechanical system (MEMS) in the mid 1980's, Manz and Widmer introduced the concept of a miniaturized total analysis system (μTAS) in late 1989,[2] which set a signpost leading to rapid development period of microfluidics. Because of features of small volume, low cost, and diversified processing methods, this technology has already been widely used in life science research, analytical device, and point of care diagnosis.[3, 4]

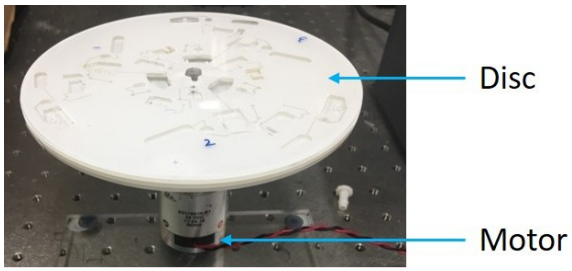

Figure 1. Photo of centrifugal microfluidic disc and motor.

The centrifugal microfluidic chip system (Figure. 1), also called lab on a disc (LOD), is a prevailing branch of microfluidic technology. Centrifugal force (CF) is used as the driving force

of liquid flow to realize a microfluidic system for detection and analysis. The power for the system comes from a simple motor with low power consumption, requiring small space, similar in deisgn to a compact disc player. CF is suitable for driving fluids in pipes of different size ranges. It has been successfully implemented to drive liquid flow in channels with diameters ranging from 50 to 500 μm. As far as the current level of development, CF can drive from 5 nl/s to ~ 0.1ml/s. The flow rate in the range of 0.1 mL/s is larger than that of several other pumping technologies. The flow rate can be continuously adjusted by changing the speed of the motor. The multi-parallel analysis unit of the centrifugal flow chip can detect multiple samples online. The literature has reported the successful development of a 96-fold parallel analysis unit.[5] Being relatively insensitive to the physicochemical properties of fluids (excluding viscosity changes), CF can drive biological fluids such as blood, urine, and some organic solvents. CF can drive not only liquids but also gases to be used in a wide range.[6] The on-disc function utilizes micro-fabrication technology to create valves, flow tubes, mixing reactors, heaters, separation devices, etc., in order to realize sampling, pre-treatment, derivatization, mixing, and detection of chemical analysis.[7] The detector and other components may be miniaturized, and integrated on a CD-shaped chip. When this microfluidic system is combined with temperature control, detection, signal access and data processing, it can be capable of running various comprehensive analyses.

In the 1970s, the first articles on centrifugal microfluidics were published.[8] The centrifugal analyzer from Oak Ridge National Labs' N. Anderson was the highlight of the first developments. Researchers began to study the centrifugal CD system in the mid-1990s systematically, and more than a dozen related publications reported the early progress of the system. Lab-on-CD led to the rapid development of centrifugal microfluidic systems and their biochemical and clinical analysis applications. The first clinical chemistry blood analyser CD was released by Piccolo Xpress® in

the mid-1990s. The second commercial CD system-labCD™ was from Gamera Bioscience Corporation (acquired by Tecan in 2000),[9] which was developed for drug development research and metabolism study.[10] The third system was Gyroslab® from Gyros, which was mainly used to prepare proteins as peptides for mass spectrometry analysis. Gyros and Tecan fostered a wide variety of intellectual property in the early 2000s by developing new centrifugal microfluidic applications, such as immunoassays.

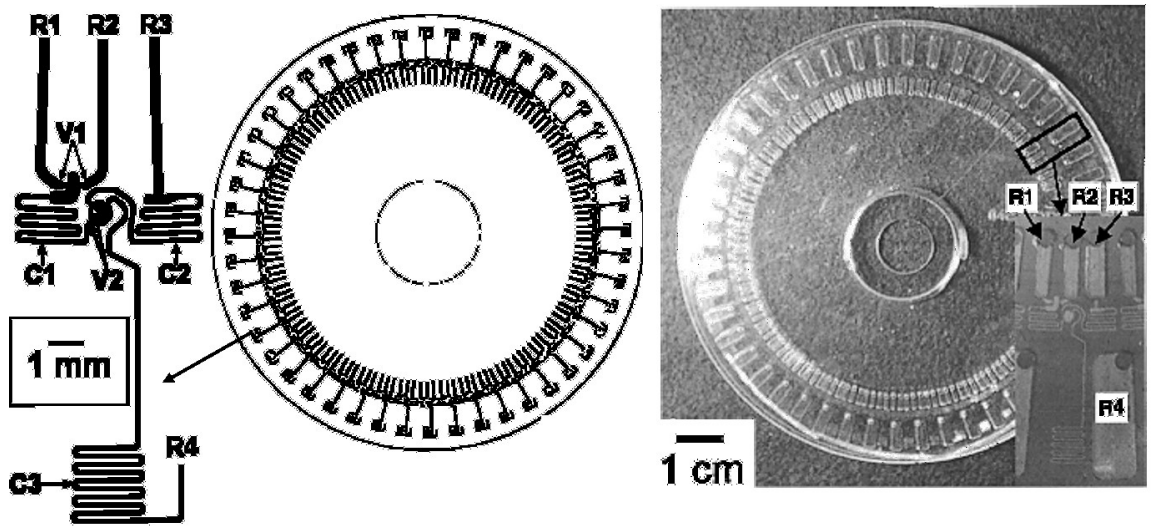

Figure 2. Design and the PDMA replica photomask for centrifugal disc carrying out 48 parallel enzymatic assays. © American Chemical Society 1999.

The centrifugal CD-like microfluidic chip system has developed rapidly in recent years due to its advantages of high throughput, multiple parallel analysis, easy operation, and integration. It has shown broad application prospects in many fields such as biomedicine, high-throughput drug screening, health quarantine, and environmental detection and protection. Examples of the progress and capabilities have appeared over time, as exemplified by some of the following landmark publications. Duffy reported a centrifugal chip colorimetric detection system integrated with 48 enzyme analysis units in 1999.[11] The chip structure is shown in Figure 2. This system can perform sample reagent mixing, reaction, detection, and other operations required for enzyme

analysis during chip rotation. In 2001, Johnson et al. reported a centrifugal chip analysis platform integrated with an ion-selective photoelectrode.[12] The PMMA (polymethyl methacrylate) chip of this system is fabricated by CNC technology. The ion-selective photoelectrode film is made of polyvinyl chloride (PVC). The results show that the detection method of unknown concentration can also control the error within 3% by using the absorbance detection method. In 2004, Lai integrated a series of microchannels on a CD and applied it to mouse IgG's enzyme-linked immunosorbent assay (ELISA).[13] The chip had 24 independent analysis structures, which could complete large quantities of sample analyses in a short time. The test results compared the ELISA-CD chip platform and the 96-well plate format used to determine IgG in mice, and the same detection range could be obtained. The former system has a significant advantage due to its small sample consumption and short analysis time.

Now, global players such as 3M, Roche, and Samsung have joined the industry of centrifugal microfluidic devices, and a slew of startups are planning to enter the market soon.[7] For example, Roche launched Cobas b 101 system aiming to detect metabolic syndrome in 2012.[14] The system includes a compact instrument to run the disc and read the result, and cartridges targeting different biomarkers. The cartridge products released so far cover blood lipid disc, hemoglobin A1c test, and c-reactive protein test. All these cartridges are prepacked with reaction reagents, less than 20μl whole blood is required to load before testing. This system is proposed for professional application in clinical laboratories and at Point-of-Care locations, and it gives quick and reliable results.

Microfluidic techniques for convenient small-volume biological sample preparation are often suggested, but rarely realized. One of the challenges is that a sample placed within a chip occupies too low a volume to be recovered for off-chip analysis, but integrating all of the detection

components makes for an expensive single-use, disposable device. Centrifugal microfluidics features a simple control system and inexpensive device fabrication, and can duplicate many laboratory steps, and may facilitate high-throughput sample processing.[15, 16] A key feature is that the volume of fluids within a disc can be made relatively large, so that there is sufficient material available to then remove the disc-prepared solution and transfer it to a lab-based analytical instrument. In this manner, the device becomes a chip-in-a-lab, which can be integrated into a larger laboratory workflow, to optimize analysis times. While the phrase chip-in-a-lab has at times been used in a negative fashion to describe microfluidic technologies, the integration of the best approaches from lab-based and chip-based technologies offer a promising route for further adoption of the technology.

In this thesis, we have first compared the performance of the centrifugal sample preparation disc for sample cleanup for SALDI-MS with cleanup for LC-MS. Reproducibility and recovery of several identified metabolites obtained from disc-based serum preparation with SALDI-MS detection are evaluated. In later work in the thesis, we have integrated a unique sensing element, in the form of particle-based etalons, returning to the sample-to-answer philosophy that has often guided microfluidic design. Etalons have not previously been incorporated in centrifugal microfluidic devices, and they represent a unique form of simple, integrated detection schemes in microfluidic systems.

We adopted different disc fabrication and on-disc fluid control techniques to optimize disc performance within the thesis work, as well as different detection systems. The systematic introduction of centrifugal microfluidic principles, fluid control methods, and device fabrication

in this chapter provides background information for the investigations reported in the following chapters.

Also, this chapter covers the detection methods employed, such as MALDI-MS and HILIC-MS, and etalon-based particles as sensors. Figures are cited with permission to illustrate these technologies and concepts. The details of how centrifugal microfluidic devices are combined with different detection methods for biochemical applications will be discussed in the following chapters.

1.1.2. On disc fluid control

In a centrifugal microfluidic chip, the microchannels are distributed along the radial direction of the disc, which is consistent with the direction of the centrifugal force (radial outward). Usually, the fluid is pre-packed in a container near the center of the disc. The fluid moves away from the center of the disc along with the microchannel network under the effect of centrifugal force when an electric motor drives the disc. Because discs made of polymers usually have a hydrophobic surface, capillary forces in the channels are almost zero. But due to the non-inertial nature of this condition of reference, both the Euler force density f_E and the Coriolis force density f_C also appear in the hydrodynamic motion, along with the centrifugal force density $f\omega$ (Figure 3)[17].

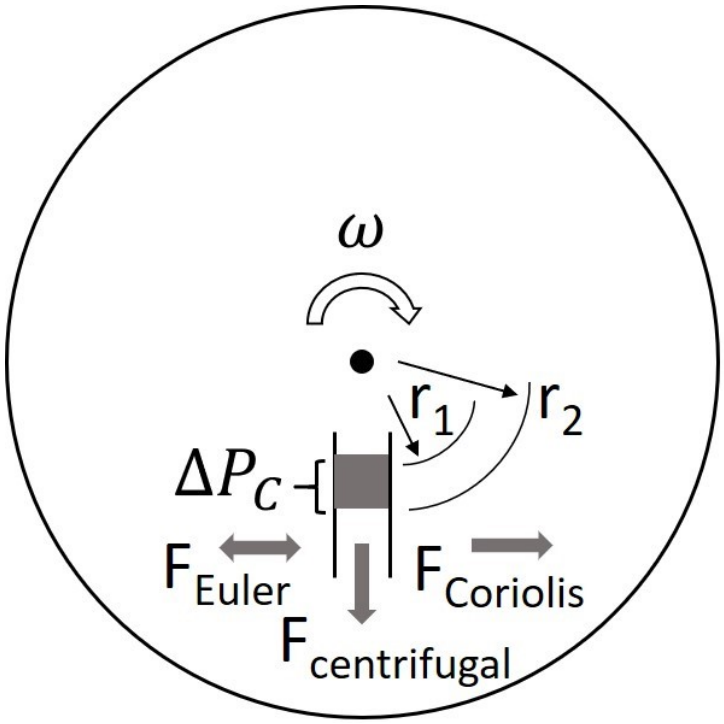

Figure 3.Forces and geometry on a spinning disc with an angular velocity vector ω.

Equations for these three pseudo forces are given below:

Centrifugal force is described by

$$f_\omega = \rho\omega^2 r \tag{1}$$

The Euler force is given by:

$$f_E = \rho r \frac{d\omega}{dt} \tag{2}$$

and the Coriolis force is described by:

$$f_C = 2\rho\omega v \tag{3}$$

where r is the radial position, ρ is the mass density, v is the velocity of the fluid, and ω is the vector angular velocity. These equations describe the common situation where ω is perpendicular to the vectors r and v.

It is more convenient to use scalar differential pressures p rather than vector forces, F, for the basic design of fluidic elements centrifugal flow. The simple equation $\Delta P = \rho g h$ defines the hydrostatic pressure in a non-rotating frame of reference under gravity, where g is the gravitational acceleration and h is the height of the liquid column. Similarly, the hydrostatic pressure induced by centrifugally spinning is determined by the location of the fluid column. r_1 is the radially inward location, and r_2 is the radially outward location of the liquid column (Figure 3), respectively. Pc stands for angular velocity induced pressure,

$$\Delta Pc = \frac{1}{2}\rho\omega^2(r_2^2 - r_1^2) \quad (4)$$

where r_1 is the inner radial point, and r_2 is the outer radial point of the liquid column. This equation is often presented in the literature as:[18]

$$\Delta Pc = \rho\omega^2\Delta r\bar{r} \quad (5)$$

Where Δr is the liquid column's radial height ($\Delta r = r_2 - r_1$) and $\bar{r}$ is the liquid column's radial centre ($\bar{r} = (r_2 + r_1)/2$).

Non-pseudo forces exist in both rotating and non-rotating systems. As a result, they are not limited to centrifugal platforms, but they play a significant role in the operation of many centrifugal units. The viscous force, the pneumatic force exerted by a pressurized gas, capillary force, and fluidic inertia are the most effective and employed non-pseudo forces. When centrifugation alone is

insufficient to complete the tasks in a centrifugal microfluidic cartridge, extrinsic forces are introduced. Magnetic, electric, or pneumatic forces are examples of those forces that assist fluids or particles in transferring. Extrinsic forces are used for various purposes, from mixing liquids with magnetic beads, to pneumatic stirring, to pumping liquids, and even dielectrophoretic separation. External magnets attract paramagnetic beads, which are widely used in suspensions on- or off-chip. Electrodes, which are usually integrated into the microfluidic cartridge, should apply electric forces in centrifugal systems. This allows samples to be exposed to an electric field for electrolysis, dielectrophoresis, and other separation processes on a permanent and proximal basis. The use of non-contact external pneumatic pressure in centrifugal microfluidics can be achieved by shooting a pressurized gas jet at specific openings of a rotating platform. As a consequence, the gas's impact pressure is introduced to the microfluidic system.[19]

Centrifugal microfluidic systems involve a broad range of fluid cell operations such as liquid transportation, metering, mixing, and valve control based on the interaction of the forces mentioned above.[20] The available functional properties cover all aspects of automated liquid control requirements and allow efficient parallelization, miniaturization, and inspection integration. Here we give explanations of several typical on-disc operations.

Passive and Active Valving

In centrifugal microfluidics, valves are one of the most crucial functions.[21] Valves regulate the fluid flow in the subsequent channel networks. Valves are commonly used in advanced application devices to enable the sequential releasing of pre-stored reagents. Active and passive valves are two main types of valves; active valves are regulated by external forces, while passive valves are

controlled exclusively by centrifugal forces.[22] Passive actuation is more convenient as it eliminates the need for an external approach, then reduces the overall sophistication of the centrifugal microfluidic device.[10] Some literature sorts different valves by other principles, such as defining valves as sacrificial and non-sacrificial.[23] In the following paragraphs, specific valves are only charactered as active or passive, to avoid crossing referencing.

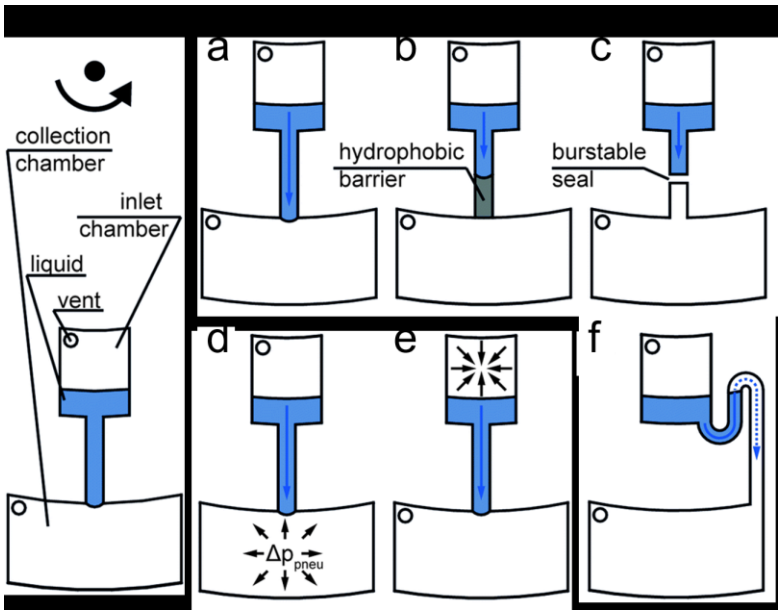

Figure 4. Examples of passive valves on centrifugal microfluidic disc : (a) the capillary valve, (b) the hydrophobic valve, (c) the burstable seal valve, (d) the centrifugal-pneumatic valve, (e) the centrifugal-pneumatic valve under pressure (the top chamber is sealed while the bottom chamber is connected to the atmosphere), (f) the capillary siphon valve. © The Royal Society of Chemistry 2015.

The initial status of integrated passive valves in centrifugal microfluidics is usually closed.[24] Centrifugal pressure, capillary forces, or instability at interfaces could trigger a closed passive valve to burst (Figure 4). Without knowing the radial location, radial length, and density of the liquid column, the commonly used rotational frequency is ineffective in explaining the valving principles. Therefore, analysing centrifugal pressures is a better way to explain them. Passive capillary valves are the most investigated passive valves in the early stage. The capillary force (due to fluid interfacial tension), and the centrifugal force, play important roles in balancing passive

capillary valves. When the centrifugal force exceeds capillary force caused by liquid interfacial tension, the fluid begins to shift and is released, such as transferring from one reservoir to another.[25] Controlling flow sequencing is possible with proper configuration of reservoirs on a microfluidic disc, and the layout of connection channels. The burst frequency is the rotational frequency at which the centrifugal force overcomes the capillary force to open the valve and transfer the fluid. In complex assays, precise operation of the burst frequencies on a CD enables sequential fluid release.[13] It is important to note that passive valving has certain disadvantages. These valves can't be used for long-term sample storage or heating without air-tightness.[26] Valve fabrication requires high precision, because the effects are strongly dependent on the channel interface geometry, and coatings are needed to adjust surface tension of the materials. These valves are also very susceptible to how the sample matrix may change viscosity and surface tension affects.

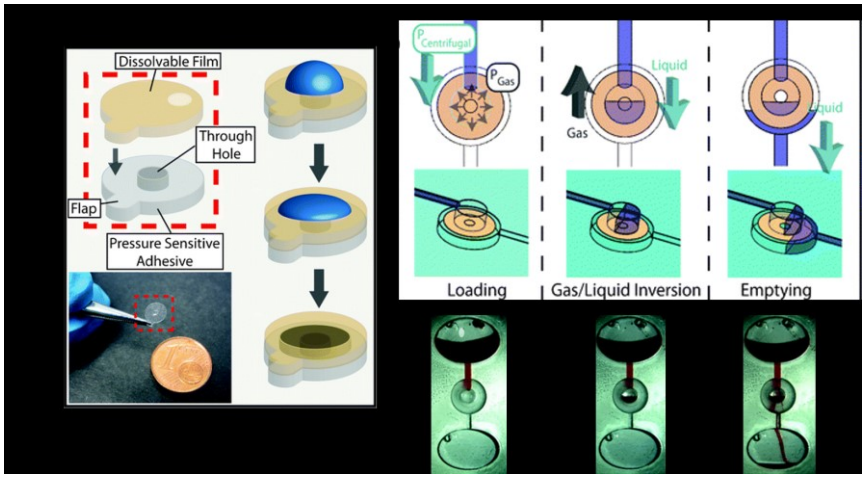

Figure 5. (a) Fabrication of the DF valving tab, (b) Schematic diagram (top), and photos (bottom) that demonstrate centrifugal-pneumatic valving procedures. © The Royal Society of Chemistry 2012.

Vapor-tight valves were developed to accommodate volatile reagents. Hoffmann et al. illustrated a valve that applied centrifugal pressure on an integrated sealing foil to open the fluidic channel,

which is defined as a "burstable seal valve".[27] It takes thirty-one seconds to release under a centrifugal pressure of two bar. In another approach, polydimethylsiloxane (PDMS) membranes were bonded to a thermoplastic cartridge to shut down the fluidic pathway. The membrane is pulled back and opens the fluidic channel when centrifugal pressure increases. Various flow rates were tuned by adjusting membrane thickness and spin rate.[28]

The centrifugal pneumatic valve is another strategy for eliminating the necessity of additional surface coatings and high-precision fabrication. The normal state of this valve is closed, because of the interaction between capillary counter pressure that happens at the channel-chamber interface and the pneumatic counter-pressure produced by the compressed air within a sealed chamber. The centrifugal pneumatic valve only opens when the centrifugal pressure conquers the counter pressures.[29] The Rayleigh–Taylor instability of the interface between the air and liquid phases facilitates optimum liquid release after the breakthrough. Afterward, a water dissolvable film (DF) was introduced to assemble the centrifugal pneumatic valve (Figure 5).[30] Compared to pneumatic valve relying on hydrophobic constrictions, the application of DF film broadens the range of rotational speeds and enhance the reproducibility of burst frequencies. The film was applied to seal the outlet of the dead-end chamber where the air pocket was trapped, enabling centrifugal pneumatic valving to take place. The DF usually dissolves within ten seconds after wetting by the liquid, then releases the fluid for downstream processing.

Both hydrophobic and hydrophilic passive capillary valves are useful. The channel of hydrophobic valves is fabricated by a hydrophobic material or by applying hydrophobic material to a particular area.[31] Another method to increase the hydrophobicity of a certain region is to introduce air gaps into the channel. Fishbone valves are structural tunnels that could fulfill this feature.[32] A

hydrophilic valve occurs when a narrow hydrophilic channel opens into a wider reservoir.[33] Capillary valves based on this geometry become increasingly unstable for liquids with touch angles less than forty-five degrees.[34] Hydrophobic surface coatings have been introduced to improve the comparability with liquids that have low contact angles. The corresponding valves are called "hydrophobic valves" (Figure 4b) designed to halt a liquid flow by the hydrophobic coating. Hydrophobic valves open when the centrifugal pressure conquers the capillary force. Many of the surface coatings used in publications are achieved by spraying or dispensing fluorinated polymer solutions on specific locations. Honda et al. created a highly parallel on-disc integration of hundreds of hydrophobic valves.[35] The contact angles of de-ionized (DI)-water increased two times on printed toner spots using a rapid surface modification for hydrophobic valves by the laser printer. Burst pressures were successfully tuned by changing the density of the toner spots.[36]

The capillary siphon valve is another kind of passive valve extensively investigated on centrifugal microfluidic platforms. Most passive valves open as centrifugal pressure increases, however, siphon valves only burst under low centrifugal pressure (Figure. 6).[37] The siphon valve is usually achieved in a hydrophilic system, where the siphon channel is primed exclusively by capillary forces.[38] The conventional siphon valve system consists of a reservoir filled with liquid and an attached reversal U-shaped channel. The peak of the reversal channel extends higher (towards the radial centre) than the radial position of the liquid level in the reservoir. In contrast, the end of the channel reaches lower than a radial position below the connection point. Centrifugal forces retain the liquid within the chamber and below the summit of the reversal channel in high-speed rotation. With the decrease of centrifugal forces in slow enough rotation speed, capillary forces within the siphon channel overcome the centrifugal forces (Figure 6). Capillary forces drive the fluid to climb the crest of the siphon and flow down to the outlet end, which is radially lower than the chamber.

Siphon priming is realized as the fluid meniscus is radially below the bulk liquid within the upper reservoir. A hydrophilic channel is required for siphoning, so the hydrophobic surface needs to be surface coated or treated to enable siphoning.[39] Larsson et al. treated polycarbonate with oxygen-plasma to create a hydrophilic surface. The treated surface still maintains improved hydrophilicity after six months of storage.[40] Furthermore, siphons are not only useful for valving on centrifugal microfluidic platforms, but they also play critical roles in pumping and liquid metering.[41]

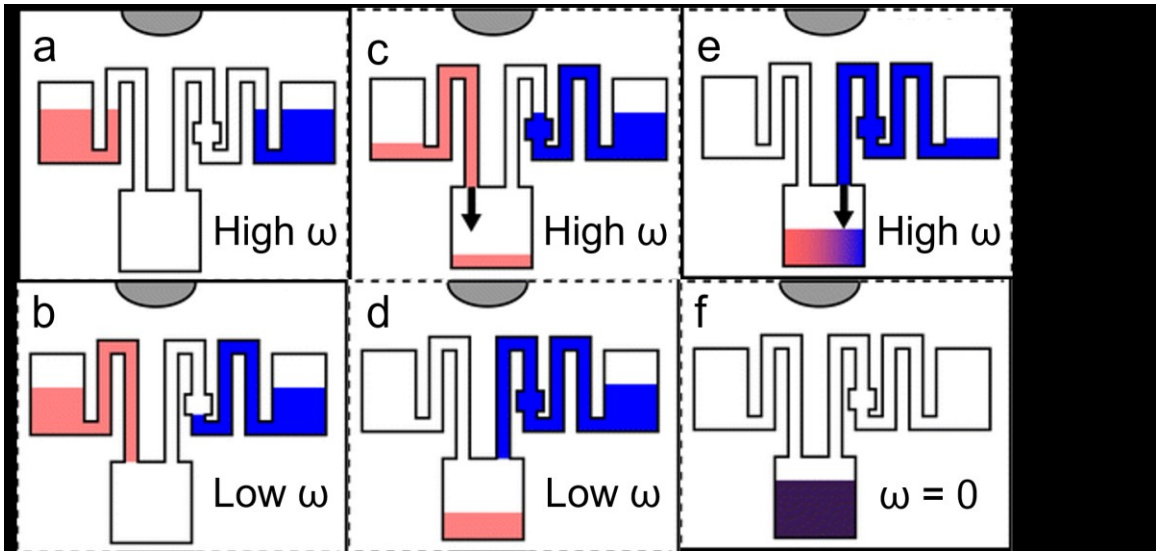

Figure 6. Schematic diagram of two serial siphon valves, the second siphon valve (right, blue) structure contains a capillary valve that preventing the prime of the right siphon channel during the first pause. © Springer Nature Switzerland 2009.

Some passive valves do not depend on centrifugal pressure to release liquids, instead adopting a time-dependent method. Schwemmer presented a microfluidic timer that could achieve liquid actuation regardless of the spinning speed. The timer is released after a defined period by introducing temporary storage of pneumatic pressure. At high rotational speeds, flushing in the first pneumatic chamber allows fluid to pump into the secondary pneumatic chamber, through a narrow channel which triggers the timer.[42] A paper strip was inserted into a centrifugal microfluidic disc by Kinahan.[43] The paper connected and wetted multiple dissolvable films in a

specific order to open fluidic pathways sequentially. Ukita presented a microfluidic clepsydra (hourglass using water instead of sands) configuration for the sequential release of liquids associated with the venting of a loading structure. The liquid level in the clepsydra drops with time, allowing the venting for the single loading components to open sequentially.[44]

Although passive components are relatively easy to fabricate and incorporate, there are many disadvantages to using them in practical applications. Capillary valves suffer unpredictable fluidic responses due to wetting and contact angle hysteresis.[45] The footprint of the microfluidic chip is dramatically increased by intermediate channels and supplementary metering channels, employed to time the fluidic motions in devices dependent on hydrostatic suction and water-clock methodologies.[46] In contrast, platforms that incorporate active valving controls make centrifugal microfluidics more functional. They enable important fluidic operations like aliquoting, metering, and mixing, resulting in easier integration and automation. In the following paragraphs, the principles and working mechanisms of active valves are discussed in the scope of recent developments in instrument design and manufacturing.

Active valves usually depend on additional external settings to realize fluidic control. Active valves can be either normally open or normally closed during on-disc processing, offering more flexibility than passive valves.[47] For example, Cai, Z.[48] presented a novel pin-type valve for centrifugal microfluidic platforms actuated by an external setting makeup by a spring plunger and a flyball regulator.[48] Its normally close state is realized by applying pressure via the spring plunger on the PDMS microchannel. When the flyball spinning speed reaches a specific value, it drives the spring plungers to reduce the pressure and make the valve open. The valve performed promisingly, and the control is simple to tune by adjusting mechanical parameters.[48] Different

active valving principles have been exploited, such as wax and ice valves, laser burst membranes valves, xurography-enabled approach, and electromechanical vents. The following discussion will focus on more detailed illustrations of their principle and external settings.

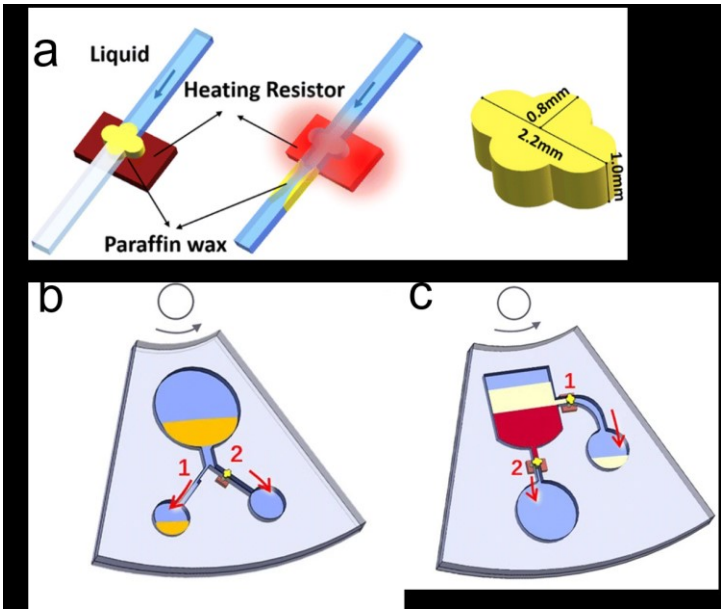

Figure 7. Working principle of the paraffin wax valve(a), the combination of the capillary valve and the paraffin wax valve(b), and the paraffin wax valve design for on-disc separation(c). The sequential loading priority is labeled by number. © Springer Nature 2019.

Paraffin wax has been integrated into centrifugal microfluidic cartridges for valving use due to its low melting point.[22] The fluidic pathway wax was melted to open the fluidic pathway under rotation using a stationary infrared setting (Figure 7). Utilizing waxes with diverse melting temperatures, the sequential activation of valves has been revealed. A sequential actuation of nine valves was reported to finish within a reaction time of 25 seconds.[21] For the melting of wax valves, another system adopted portable heat guns rather than infrared lamps.[49] Meanwhile, possible interference with on-disc reagents caused by molten wax and heat input raises concerns. Al-Faqheri [22] eliminated these drawbacks by configuring the wax valves apart from the reagents to avoiding direct contact. In a few cases, valves are melted to open or close the connections to the vents rather than opening the fluidic channel[22]. Ice valving was developed by Amasia.[50] by

freezing liquid plugs in specified channel areas via thermoelectric modules, in order to prevent evaporation in polymerase chain reaction (PCR) thermocycling. Park et al. developed single addressable and low energy input laser-irradiated ferrowax microvalves(LIFM),[47] which were implemented for various devices. Iron oxide nanoparticles were added into the wax for more efficient heating by laser, enabling valve actuation with low-power lasers and yielding a fast response. This melting principle ensured that only the nanoparticles were heated by the laser rather than the surrounding liquids. The normal state of laser-irradiated ferrowax microvalves could be closed or open, also reversible valve actuation is possible in this platform. Furthermore, LIFM could bear high centrifugal pressure as about 400Kpa and stay leak-free, enabling versatile applications of this technology.[51]

In the first xurography-enabled automated valving system, the vents connected to the centrifugal pneumatic DF valve are sealed by pierceable adhesive tape.[52] A commercial blade is installed on an XY-axis robotic arm and fixed above the disc, dropping during disc spinning to puncture the adhesive tape. Once the pneumatic chamber is vented to the atmosphere by breaking the sealing tape, wetting and opening are triggered. As the blade is placed above the rotating disc, only these tape-sealed vents in the same orbit are actuated simultaneously. Moreover, xurography-enabled automated valving is compatible with pneumatic overpressure or vacuum compression[22] flow control without the use of DFs. But the drawback is the limitation of spin rate with the absence of DFs.

Volume metering and sequential Loading

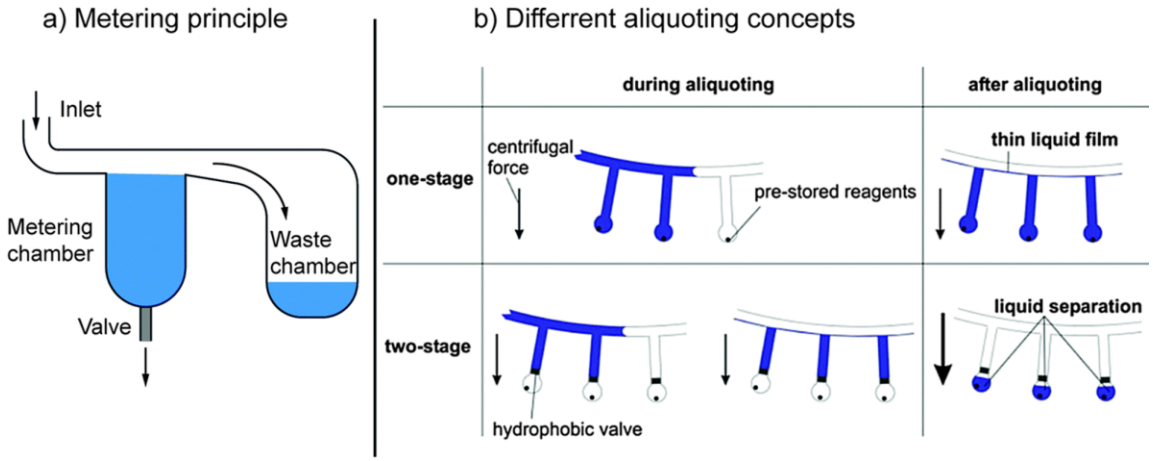

Figure 8. Schematic diagram of the simplest metering structure (a) and metering unit coupled with valves (b). © The Royal Society of Chemistry 2015.

To obtain quantitatively repeatable results, most microfluidic integration applications require precise liquid volume input in each step. As a consequence, one commonly used unit operation is measuring liquid volumes. In the simplest embodiment, the metering structure includes a channel connected to the inlet, a metering chamber having a defined volume, and an overflow to the waste chamber to obtain the excess volume (Figure 8a).[53] For additional fluid handling, the metering unit may be coupled with valves such as hydrophobic (Figure 8b),[54] siphon,[41] and centrifugal pneumatic valves[29] at the radially outer end of the metering chamber. Metering accuracy is primarily affected by variations in lumen size within manufacturing tolerances and the effect of capillary force on the core suction at the liquid interface. Capillary force can be offset by centrifugal force, and centrifugal microfluidics can achieve high metering accuracy even at nanoliter volumes.[55] The metering structure includes a channel connected to the inlet, a metering chamber with a given volume, and an overflow to the waste chamber to obtain the excess volume. However, wicking effects that occur on liquid interfaces caused by capillary forces tend to decrease metering accuracy. Steigert et al. had developed design approaches to combat this effect and have achieved a variability coefficient of 5% when the metering volume was 300 nL.[55]

Sequential loading means that the fluids are transported to a specified chamber in a given order. Sequential loading usually appears in the same on-disc protocol with metering, as both accurate reagent volumes and loading sequences are important in many reactions or diagnoses, especially in nucleic acid extraction and immunoassay protocols. The critical technique for regulating the flow of different liquids in microfluidic networks is using various valves. Active valves have been used in the sequential transport of different liquids in some published applications, such as the laser-irradiated ferrowax microvalve.[51] The active valves must be actuated by various external instruments, which leads to the overall system's complexity.[56] Sequential capillary valves are an example of passive valves applied to release liquids into a reaction chamber in a proper sequence[25]. Since the capillary valves cannot withstand the high angular velocity, they are useless in high-speed operations. Other kinds of passive valves that are commonly used for flow sequencing are siphon valves.[37] These valves are designed to tolerate high angular velocities. But the main disadvantages of these methods are the fairly complicated structural design, the obligation of surface modification, and substantial dead volumes existing in the microchannel. Park presented a system in which three different microfluidic channels (120, 40, and 20 μm) were manufactured as passive capillary valves with different threshold values.[57] The centrifugal force directed the reagent loading in order. This sequential loading model was used for the purification of H1N1 viral RNA. Jung et al. proposed a similar method employing both capillary valves and siphon channels to realize sequential loading. An autonomous sequential loading of reagents in a continuously rotating centrifugal microfluidic system based on the water-clock technique was recently proposed by Ukita.[58] By supplying air to difference sealed sample chambers in time order controlled by the water-clock, the sequential sample transfer is achieved.

On-disc Mixing

In microfluidics, the aim of mixing is to achieve a maximum distribution and homogeneity of sample and reagent molecules to accelerate chemical reactions. Stirring, shaking, and vortexing are the most common techniques for mixing in macroscopic standard laboratory processes. However, mixing is difficult to realize on a centrifugal microfluidic platform because the disc is rigidly connected to a motor shaft, which spins the disc with a high angular velocity.[59, 60] The centrifugal microfluidic platform is extremely effective for separating phases with different mass densities but not for mixing, due to the artificial gravity generated by the rotation. Simple diffusive mixing is inefficient for liquid volumes varying from a few hundred nanoliters to a few milliliters.[61] Since mixing is still important for many biochemical assays, several methods for mixing fluids on the centrifugal microfluidic platform have been investigated.

Grumann[59] stated a concept for "Batch-mode" liquid mixing that depended on continuous changes in the spin speed of the centrifugal microfluidic device (Figure 9). Euler forces were induced by the angular momentum produced by acceleration or deceleration, causing layer inversion of the liquids in the microfluidic chamber. The standard deviation of all the observed pixel distributions of a solution containing dyed and undyed liquids was calculated by image processing to indicate mixing efficiency. The recorded mixing time could be reduced by half, from 7 minutes for merely diffusional mixing to 3 seconds for shake-mode mixing. The mixing efficiency was affected by acceleration and deceleration speeds and the angular span of the rotation, and the radial location of the reaction chamber. The mixing time has been further reduced to 0.5 seconds by introducing magnetic beads. A series of external permanent magnets pulled the magnetic beads inside the mixing chamber to move radially inward and outward, causing a faster mixing.

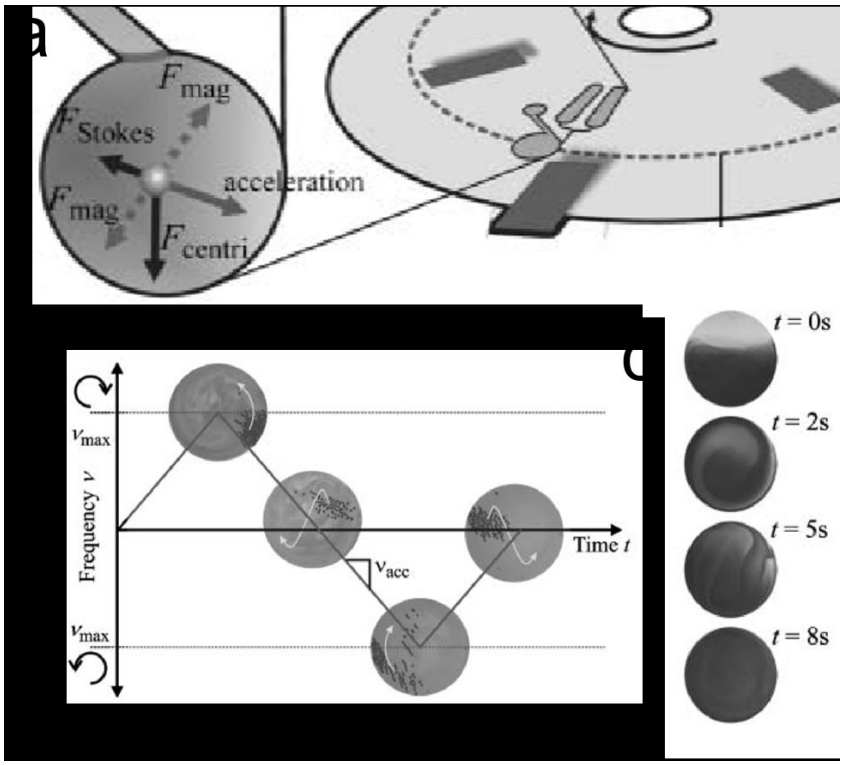

Figure 9. Demonstration of acting forces facilitating on-disc shake-mode liquid mixing(a), accelerated blending by altering the rotation with paramagnetic beads (b) and without paramagnetic bead (c). © Elsevier B.V. 2005.

Haeberle[62] presented mixing based on coriolis pseudo-forces. In his work, two liquids were distributed to two separate microfluidic inlets on the centrifugal microfluidic device. Both liquids flowed into a Y-shaped channel combined by lateral convection due to the coriolis forces acting perpendicular to the flow direction. Then the liquid was spun from the cartridge to the receiving chamber, allowing for continuous mixing. Coriolis force-based mixing was further studied by a Y-shaped microchannel at moderate spin speeds. The mixing efficiency was determined by the channel geometry, rotational speed, and flow rates. To improve overall mixing performance, coriolis mixers have recently been used in zigzagging configurations that also combine the dean effect in channel turns[63]. Coriolis mixing is ideal for applications on a wide variety of processing equipment, such as regular laboratory centrifuges, due to its independence from spin speed changes.

The flow rates of the fluids entering the mixing channels must be precisely controlled, making the integration of coriolis mixing a challenge.[64]

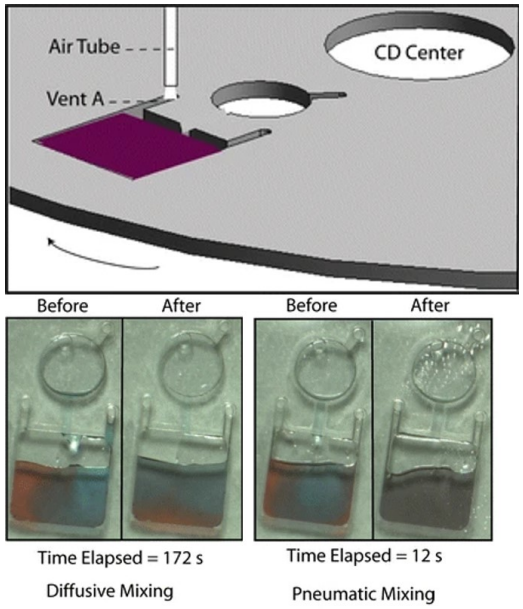

Figure 10. Comparison of on-disc mixing efficiency of diffusive mixing and mixing with pneumatic agitation. The volume of red and blue dye is 60 µL, respectively. Strobed images are captured during rotation. © Springer-Verlag 2012.

Besides "shaking-mode" protocols, methods of mixing with a constant spin speed have recently been investigated. Burger[65] produced individual droplets and several alternating layers of two separate liquids by disrupting continuous liquid flows. As a result, the interface between the two liquid phases was substantially increased, and the diffusion mixing was enhanced. Blood plasma and PBS were combined and separated into single aliquots via droplets of 60 nL volumes. The concentrations of protein in all aliquots were in alignment with the theoretical values for the perfect mixture. Kong et al. used an external air stream to mix fluids within a microfluidic chamber. The external air stream was directed through an orifice to the configurations of the microfluid, which enabled mixing at constant frequencies of spin (Figure 10).[66] The mixing efficiency with a duration of 11.2 seconds was 30 times higher than the diffusive mixture with a 7.5 Hz spin rate.

Separation

Many biochemical processes require the separation of different components from each other as a necessary unit operation. Small molecules like metabolites, macromolecules like nucleic acids and proteins, and larger components like cells or solid particles must be separated from their matrix, meaning there is a large variety of possible targets of separation operations. Variances in the chemical or physical properties of these target substances are usually exploited for separation implementation.

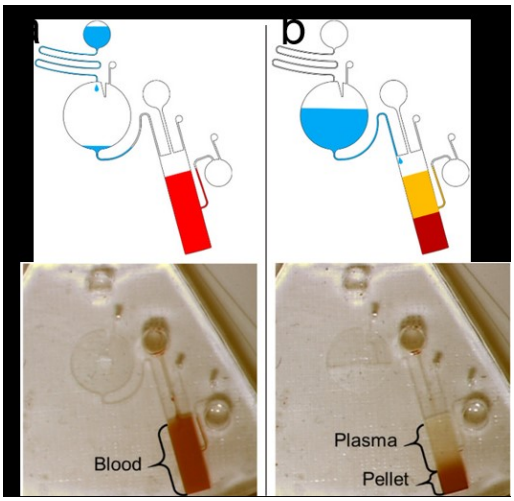

Figure 11. Schema of on-disc blood separation(a) and photograph of device operation.

Filtration and sedimentation are the most commonly used physical separation techniques performed on centrifugal microfluidic platforms. Filtering could be used in microfluidic systems to isolate or collect solid particles from a liquid phase, depending on particle size. Suppose the filtrate, or liquid that passes through the filter, is analysed in the downstream application. In that case, pre-filtering is required to prevent clogging microfluidic channels, or to avoid negative interaction with the assay.[67] Filtering is adopted in other systems to increase assay sensitivity by trapping cells or bacteria, to concentrate the material retained by the filter. Sedimentation takes

advantage of density differences between the separated component and the matrix media rather than particle size. Denser components sediment radially outwards along the centrifugal force vector, while the lighter supernatant can be transported to downstream microfluidics, pushed by centrifugal forces. The removal of solid particles or blood cells (Figure 11) is a promising application for centrifugal sedimentation.[68]

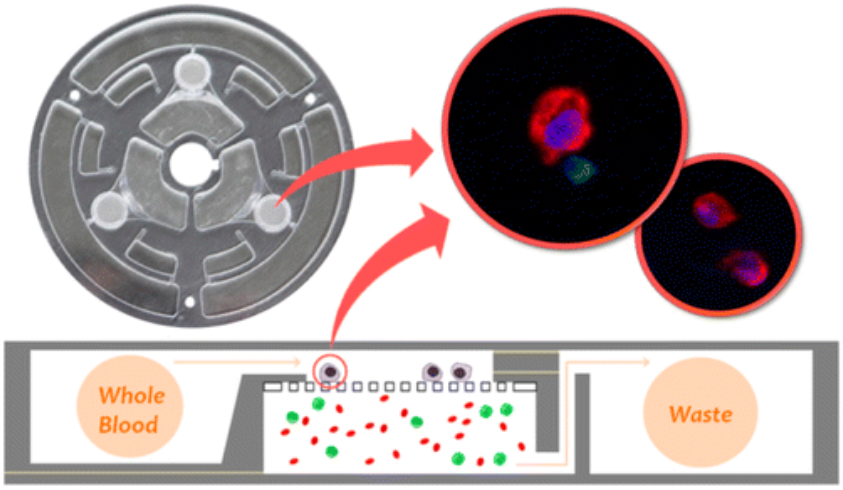

Figure 12. The working principle of size-selective circulating tumor cells isolation disc with embedded track-etched PC membranes (pore size of 8 μm). ©American Chemical Society 2014.

Numerous researchers have explored geometry-based methods for isolating cells and particles on centrifugal microfluidic systems. Nwankire et al. developed a size obstacle array for tumor cell isolation in whole blood.[69] Particles are captured in claw-like structures after displacement for further processing. The displacement approach was first reported to sort seven bead populations with different diameters from the same mixture. Other than geometric restrictions, filter membranes have been successfully applied on centrifugal microfluidic devices to extract bacteria from water samples or specific particulates from soil.[70] Both publications claim that almost all of the particulates analysed were filtered (Figure 12).[71] Martinez-Duarte and colleagues demonstrated specific filtering employing di-electrophoresis and the electrical polarizability of targeted substances. Carbon electrodes were built into the device and operated by electrodes with a slip-

ring on the rotor, allowing filtration of yeast cells from a slurry of yeast cells and latex particles.[72] Boettcher[73] demonstrated particle and cell separation within a spinning microfluidic di-electrophoresis chip. The chip was powered by two co-rotating batteries, with the alternating currents supplied by a co-rotating generator. Sediment cells and particles could be driven to a designated branch of a Y-shaped channel using the mentioned di-electrophoretic setup.[73]

LaCroix-Fralish[67] demonstrated a unit procedure for sedimentation of solid particles in colloidal samples and subsequential transportation of liquid supernatant. The connection between two microfluidic chambers was manufactured by fine fused silica capillaries. By inserting one end of the capillary in the upstream chamber, the liquid above the condensed fraction of solid particles was decanted. Saw-toothed obstacles designed in the inlet chamber were used to retain sediment particles from seawater samples in another study.[74] A wax valve will open after sedimentation to transfer the clear seawater into the aliquoting chamber. Blood-plasma separation based on the sedimentation of the denser cellular blood material has used similar principles. The implemented unit operations for plasma transfer after sedimentation were pneumatic valving, pneumatic siphon valving, capillary siphon valving, decanting,[75] or integrating a Y-channel enabled denser cells to reach the radially outward branch of the Y-channel when plasma was delivered into the subsequential chambers.[76]

Chemical separation in centrifugal microfluidics is based on the affinity of a target molecule with a matchable mobile or non-mobile substrate. The target molecule and specific assay reagents must be brought into contact with the mobile or non-mobile substrate sequentially. To enable the sequential transport of the sample and reagents, non-mobile supports must be integrated into the workflow of microfluidic on-disc transfer, valves, and switches, while mobile supports can

dynamically be transferred to the location of the sample. Non-mobile disc-integrated silica membranes,[77] glass bead columns,[78] and silica sol–gel[57] have been reported. Taking advantage of the hybridization between nucleic acids to complementary strands modified on the disc surface is another separation strategy.[79, 80] The binding of antibodies to antigens is the affinity mechanism utilized in immunoassays and immunoseparation. Antibodies (or under limited occasions, antigens) are caught by stationary substrates such as embedded antibody-coated beads (made by polystyrene, glass, or silica),[81-83] PMMA discs,[13] and nitrocellulose membranes,[84] which are then isolated from other components of liquid reagents. One of the reported implementations of mobile support is a simple approach for separating nucleic acids by using magnetic silica beads as the mobile support.[85] The beads could be transported through reagent-filled microfluidic chambers relying on the location of the centrifugal microfluidic cartridge with reference to an external magnet. For pathogen capturing and immuno-magnetic isolation from a whole blood sample, Cho[51] employed antibody-coated magnetic beads. A cartridge-integrated magnet and an external magnet established on a linear gear were used to control the beads. This setting allowed the mixing of the beads or their temporary stop in a dedicated location while the surrounding media were transferred. Chen and colleagues showed another method for immuno-magnetic separation, in which antibody-labelled magnetic beads were used to seize target cells. A co-rotating magnet captured the beads after target cells were bound, and the cell sample was decanted into a waste reservoir.[51]

1.1.3. Device fabrication and sealing

Materials currently used in microfluidic chips include polymethyl methacrylate (PMMA), polycarbonate (PC), polydimethylsiloxane (PDMS), and polystyrene (PS), polypropylene (PP), polyethylene (PE), polyethylene terephthalate (PET), etc.[86] The chemical structures of various

materials are different, and the physical and chemical properties of their surfaces and bodies are also different. At present, the centrifugal discs reported in the literature mostly use two materials, PMMA and PDMS. The processing technology of these two materials is relatively mature, but the investigation of other materials such as cyclic olefin copolymer (COC)[87] and 3D printing filament[88] is also in progress. As we adopt PMMA in the experimental section, introduction of the fabrication and application of PMMA are emphasized in the following paragraphs.

The main technologies available for PMMA substrate fabrication are molding and direct fabrication. Molding involves duplicating a microstructure by applying the substrate to a mold with the corresponding microchip channel.[89] There are three main kinds of molding approaches, including replica molding, injection molding, and hot embossing. Also, there are many types of materials for the mold and corresponding techniques for producing the mold. Overall, molding is a low-cost fabrication technology, because the repetitive use of the high cost mold amortizes the total cost in mass production. Unlike molding, a direct fabrication technology is to process the desired microstructure directly on the polymer without making a mold. This method can process individual micro devices quickly, but it takes much longer for mass production. Direct fabrication technology such as laminating and 3D printing has become more and more prominent due to its convenience and easy operation.

Laminating

Laminating means cutting a set of individual layers, which are bonded together to construct microfluidic channels and features.[90] Each layer can serve as a planar flow structure, and the thickness of the material determines the channel height. Material selection, cutting, and bonding

are the main steps in building a laminate device. Laminating techniques employ various materials, such as transparent plastics and thermoplastics.[91, 92] Adhesive tapes, polymers, and glass sheets are three of the most commonly used materials in laminate fabrication[93]. While the adhesive transfer tape may have reagents/particle absorption issues, it is still preferable due to the inherent bonding function (Figure 13). The advantages of polymers and glass layers are optical transparency, cost-effectiveness, and reagent compatibility. Although these three materials are listed as the most used materials, many other materials can be adopted in laminate production. Laminate is compatible with a broad range of materials, because of the ease of combining different types of bonding methods and materials.

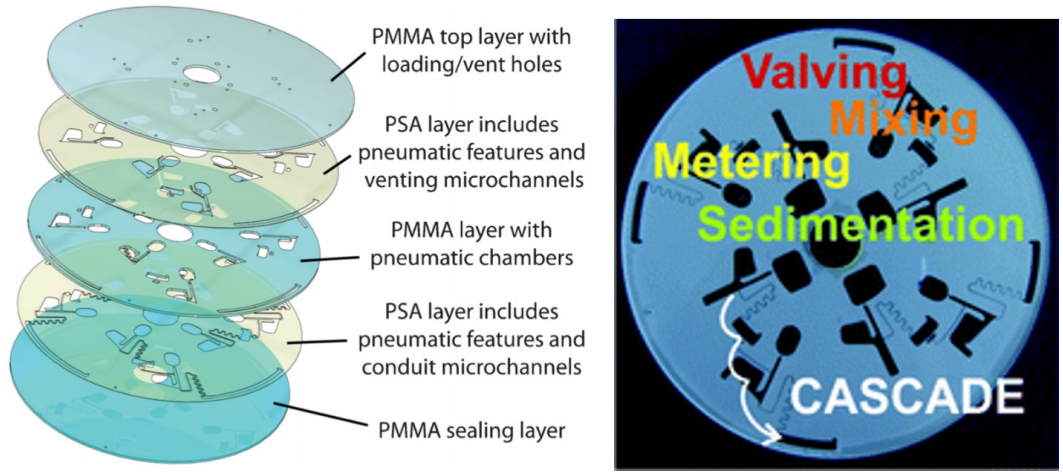

Figure 13. A laminating disc is composed of five layers: three PMMA layers and two PSA layers. © The Royal Society of Chemistry 2013.

As each layer of a laminate microfluidic system is cut separately, the technique of cutting has a direct impact on the dimensions and features of the unit. Cutting is mainly performed with a knife plotter or laser cutter for prototyping and research work, due to the speed and flexibility that each tool provides. The cutting plotter delivers patterns by cutting material with a blade when the laser cutter, usually CO_2 lasers, employs a focused beam. The fundamental process is the same in both methods: CAD (Computer-aided design), software designing, cut the structure by either method,

clean the entire assembly, and bond layers together to close channels. The choice between these two methods depends on the material's property and the required accuracy. Laser cutters are more compatible with different materials and layer thicknesses, though they are more expensive.[94] Walsh provide a thorough comparison of the advantages and disadvantages of each cutting approach under laboratory and prototyping scenarios.[95] Other than the cost, another drawback of laser cutting is caused by the vacuum pump, which is a necessary component for a laser cutting machine. Burn residues left by the vacuum pumping system may contaminate the channels, which affect the device's output. The setting of a cutting plotter is usually more straightforward than a laser cutter because it is more affordable and does not rely on the vacuum system. However, there are drawbacks of plotter cutting techniques such as low resolution, materials, and thickness restriction. After figuring out optimal parameters, it takes almost the same time for the knife plotter and laser cutter to finish cutting one piece. The two cutting approaches work similarly in many situations, therefore a choice can be made based on ease of access.[91]

Scalability is one of the primary advantages of the laminate technique over other fabrication methods, particularly after production volumes exceed one hundred thousand units. Each fabrication step can be automated and operated in a parallel way, so lamination is highly scalable. The cutting technique could prepare thousands of devices per minute in a modernized fabrication process because fabrication scales up to enable the application of other advanced microfluidic fabrication techniques. The concept of the Lab-on-a-Foil fabrication that uses and often combines thermoplastic and laminate based designs to produce low-cost, massive, and disposable devices was developed out of this fact.[96]

Molding

Modern micro-machining technologies such as sewing, cutting, grinding, honing, etc., can already process micro-mechanisms with a size of tens of microns. These technologies can transfer the designed channel microstructure graphics to the mold substrate under the digital control of the computer, which can process graphics with different depths, becoming an ideal method for processing three-dimensional microstructure male molds. Mecomber et al. reported that computer numerical control (CNC) machining aluminium molds are used to make chips[97]. The results show that CNC technology chips and chips made with the LIGA (German abbreviations of Lithograghie-lithography, Galvanoformung-Electroplating, and Abformung-Moulding) method have comparable electrophoretic separation capabilities. Limbach et al. reported an improved CNC technique for machining and fabricating aluminium molds to replicate plastic chips. This method uses several advanced techniques such as high-density carbon drilling to improve the CNC machining process and overcome the limitations of the usual CNC technique. This method can reproduce microchannels with an error of 4 μm, which is 10 times less than usual CNC processing.[98]

Hot embossing

The hot embossing process uses pressure and heat to precisely mold melted substrate at high temperatures (Figure 14). The hot embossing method utilizes thermoplastics or polymers and a mold to press them under the heat deformation temperature of the plastics.[99] Unlike melting thermoplastics or polymers before injection, the whole mold chamber is heated to casting the mold to the sandwiched material. Then the mold and the polymer substrate are cooled together below the glass state temperature under pressure, and the desired microstructure is obtained after demolding. The hot embossing method is suitable for thermoplastics such as PMMA, PC, PS, and

COC.[100] Hot embossing has tremendous commercial adoption in the microfluidic industry due to its cost-effectiveness, accuracy, and high throughput.[101] Drawbacks of this technology include a limitation of thermoplastics and the challenge of fabricating sophisticated three-dimensional structures.

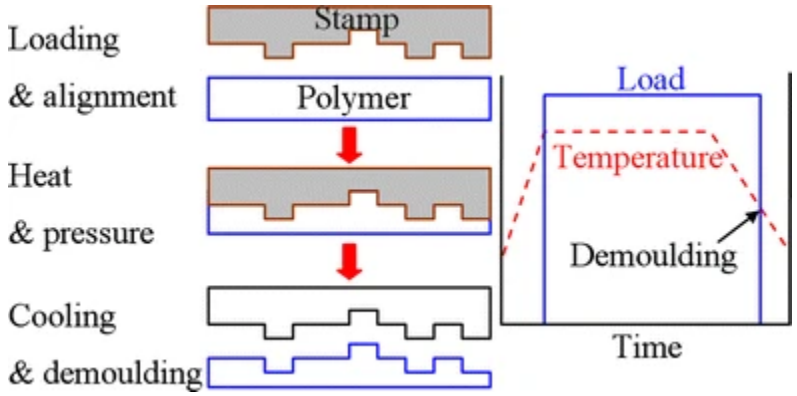

Figure 14. The process of hot embossing. © Springer-Verlag 2007.

Packaging

The microchannels and chambers are open after fabrication, so it is usually necessary to seal with a cover sheet. The bonding method and material should not block the channels or change the physical parameters or dimensions of the channels. Before sealing, holes are usually punched or fabricated in the corresponding position of the substrate or the cover sheet to allow the reagents, etc., to enter or exit the microchannel/microchamber. Adhesive bonding[102] and thermal bonding[103] are the most popular and simple bonding methods, with the choice of the proper bonding technique inherently dependant on the materials used.

Thermal bonding is usually realized by a heat press machine, which is sold as a commercial machine or custom assembled. To complete thermal bonding, the temperature is raised to a temperature above the glass transition temperature of one or both components, then pressure is

applied to facilitate thermal bonding. Thermal bonding is extremely suitable for sealing for PC[104] and polylactic acid (PLA),[105] but not all materials can be thermally bonded. Some simplified heat-pressing operations to seal the chips have been reported in the literature. Manynova et al. clamped the PMMA substrate and coverslip with two microscope coverslips and placed them in an oven at 108°C for 10 min, which could completely sealing the chip.[106]

The main drawback of thermal bonding is the tendency of feature distortion to occur during the system heats up or cools down. Efforts are made to reduce this side effect out of heating based on the physical properties of materials. Kelly reported an easy-to-operate method for sealing PMMA chips in boiling water.[107] The substrate and coverslip were paired together with an external microscope slide and aluminium sheet, clamped with two C-shape clamps, and immersed in boiling water for 1 h to make a sealed device. With this boiling method the temperature is constant and homogeneous, the reproducibility is good, and the temperature is just under the glass transition temperature of PMMA (105°C), so the polymer has sufficient rigidity to avoid collapse of the channels. Li[108] demonstrate a novel low-temperature ultrasonic bonding approach for PMMA microdevices. Strong bonding is achieved at only 60 °C, because of the ultrasonic energy spot effect, avoiding channel deformation.

There are different sorts of adhesive bonding: wet and dry. The surface is commonly glued with SU-8,[109] wax,[110] or UV (ultraviolet) curable epoxy [111] in wet adhesive bonding. This adhesive bonding approach significantly broadens the material selection range with the introduction of adhesive media which can hold most materials together. On the other hand, the thermoplastic surface could be activated by plasma or chemicals and become adhesive without introducing external glues. While this technique has been explored as a feasible solution for polymer bonding,

successfully cases are rarely reported due to the issue of channel blockage. Channel clogging can be avoided by using certain types of microchannels which require special designs.[102, 112] In addition, uneven adhesive distribution can lead to a weak bonding performance.

Dry adhesive tape bonding is the most simple, efficient, and low-cost technique for sealing microchannels, compared with other bonding methods.[113] Unlike introducing liquid glue or activate the plastic surface in wet bonding methods, tapes are employed for bonding microfluidic chips in dry adhesive bonding methods. The easy access to different adhesive tapes facilitates large-scale microfluidic device production. Furthermore, dry adhesive offers high strength for heterogeneous material bonding, including thermoplastic, glass, and metal surfaces[114, 115]. Reversible sealing and multifunction integration are also possible with dry adhesive. Based on these properties, the adhesive tape bonding technique has been widely used in different microfluidic systems, such as electrochemical microfluidic platform, immunoassay device, and optical biosensors.[116, 117] Dry adhesive bonding offers excellent biocompatibility, if choosing the proper tape. As a result, dry adhesive bonding methods have already been successful applied in biomarker detection,[118] DNA (Deoxyribonucleic Acid) amplification[119] and cell culture microfluidic devices.[120]

1.1.4. Detection

As well as fluid control and separation, the detection of analytes is also a significant operation for to complete on-chip analysis. Optical detection, electrochemical-based techniques, and mass spectrometric methods are the most common on-chip detection schemes.[121] Centrifugal microfluidics is already a mature technology for resolving a series of challenges such as liquid

metering, valving, mixing, and separation, allowing for the easy integration of a variety of assay protocols.[122] However, detecting and reading results on centrifugal platforms faces some additional challenges, as the microfluidic disc spins when the assays are conducted.

Optical detection

Optical detection methods play an important role in microfluidics research due to their specificity, high sensitivity, and well established assay schemes. Although techniques like electrochemical-based detection systems have some advantages over traditional optical detection in terms of portability, cost, and ease of alignment, smaller optical components embedded on-chip can conquer these shortcomings.[123]

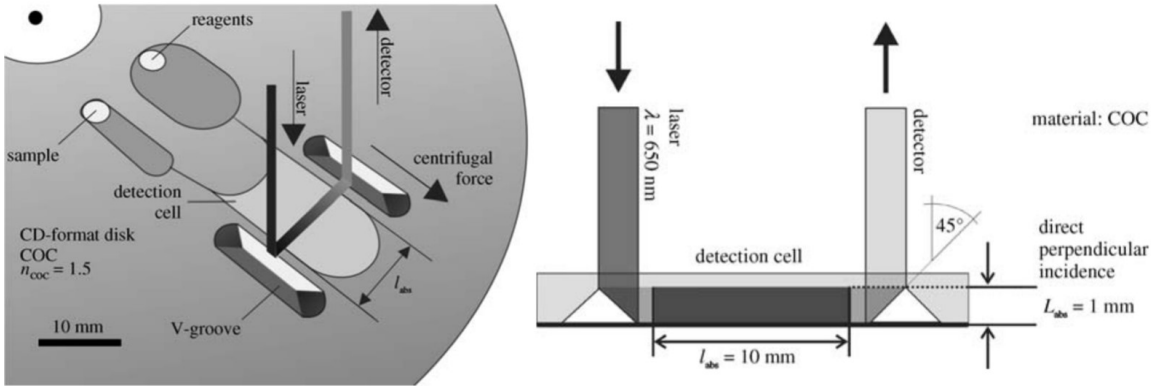

Figure 15. The diagram illustrats that the optical path length is ten times enhanced by TIR. © Springer Science Business Media, LLC. 2006.

The detection of absorption shift caused by the presence of an analyte is one of the simplest methods on a lab-on-a-disc device. Both academic and commercial implementations have used absorbance-based methods in centrifugal microfluidic systems. However, the optical path, which is a variable in the Beer-Lambert law, is relatively short in a typical absorption detection setting in a centrifugal microfluidic system, because the light source and detector are usually perpendicular to the disc surface. Grumann presented a device using total internal reflection (TIR) (Figure 15) to

increase the length of the optical path, by deflecting the perpendicular light beam by 90 degrees, making it parallel to the disc.[124] The deflection is realized by simple grooves on the disc polymer, which enables easy disc integration. This method has been used in a series of assays, including testing haemoglobin,[125] glucose, and alcohol in blood samples.[41]

Fluorescence-based assays have become prevalent in clinical laboratories because of their high sensitivity.[126] Meanwhile, the drawbacks are the high-cost and sophistication of fluorescence excitation and readout equipment. The fast development of fluorescence-based POC (point-of-care) devices benefits from the declination of the cost and size of fluorescence components over the years. Another benefit comes out of the prevalence of commercially available assay reagents since they have been used in clinical settings for many years. A main concern is that the disc needs to be stopped for readout or even moved to another system with most fluorescence-based centrifugal microfluidic assays. Hillig established a detection system for CytoTrack rare cell assessment which is substantially a fluorescence microscope coupling with a disc-shaped sample carrier[127], illustrating the possibility to accomplish fluorescent detection in the rotating condition. Kubo et al. demonstrated a microbead-based chemiluminescent ELISA for the detection of bisphenol A (BPA) on a centrifugal platform. The on-disc detection range was from 3.9 ng/ml to 250 ng/ml, and successful analysis of BPA-spiked rat serum was demonstrated.[128]

Imaging based detection

In microfluidics, optical imaging protocols are critical for monitoring and analysing biological or chemical samples. Imaging in microfluidics has traditionally been conducted by bench-top microscopes or large footprint, expensive imaging devices. Considering the spinning state of the

disc, considerable effort has been put into combining optical imaging techniques with centrifugal microfluidic platforms. Placing the imaging detector on a linear stage enables imaging of the entire disc region. This kind of centrifugal "test stand" was designed primarily for disc development in advanced labs where the relatively large size and high cost are applicable.[129] Given the cost decrease and improvement of optoelectronic components in recent years, test stands with cheaper components have shown sufficient quality to meet the requirements of the majority of labs. The selection of either bulky imaging systems or compact imaging systems depends on resolution requirements, sample properties, and budget.

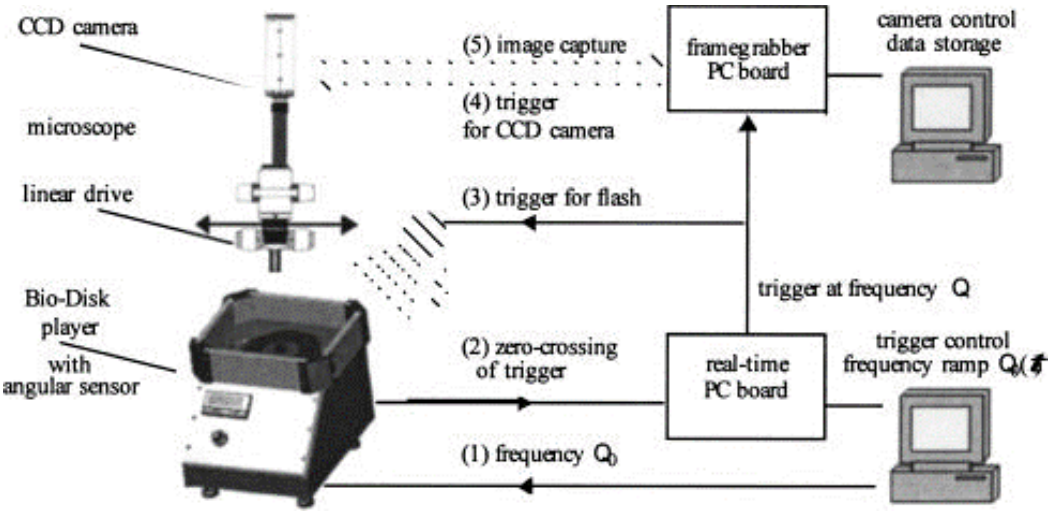

Figure 16. The experimental configuration of the spin-stand with a CCD camera and a stroboscopic flash for real-time on-disc process monitoring. © AIP Publishing 2005.

The first advanced microscopic imaging system for spinning discs is developed by Grumann. This setup includes a motor for driving the disc, a camera attached to a microscope with a minimum exposure time, as well as a strobe light (Figure 16).[130] The acquisition of images is synchronized to the motor rotation, allowing the real-time observation of a certain region on the disc. Using a similar technique, Riegger performed bead-based fluorescence immunoassays for testing hepatitis

A and tetanus [126] Individual fluorescently stained particles or cells were trapped in trapping slots and imaged by the same setup mentioned above. Furthermore, the emerging imaging system for spinning discs enables complex on-disc procedures such as nucleic acid amplification and sample preparation. Kim proposed a centrifugal microfluidic device that integrated DNA amplification and identification steps for detecting pathogens.[131] The color change of the embedded paper strip immunoassay in the presence of bacterial DNA was collected by the integrated CCD (charge-coupled device) camera.

Electrical-based techniques

Electrochemical detection is used in many primary biosensors, such as the most well-known example of an electrochemical glucose monitor.[132, 133] There are different ways to realize the integration between miniaturized electrochemical sensors and centrifugal platforms. Commonly, electrodes are easy to integrate, but the disc needs to stop spinning for electrical testing after the sample processing. These approaches are not ideal, because the capacity to execute electrochemical detecting during spinning is critical for real-time analysing and simultaneous adjusting of measuring parameters. Overall, integration of electrodes on a centrifugal microfluidic platform still provides additional possibilities for new sample manipulation, sample pre-treatment, and detection principles.

In the widely used amperometry detection methods, the constant potential is delivered by the working electrode, and a current-time curve is recorded to reflect the oxidation or reduction of electroactive species. Li demonstrated a whole blood analysis platform for multi-analyte detection, including glucose, uric acid, and lactate.[134] The nanoporous structure of the gold electrode and

multi-wall carbon nanotubes attached to the electrode significantly enhanced the overall surface area, where the catalyst and enzymes were immobilized. This method only requires 16 μL of blood sample and yields comparable results with conventional approaches. An on-disc cyclic voltammetry measurement system was presented by Andreasen,[135] using a low noise electrical slip-ring. The authors realized real-time monitoring of a complete electrochemical experiment during disc rotation. The mechanism of impedance measurements is that the binding of target molecules/cells on the electrode surface decreases the electrode capacitance, which is reflected by the increase of measured electrochemical impedance. Nwankire et al. reported on-disc impedance-based tests for identifying cancer cells in a blood sample.[136] To realize the specific capture of target cancer cells, the electrode was modified by anti-EpCAM antibodies, as EpCAM is a protein existing on the cancer cell membrane. The detection limit is equal to about 2% coverage of the electrode surface, while five parallel assays could be conducted simultaneously.

Mass Spectrometry (MS) Detection

Many efforts have been put into the coupling of microfluidics with mass spectrometry because the MS's ability to classify trace analytes significantly complements microfluidics' capacity to process and separate small volume samples.[137] The flow rate on microfluidic platforms is similar to electrospray ionization (ESI)-MS, which is the basis of numerous studies developing suitable on-chip tips for electrospray. When it comes to centrifugal microfluidics it is hard to realize online coupling with ESI-MS for liquid samples. However, in the coupling with matrix-assisted laser desorption/ionization (MALDI)-MS analysis, the planar centrifugal microfluidic disc can directly serve as a MALDI plate. Also, on-disc crystallization avoids the procedures of sample transfer and deposition onto another substrate before MALDI-MS measurements.[138]

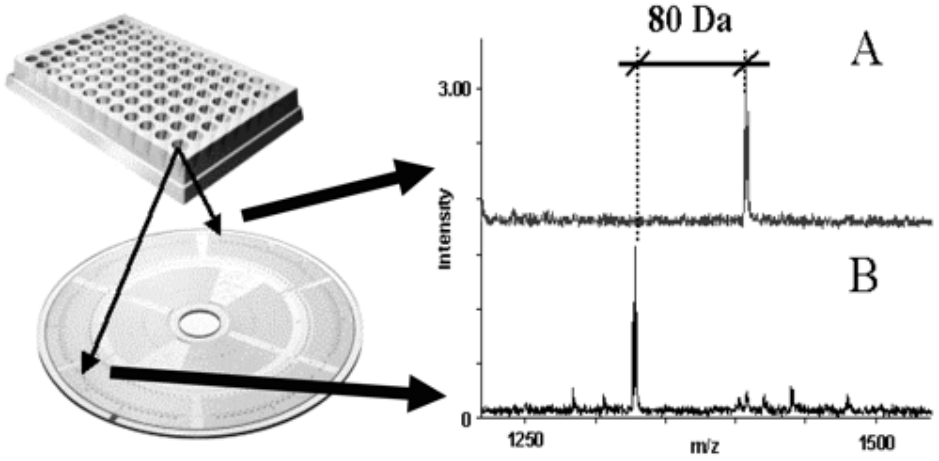

Figure 17. MALDI mass spectra are illustrating the phosphopeptide detection approach employing on-disc immobilized metal affinity chromatography and enzymatic dephosphorylation. There are 96 on-disc microcolumns, half of which were utilized for phosphopeptide enrichment and alkaline phosphatase dephosphorylation. Two aliquots of each sample from the 96-well microtiter plate were transferred into corresponding two types of the on-disc column by robotics. © American Chemical Society 1999.

Gustafsson et al. successfully conducted both on-disc proteolysis as well as on-disc MALDI-MS detection realized via crystallization.[5] This 96-unit chip system completes the mass spectrometry characterization and identification of peptides with a detection sensitivity of 200 Åmol and a detection limit of 50 Åmol. This integrated technology obtained a much higher success rate in phosphopeptide analysis than the MALDI and C_{18}ZipTips methods. In the same year, Hirschberg introduced a centrifugal chip system-mass spectrometry method for the selective detection and analysis of phosphoric acid based on the above research.[139] The research combines IMAC (immobilized metal affinity chromatography) and enzyme dephosphorization technology to perform online MALDI in a 96-unit CD chip system (Figure 17). The dephosphorization effect of peptides is enriched by IMAC, and selective detection of phosphorus peptides can be conducted in different mass spectrum regions. The detection limit reaches a fmol level,with the detection success rate of phosphorylated peptides exceeding 90%.

Thanks to extensive research of on-disc fluidic control, including metering, valving, mixing, and separation et al., lab-on-a-disc systems are already a well-known technology for automation and miniaturization, and easy operation. However, on-disc readout is more challenging than in other microfluidic devices due to the actuation principle of centrifugal platforms. The development of sensor integrations into centrifugal microfluidics is still ongoing. Integration of individual sensors is already widely investigated, and integration of multiple sensors enables multi-function analysis.[122] The selection of a sensor is determined by requirements of on-disc detection and commercial concerns.

1.2. **Mass spectrometry**

1.2.1. Overview

Over the last 30 years, mass spectrometry has developed dramatically through its wide range of applications in life and health sciences.[140, 141] Mass spectrometric results reveal crucial information on analytes, such as structure, sample composition, and quality (purity) .[142] The fundamental principle of mass spectrometry is the separation of charged gas-phase ions in an electrical (or magnetic) field according to each ion's mass-to-charge ratio (m/z). The x-axis in an MS spectrum indicates m/z values, while the y-axis represents total ion counts. In other words, "mass-to-charge spectrometers" is a more accurate description of mass spectrometers.

The first mass spectrometer was built in 1919 by Francis William Aston to identify isotopes.[143] Its target analytes expanded from small inorganic molecules to bio-macromolecules with literally no mass limitations. The innovations in soft ionization methods, including matrix-assisted laser

desorption ionization (MALDI)[144] and electrospray ionization (ESI),[145] allow the charging of biomolecules for mass spectrometric analysis of proteins and other biomolecules. The interface between ESI-MS and upstream separation methods such as gas chromatography (GC) and liquid chromatography (LC) have had a profound impact on life and health studies. Meanwhile, MALDI tends to transform peptides and proteins to single charged ions, which significantly eliminates spectral complexity.

Both quadrupole(Q) and time-of-flight (ToF) mass spectrometers are commonly used, and they can be configured together to form a QToF tandem mass spectrometer.[146] As the name implies, tandem mass spectrometry (MS/MS) is the sequential separation of ions twice or more, usually realized by coupling two or more mass analyzers together.[147] There are four main analyzers widely used by mass spectrometers, including quadrupole, quadrupole ion trap (QIT), time-of-flight, and Fourier transform ion cyclotron resonance (FT-ICR). These analyzers differ in size, price, resolution, mass range, and the ability to perform tandem mass spectrometry experiments (MS/MS).[148] While the QIT is capable of performing multiple mass spectrometry experiments, the FT-ICR is very powerful in terms of accurate mass measurements.

1.2.2. Matrix-assisted laser desorption/ionization (MALDI) mass spectrometry

MALDI is a soft ionization technique for the analysis of large non-volatile molecules. The MALDI process irradiates a dried mixture of specific analytes dissolved in a suitable matrix compound by a pulsed laser beam, producing pseudomolecular ions of the analyte. Typically, a short pulse laser beam with 1 to 100 nanoseconds pulse length is used for ionization, and the nitrogen laser is the most common one.[149] MALDI is a primary ionization source currently used for proteomic studies

and protein sequencing, usually combined with ESI techniques. For example, Banoub's group has successfully characterized a fish biomarker, Vitellogenin, using both MALDI ToF MS and ESI Q-ToF MS/MS.[150] Furthermore, MALDI can also be used to study DNA,[151] lipids,[152] conjugates,[153] and polymers.[154]

A typical MALDI experiment consists of the following steps. First, the sample is dissolved in a proper solvent and mixed with an excess of a suitable matrix. Depending on the nature of the sample to be analysed, several sample preparation techniques have been developed. The commonly used techniques are the dried droplet,[144] the fast solvent evaporation,[155] the two-layer sample preparation,[156] and the solid/solid compression for insoluble samples.[157] The dried droplet method is most widely adopted due to its simplicity. Subsequently, in the dried droplet method, the mixture is spotted on MALDI plates and air-dried. Then the sample co-crystallizes with the matrix on the plate, but this procedure tends to produce inhomogeneous matrix crystals which leads to poor spectral reproducibility.[158] In the next step, the laser beam hits the sample-matrix crystal, resulting in absorption of laser energy and subsequent desorption and ionization. After the desorption/ionization, the produced gas-phase ions are introduced into the mass analyzer and separated according to their mass-to-charge (m/z) ratio. Time-of-flight mass analyzers are usually coupled with MALDI for advantages such as cost-effectiveness, simplicity of design and use, high ion transmission, unrestricted mass range, high-throughput, fast analysis, and compatibility with pulsed ionization methods.[159]

1.2.3. MALDI MS analysis of small molecules

Due to the coupling of the MALDI source to the time-of-flight analyzer, an unlimited range of masses can be theoretically inspected. In practice, single charged molecular ions with a molecule weight of 1.5 million Da have been observed. Despite the advantages of tolerance to contamination and high absolute sensitivity, MALDI has not gained broad application in the characterization of small molecules. Some drawbacks are attributed to the inefficiency of the first generation TOF MALDI which results in low resolution, matrix interference, and detector saturation when performed within low mass range. Also, in contrast to ESI, it is hard to couple MALDI with an online separation technique like liquid chromatography. Therefore, MALDI has been regarded as an ineffective or even useless tool for analysing low molecular weight compounds. However, with the development of TOF systems, especially significant improvements in MALDI-TOF resolution,[160, 161] MALDI has retrieved its application in studies of small molecules.

The selection of substrate is crucial to the successful implementation of MALDI MS. In MALDI, the matrix performs several functions. It absorbs the laser energy, isolates sample molecules, and provides photoexcitation sites for sample ionization during ion/molecular collisions.[162] Although the details of energy transfer, sample desorption, and sample ionization are still under investigation,[163] the general principle is that the energy from the laser beam is absorbed by the matrix and quickly expanded into the gas phase with the incorporated analyte molecules. Proton transfer between excited matrix molecules and analyte molecules in the solid phase and the expanding vapor causes ionization. Then ions are introduced into a mass analyzer, which tests m/z with ion abundance. Based on this mechanism, characteristics such as analyte in-corporation, the

capability of energy absorption, analyte ionization efficiency, and less analyte fragmentation should be taken into consideration when evaluating matrices.

As most "first generation" MALDI matrices are small molecules with molecular weights below 300 Da, it is obvious that they are unsuitable for MALDI analysis of LMW (low molecule weight) analytes. Therefore, strategies such as matrix additives, sample pre-treatments, sample derivatization, and novel deposition methods were developed to reduce interference from the matrix[164]. Employing high molecular weight (HMW) matrices instead is an alternative way to avoid the matrix issue in the low m/z range. Chen et al. realize the detection of femtomole level small molecules including vitamins, amino acids, and peptides when DHPT(3,4,5-tetrakis(3',4'-dihydroxylphenyl) thiophene) serves as matrix.[165] Derivatization of the classic CHCA also could shift its spectra to a high m/z range to reduce background in the low m/z range. Porta et al. realized 30% signal-to-noise ratio (S/N) improvement by derivatizing CHCA.[166] New MALDI MS deposition methods of using conventional matrices for LMW analysis detection have been developed. Shuai et al presented an electric field-assisted spraying system that generates tiny crystals of matrices to enhance the detection sensitivity of monophosphate, nucleosides, and fatty acids in cancerous tissues.[167]

The second generation of organic matrices emerged with different classes/functions such as negative ion mode matrices, reactive matrices, and nanomaterial-based matrices et al. Designed matrices with molecular recognition function have been proposed, and they are expected to bring new opportunities for targeted MALDI MS analysing. In the negative ion mode, proton transfer is usually determined by the gas-phase basicities of the deprotonated matrix and the deprotonated analyte.[168] 9-Amino acridine is widely used in the analysis of LMWC (low molecule weight

compound) in bio-samples for metabolomic studies as well as natural resins and cultural artifacts. New matrices, such as 1,5-diaminonaphthalene,[169] 4-phenyl-cyanocinnamic acid amide,[170] and quercetin[171] are also have been designed for negative ion mode MALDI MS analysis of LMWC.

Nanomaterial-based laser desorption/ionization mass spectrometry exhibit impressive advantages in real sample analysis.[172] The introduction of nanostructure materials to the MALDI substrate stimulated the development of a variety of laser desorption/ionization (LDI) approaches such as surface-enhanced LDI-MS((SELDI-MS)) and surface assisted laser desorption/ionization (SALDI-MS). For the study of small molecules, nanoparticles overcome the limitations of typical organic matrices as nanoparticles provide a simple background without interfering peaks, prevent fragmentation of thermally labile molecules, and enable the ionization of samples with weak noncovalent interactions in most cases. There are two main kinds of nanomaterial, one group is silicon-based matrices including silicon nanopillars, silicon nanowires, and silicon nanopost arrays, while another group is metal-base matrices.[173]

The porous silicon surface was firstly adopted by Wei et al. in the matrix-free MALDI procedure. Chemical modification on the porous silicon surface is possible since the surface could be easily oxidized. It has been demonstrated that the silylation of oxidized porous silicon improves sensitivity, storage stability, and modification efficiency.[174] Additionally, these modified surfaces could extract analytes from a complex background selectively.[175] Picca presented a novel nanostructured surface by hybrid arrays of silicon nanowires (SiNWs) and Ag nanoparticles (AgNP) to form AgNP/SiNWs for efficient SALDI-MS analysis of low-molecular-weight unsaturated food compounds and vegetable oils.[176] The hybrid surface combined advantages of both silicon-based substrates (salts tolerance, limited fragmentation) and metal nanoparticles

(good thermal conductivity). Hashim successfully fabricated vertically aligned silicon nanopillars (SiNPs) via nanosphere lithography and chemical etching, which is used for SALDI-MS detection of small peptides and methadone. Parameters such as porosity, length, and diameter of SiNPs are tuned to achieve maximum analytical efficiency, and the ability of SiNP arrays to identify methadone in clinical samples is proven.[177]

1.2.4. Nanostructures by glancing angle deposition

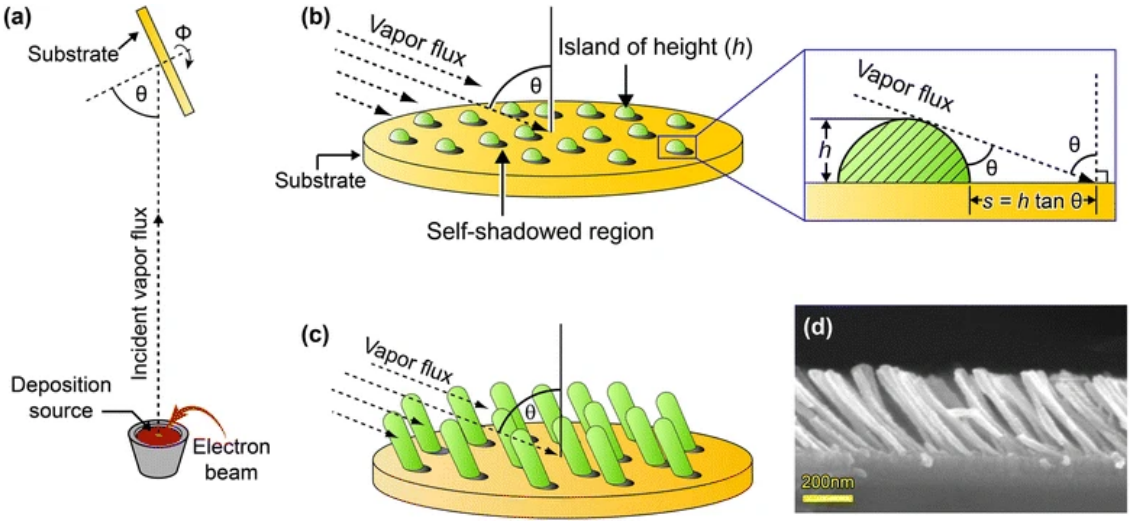

Figure 18. Schematic of glancing angle deposition. © Springer Nature 2015.

The Glancing angle deposition (GLAD) method is based on physical vapor deposition at oblique angles to engineer micro-and nanoscale columnar structure on thin films. The oblique incident angle means the incident vapor flux is not ninety degree vertical to the substrate but tilts at a certain angle, allowing films to bear anisotropy intrinsically. Early-stage studies deduced that anisotropic properties such as birefringence, dichroism, and anisotropic resistivity were caused by film morphology rather than film nonuniformity.[178] With the optimization of the GLAD process, techniques of rotating the substrate during deposition were invented which could further change

the film structure (Figure 18).[179] Substrate rotation alters the shadowing effect dynamics, allowing the continuous growing of columns along with different directions. Adjusting operation conditions such as the glancing angle and the rotation of the substrate will affect nucleation and crystal growth on the substrate, resulting in films of nanostructures with various morphologies. Different inorganic materials, such as silicon,[180] metals, and metal oxides,[181] have been successfully manufactured using the GLAD technique.

The porous silicon substrate has proved to be one of the most promising nanoporous surfaces in MALDI-MS small molecule detection, yielding results that are comparable or better than other MALDI methods. Compared to MALDI methods relying on chemical matrices, the utility of physical deposition thin film substrate avoids chemical contaminate interferences. Porous silicon was firstly used in MALDI MS for effective small molecule detection and identification by Wei.[182] However, it is hard to control pore sizes and pore density which have an effect on the detection sensitivity and detection limits by chemical etching. Fortunately, many parameters such as the deposition angle and the substrate rotation angle are tunable in the modern GLAD process, enables extensive engineering of the film properties such as porosity, thickness, and spatial structure. Furthermore, the movement of the substrate in the modern GLAD process is monitor by a computer, which makes the produced substrates have high reproducibility.

GLAD films have also been found to be useful in numbers of biosensing and chemical applications by other studies. A GLAD-fabricated ultra-thin Ag nano-rod array has been used as a promising transducer for LSPR (Localized surface plasmon resonance) biosensing.[183] Chu reported a portable fiber Surface-enhanced Raman spectroscopy (SERS) composed of Ag nanorod array fabricated by GLAD.[184] With optimization and investigation of the physical properties of GLAD films, GLAD

nanostructures are positioned at the forefront for both biosensing and engineering applications.[185, 186]

Our group has developed surface -assisted laser desorption/ionization (SALDI)-MS on silicon GLAD films of highly reproducible morphologies in collaboration with Michael Brett's group, who has focused on fabricating inorganic nanostructured materials with controllable properties.[187] Molecules with different weights, including metabolites, peptides, and drugs, were detected. Ya et al. furtherly modified the silicon GLAD films with (1H, 1H, 2H, 2H-perfluorooctyl) dimethylchlorosilane to create a silanol-rich surface.[188] This hydrophobic surface facilitated the segregation of crystallized salts during SALDI MS sample spot drying, thus significantly reducing the interference of electrolytes in biofluids. Several free amnio acids (MW<200 DA) were detected with low background noise in ultrafiltered serum samples on these perfluoro-coated nanoporous GLAD films. Recently, Yufeng et al. successfully used this modified silicon GLAD film for SALDI MS detection of free amino acids in the microfluidic processed serum sample. The results are in good agreement with hydrophilic interaction liquid chromatography (HILIC)-MS results.[189]

1.2.5. HILIC-MS

HILIC is based on a polar stationary phase and a low water/high organic mobile phase, which serves as a vital complement to reversed-phase liquid chromatography (RPLC) for the retention of polar analytes.[190] RPLC is widely used for most small drug molecules that are separated by the degree of hydrophobic interaction with the stationary phase. In contrast, the retention and separation in HILIC rely on the strong interaction of polar compounds with a hydrophilic stationary phase. With the introduction of HILIC columns, new applications, e.g., AA analysis,

became much more accessible. Semi-quantitative analysis of AAs was performed in fruits, rat brain, and animal tissue hydrolysates.[191-193] Hubertus developed a rapid, sensitive, and specific method for analysing and quantifying AAs in human plasma using HILIC tandem MS without derivatization.[194] The ISO medical laboratory accreditation standard validates the method to diagnose patients with inborn errors of amino acid metabolism. Also, the results are comparable with conventional ion-exchange chromatography.

HILIC solid phases are usually prepared by chemically modifying silica gel with functional groups such as a diol, amino, and amide. Chemically bound diol phases have hydrogen bonding, high polarity properties, and exclusive ionizable groups of silanols, making them ideal for HILIC mode.[195] Yajing[196] prepared silica-based amino stationary through click chemistry to separate polar analytes such as nucleosides and organic acids, which showed strong hydrophilic interaction liquid chromatography (HILIC) properties. Despite considerable research of novel HILIC separation materials, unmodified bare silica gel still holds some advantages for HILIC. In contrast to chemically bonded stationary phases, unmodified bare silica gel does not gradually lose efficiency. There are three types of bare silica gel sorting by their surface properties, which are silica type A, type B, and type C. Type A silica gels are acidic because surface silanol groups are activated by metals during precipitation. Silica gels type B provides better separations, particularly for basic samples, as it contains small amounts of metals and is stable at a higher pH environment. The surface of silica gel type C is covered by nonpolar Si-H groups instead of silanol groups, making it less polar and suitable to be used in a more organic solvent.

HILIC could be easily coupled online with electrospray mass spectrometry (ESI-MS) because HILIC usually employs high water content mobile phase to facilitate hydrophilic interactions

between the stationary phase and the analyte.[197] Typical mobile phase for HILIC gradient elution is composed of 50%–95% percent water-miscible organic solvents and water/volatile buffer. Acetonitrile can retain polar analytes very well and only elutes as a narrow peak in the chromatograph because of its low viscosity. Therefore, acetonitrile has become the most widely used organic solvent in HILIC. The elution pH (range from 3 to 8) is controlled by ammonium salts buffer, which has good solubility in organic solvents.

In the last decades, numerous HILIC-MS methods have been developed for research on metabolic, proteomic, pharmaceutical, food, and environmental analyses.[15, 16, 198] Antonio et al. developed a HILIC–ESI-QIT(quadrupole ion trap)-MS system to analyse carbohydrate metabolites in Arabidopsis thaliana leaf.[199] Which is capable of separating and identify glucose, sucrose, raffinose, and glucose phosphate in chloroform/methanol leaf extracts. Koichi reported a HILIC-MS/MS method for quantifying nucleotides in infant formula avoiding complicated extraction procedures and separation techniques in LC/ESI-MS/MS.[200] Five protonated nucleotides were identified with LOD (limit of detection) of 5−10 μg/mL and LOQ (limit of quantification) of 10−30 μg/mL in multiple reaction monitoring (MRM) mode. Tetsuya studied 13 nonsteroidal anti-inflammatory drugs in 20 μL plasma samples by HILIC-MS/MS with short analysis time and low LOQs.[201] Also, this method shows the potential to be applied in clinical and toxicological analysis. To gain maximum analytical results, efforts still need to be put into improving matrix effect, and mass spectrometric interference of HILIC-MS/MS methods in the future.[190]

1.3. Poly(N-isopropylacrylamide) Microgel Based Etalon

1.3.1. Poly(N-isopropylacrylamide) Based Microgel

Smart materials can be defined as substances that react physically and/or chemically to impulses from the external environment such as temperature, pH, light, and specific molecules/biomolecules, resulting in specific changes in material properties. It is then necessary to carry out specific operations. This character provides the foundation of further sensing and actuating possibilities. In another word, it means that each material responds in different ways to stimuli from the environment. However, the substance's volume change due to the thermal expansion effect under increased ambient temperature or heating is not regarded as an "Intelligent" response. So it is more reasonable to define "smart materials" as materials that react to changes in their environment in a specific and functional way, and this reaction can be duplicable.[202]

For now, polymers are already employed in the production of various types of smart materials. Polymers can be adapted for a wide range of applications due to their chemical and physical diversity. In the last two decades, great interest has been shown in polymeric materials that can reversibly or irreversibly change their physical and chemical properties under the impact of external stimuli. Stimuli can be divided into two categories: physical stimuli and chemical stimuli. Examples of physical stimuli are temperature, ionic strength, light, solvents, magnetic fields, electric fields, and mechanical stress. Common examples of chemical stimuli are pH, the presence of certain analytes, and biomedical reagents. Smart polymers are very flexible in performance states such as solutions, gels, nanoparticles, films, or solids. Researchers have been attempting to apply previously discovered properties of such materials to more complex issues such as drug and

gene delivery, catalysis, detection and imaging, adaptive coatings, and self-healing materials. Unlike their low molecular weight analogues, polymer-based intelligent materials have a range of advantages in terms of structural stability, aqueous solution dispersion, biocompatibility, processing ease, and subsequent integration with detection devices.[203]

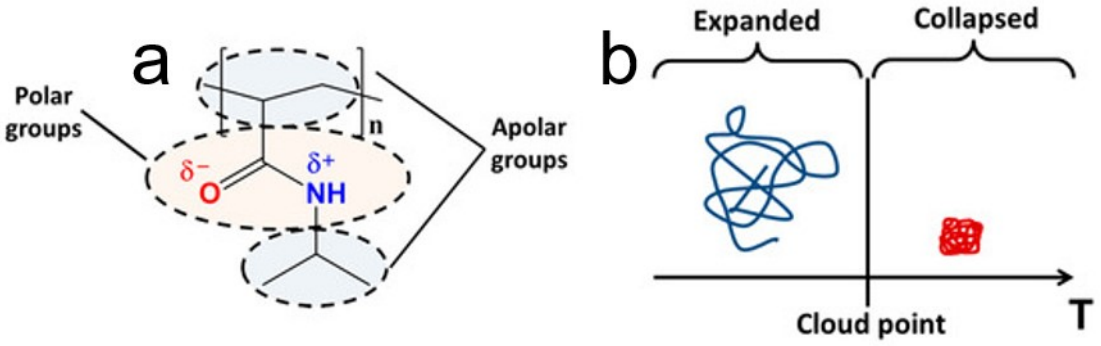

Figure 19. (a) Poly(N-isopropyl acrylamide) structure, with n indicating the number of repeating monomers. (b) Schematic showing the coil to globular conformational change. © MDPI 2017.

Poly (N-isopropyl acrylamide) (Figure 19a) is possibly the most well-known and thoroughly researched example of a stimuli-responsive polymer. The polymer is well known for its coil to globular conformational change (Figure 19b) at approximately 32 °C in water, making it of great interest to the investigation into possible biological applications.[204] In effect, linear poly (N-isopropyl acrylamide) (pNIPAm) will be soluble in water under 32 °C in a random coil conformation. When the solution is heated above this temperature, the pNIPAm will collapse into a globular conformation and no longer be soluble in water, causing the solution to become cloudy as the polymer precipitates from the solution. The structure of pNIPAm can be seen in Figure 19, pNIPAm has a hydrophilic amide group and a hydrophobic isopropyl group giving it this LCST (lower critical solution temperatures) which is in an ideal range for work with biomedical applications.[205] When synthesized with a crosslinker such as N, N'-methylenebisacrylamide (BIS) pNIPAm can form a colloidally stable microgel with the same temperature-responsive

characteristics as the linear polymer.[206] These microgels will now expel the water of salvation at the volume phase transition temperature (VPTT) at 32 °C. Of interest also is the ease with which the polymer can be functionalized with various groups. The pNIPAm can be synthesized with co-monomers such as acrylic acid (AAc) to give additional functionality by making the polymer not only temperature-responsive but also pH responsive.[207] The AAc also provides a site to be further functionalized and provide additional responsivity to analytes and biomarkers.

Due to the possibility to make pNIPAm responsive to a wide variety of stimuli, they have potential applications for sensing or possibly the mechanical force produced by the polymer response. Some of the potential uses of pNIPAm and pNIPAm based microgels are biosensing, controlled drug delivery, and biomaterials.[208, 209] For instance, by coating optical microfibers with pNIPAm, Huang et al. developed a sensitive, flexible adhesive temperature sensor.[210] The polymer chains were dehydrated and covered the microfiber surface when the temperature higher than pNIPAm's LCST. The surface refractive index of pNIPAm changed due to the interfacial phase transition induced by temperature, which furtherly changed the interferometric fringe of the transmission spectrum. This thermometry also was utilized to measure the temperature of rat breast carcinoma cells due to the micrometer-sized footprint. A recent investigation into the potential uses of pNIPAm is removing contaminants from water, which has seen work into the use of pNIPAm and pNIPAm copolymers to remove organic molecules and dyes from solution.[211] There has also been work done in using pNIPAm microgels in creating photonic materials such as basic interferometers that can respond to various stimuli.[212, 213]

1.3.2. Poly (N-isopropyl acrylamide) Microgel Based Etalons

A Fabry–Pérot interferometer, also known as an etalon, is a one-dimensional optical material that emits a certain wavelength of light determined by the resonance of light through a cavity between two reflective surfaces.[214] Recently these optical devices have been made using pNIPAm based microgels to actively tune the distance between these two reflective surfaces, dynamically changing the wavelength of light that is emitted. These tunable etalons have shown promise in a number of applications such as pH sensing, glucose sensing, and macromolecule sensing.[215]

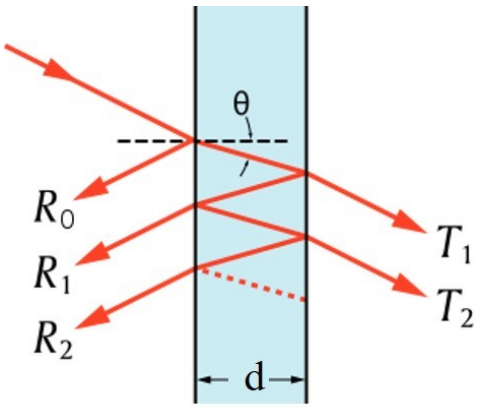

Figure 20. Light interacting with Fabry–Pérot interferometer © Wikimedia Commons

The Fabry–Pérot interferometer is in a sandwich structure with a layer of dielectric material between two semi-transparent, reflective surfaces. As light hits the device, both reflection and refraction are conducted with the reflective material; if the light is in phase, positive interference occurs; if the light is out of phase, destructive interference occurs, resulting in distinctive reflectance spectra of maximum and minimum wavelengths. Figure 20 depicts this behaviour, which is determined by the equation:

$$\lambda m = 2ndcos\theta \quad (6)$$

In this equation, λ represents the wavelength of reflected light, m is the peak order, n is the dielectric material's refractive index, d is the thickness of the dielectric material layer or the distance between the two reflective surfaces, and θ is the angle of the launched light beam.

The pNIPAm-based microgel has been used as a dielectric substrate for etalon fabrication, which shows reflected color when submerged in water and allows for dynamic adjustment of the distance between the two reflectors. Changing the temperature of the setting allows the color of reflected light to be adjusted when the system is immersed in water, as the maximum wavelength is determined by the thickness of the dielectric material or the distance between the two reflective surfaces. When increased temperature causes the collapse of pNIPAm microgels, the distance between the two reflective surfaces will decrease. According to equation 6, the wavelength is directly determined by distance when other parameters are the same. Distance decrease induces the peak wavelength of reflected light decreases, changing the device's reflected color.

In addition to this color tunability, there are lots of other potential applications for pNIPAm microgel-based etalons, including those that have previously been explored. In one publication, the microgels used to fabricate the etalon was co-polymerized with AAc and functionalized with aminophenylboronic acid (APBA) allowing the microgels to be glucose sensitive.[212] In this way, there was not only a spectral change in wavelength when glucose was added to the solution containing the device, but a visual color change was also observed. From this proof-of-concept work, the potential applications of the device in biosensing are apparent, with the possibility of visual color change indicating the results. Furthermore, there has been work done in testing the pH and temperature response of spatially isolated regions of an etalon.[216] This indicates that an etalon device can be fabricated with multiple test areas on a single device, which enables sensing for

multiple small molecules simultaneously. In addition to biosensing, the device has recently shown promise in detecting polyelectrolytes by size and charge.[217] The charge selectivity arises from the presence of pH-responsive co-monomers in the microgel and being at a pH that gives an overall charge to the microgels allowing the opposite charge to be detected. The size exclusion arises from pores in the Au layer can be controlled by changing the thickness of the top Au layer.

1.4. **Scope of the thesis**

This chapter covers the general context of the thesis's subjects, such as centrifugal microfluidic fluid control and device fabrication, SALDI-MS and HILIC-MS, and etalon sensor. Figures are cited with permission to illustrate these technologies and concepts. The details of how centrifugal microfluidic combined with different detection methods for biochemical applications will be discussed in the following chapters.

Chapter 2 introduces a centrifugal microfluidic protocol for clean-up of the human serum sample. Bench-top sample processing procedures, including proteins and lipids removal, are realized by the inexpensive PCL disc. While some operations still require stopping the disc spinning, the introduction of MeOH, C18 particles, and silica particles is proven to clean up the serum sample successfully, placing the clean-up steps on the chip. Subsequent recovery of the clean sample by pipet and transfer to a SALDI-MS plate for analysis demonstrates the viability of the chip-in-a-lab approach. The resulting mass spectra of disc-prepared samples shows a clean background and high signal to noise ratio for amino acids peaks.

In Chapter 3, we develop an automated blood sample processing disc for small molecule analysis. Large particles or molecules such as blood cells, proteins, and lipids are removed by respectively separation precipitation and solid-phase extraction. A combination of on disc operations including valving, decanting, metering, and mixing allow one-stop real-sample-in/clean-sample-out blood handling. The processed sample is employed for both SALDI-MS and HILIC-MS amino acid analysis to verify the on-disc processing efficiency.

Chapter 4 introduces a compact automized centrifugal device for P4 detection. The embedding anti-P4 DNA aptamer modified etalon in charge of on-disc detection. The anti-P4 DNA aptamer we employed has been proved to exhibit high selectivity for the target molecule, even in milk samples containing multiple steroid hormones. In addition, our aim was device development. Therefore, we didn't present data for selectivity, based on the fact that the selectivity of the anti-P4 DNA aptamer has been extensively validated. All required sensing procedures, including sample incubation, buffer wash, and salt stimulating, are automized by sequential pneumatic valves and a siphon valve. The data collecting method of image color analysis furtherly simplified the equipment setting by eliminating reliance on complex optical equipment. The green color value of the etalon sensor images shows a linear proportional relationship with P4 concentrations. These studies go toward demonstrating the use of etalons for a variety of molecular targets within a centrifugal microfluidic environment.

In Chapter 5, we discussed the perspectives of these two discs. We plan to optimize the user experience of blood preparation disc and introduce built-in algorithmic quality control to make it a practical product. We realized that etalon quality control is still an issue as a batch-to-batch variation has been observed. Therefore, enhancing product stability by standardizing the

manufacturing process and improving fabrication techniques will be in priority. Based on improved quality control, real sample preparation steps for realizing steroid for detection will be introduced. The bio-sample preparation will be realized by combining these two discs in this thesis or embedding the etalon sensor to a new microfluidic platform- digital microfluidic.

Chapter 2. Sample preparation in print-cut-lamination centrifugal microfluidic discs for human serum analysis by surface assisted laser desorption/ionization mass spectrometry

2.1. Introduction

Metabolomic studies can facilitate biomarker discovery,[218-221] diagnosis of disease,[222-226] and toxic effect assessment of drugs, toxins and food additives.[227-231] Considerable interest is focused on small molecule metabolites (< 1500 Da) such as amino acids,[226, 232, 233] lipids[234-236] and fatty acids.[232, 237] Once useful health markers are known, batch processed, spot analyses are an attractive approach to routine assays. Analyzing blood derived samples, such as serum, is of primary interest for metabolite assays,[238] but high concentration of proteins, as well as other biomolecules, usually generate interferences in the following detection step, so sample preparation is required.

Here we introduce a centrifugal microfluidic device to prepare ~ 5 µL serum samples for small molecule analysis by surface assisted laser desorption/ionization mass spectrometry (SALDI-MS). We have previously introduced a perfluoro-coated, vapour deposited, nanoporous Si film for sample desalting and SALDI-MS.[188] Our centrifugal microfluidic disc, fabricated by a simple print, cut and laminate method (PCL),[239] enables sample preparation, removing proteins and lipids from serum. The sample is recovered from the disc following clean-up, then transferred to a SALDI-chip, which provides an additional clean-up by segregating the electrolyte background from the sample salts.[188]

Conventional sample preparation methods for human serum include organic solvent precipitation and ultrafiltration.[240-243] Organic solvent precipitation methods take time and require that multiple

steps be performed. Ultrafiltration[188, 244] is often conducted using commercial ultrafiltration centrifuge tubes, requiring a high-speed centrifuge and other standard laboratory steps, and is more challenging to use for low volume samples (< 25 μL). Lower volume preparation and measurement of blood derived samples allow for multiple tests from a single sample collection and would enable metabolite detection with capillary blood samples from finger-stick tests.

Microfluidic techniques for convenient small-volume biological sample preparation are often suggested, but rarely realized. One of the challenges is that sample placed within a chip occupies too low a volume to be recovered for off-chip analysis, but integrating all of the detection components makes for an expensive single-use, disposable device. Microfluidic chips have been utilized for online separation in untargeted metabolomic profiling,[245] where samples were first prepared by various off-chip extraction/separation steps. Digital microfluidics has been utilized for sample preparation coupled with mass spectrometry in proteomic[246-250] and metabolite[251, 252] studies. Digital microfluidics requires a sophisticated electronic control system for fluid manipulation, relatively high cost for device fabrication, and the range of sample processing steps that can be translated to that format has limitations. In contrast, centrifugal microfluidics features a simple control system and inexpensive device fabrication, can duplicate many laboratory steps, and may facilitate high-throughput sample processing.[7, 10] Proteomic applications of centrifugal microfluidics have been demonstrated for mass spectrometry,[5] although the sample cleanup challenges are different than for metabolites.[253] Sample preparation with centrifugal devices for the analysis of individual metabolites, such as glucose, alcohol, lactate, or uric acids has been shown, with electrochemical[134] or optical detection.[55, 124] However, sample preparation for mass spectrometry using centrifugal microfluidic devices for analysis of a broad range of small, ionic metabolites has not been reported.[253]

Here we have targeted free amino acids, which are critical in neurotransmission. Inoshita found substantial elevated blood glutamate levels in major depressive disorder patients.[254] Concentration changes in free amino acids in probable Alzheimer's disease[255] were determined by Fonteh in various biofluid samples. Citrate, whose level has been associated with cancer,[256] and taurine, which plays a crucial role in regulation of vasoactivity,[257] were also selected. We have compared the performance of the centrifugal sample preparation disc for sample cleanup for SALDI-MS with cleanup for LC-MS. The resulting mass spectrum of the prepared sample shows a relatively clean background and high signal to noise ratio for metabolite peaks in SALDI-MS, and provides good sample cleanup for LC-MS. Reproducibility and recovery of several identified metabolites obtained from disc-based serum preparation with SALDI-MS detection are evaluated. Quantitative analysis of metabolites is demonstrated.

2.2. **Experimental Section**

2.2.1. Design of the centrifugal disc

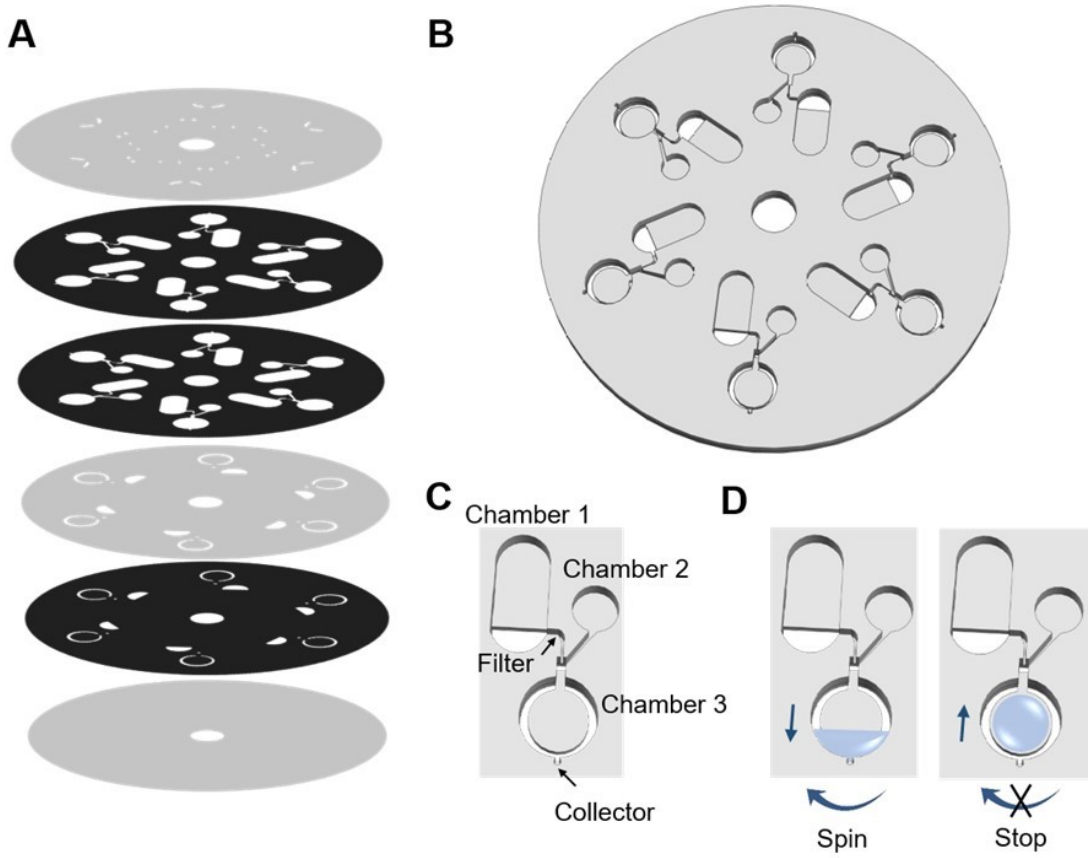

Figure 21. (A) Schematic representation of the centrifugal microfluidic device without assembly (six layers of polyester films). Transparencies with toners are shown in black and transparencies without toners are shown in light grey. Features in the top layer include vents and sample inlets/outlets. (B) Assembled device without showing the top layer. (C) Design of a single reactor. (D) Liquid movement in Chamber 3 under a spin-stop cycle.

The centrifugal microfluidic device for human serum sample clean-up consists of six layers of polyester film with 10 cm diameter and 100 µm thickness for each layer (Figure 21A). Layer 2, 3 and 5 (numbered from top to bottom) are printed with toner as bonding agent between layers. Features are cut by laser cutter and layers are aligned and laminated by hot laminator, as described

below. The assembled disc (Figure 21B) is fixed using a rubber cap on a spinning motor (0923/S010-R1, McMaster Carr), which is controlled by a DC power supply (6217A, Hewlett Packard). The spinning frequency is measured by an RPM meter (1905T22, McMaster Carr). Figure 21C represents the microfluidic design of one processing unit on the disc for sample preparation, which includes three chambers. Chamber 1 and 2 are for sample and reagent introduction, respectively. A filter is inserted in the channel between chamber 1 and 3, to separate supernatant and pellets under filtration. Chamber 3 is a two-level structure with a shallow center area for sample drying and mixing. Sample stays in the center due to capillary force when the device is not spinning. When sample is being dried under vacuum, liquid will not contact with the edge of the chamber and enter the gap between layers. When the device is spinning and the centrifugal force overcomes the capillary force, the liquid sample will be driven to the outmost region in the chamber 3. Using spin-stop cycles, the liquid is moving to accelerate sample mixing (Figure 21D). A small collector at the far end of chamber 3 (shown at the bottom in Figure 21C) is used to collect silica nanoparticles by centrifugation which is added to remove proteins in the sample.

2.2.2. Fabrication of the centrifugal disc

Centrifugal microfluidic discs were fabricated by a print, cut and laminate method[239]. The 8.5×11 inches size transparency sheets (APO09209, APOLLO) were used as substrates for printing and laser cutting. For toner-printed transparency films, the whole area of each side was printed with 3 layers of black toner at a resolution of 600 dpi with the laser printer (HP LaserJet 2055dn). The DXF format file of the microfluidic design was created in AutoCAD software for laser cutting. Each layer of transparencies was fabricated by a CO_2 laser cutter (Epilog Legend) in the 'Vector

cutting' mode. The laser cutter was manually aligned and cutting was performed with settings of 9% power, 80% speed, 1200 DPI and 5000 Hz. The fabricated layers were removed from the rest of the transparencies, cleaned with ethanol and distilled water and dried under N_2 before assembling. Transparency films were manually aligned and taped together with Scotch tape one layer a time, from bottom to top. Before adding the top layer, a small piece (~ 1 mm×1 mm) of glass fiber filter (Whatman GF/B) was inserted. The assembled device was sandwiched between two layers of aluminum foil for hot lamination at 260° F, with a Catena 35 laminator using 3 mm roller pressure and the lowest speed. The device was then removed from the foil and cooled for 1 min.

2.2.3. SALDI chip preparation

The SALDI chips were prepared as described previously[188]. Briefly, vertical silicon nano-posts were deposited on a silicon wafer substrate by using glancing angle deposition (GLAD), followed by oxidation in an air environment and surface derivatization with (1H, 1H, 2H, 2H-perfluorooctyl) dimethylchlorosilane (pFMe2SiCl, Gelest).

2.2.4. Sample preparation coupled with offline SALDI-MS

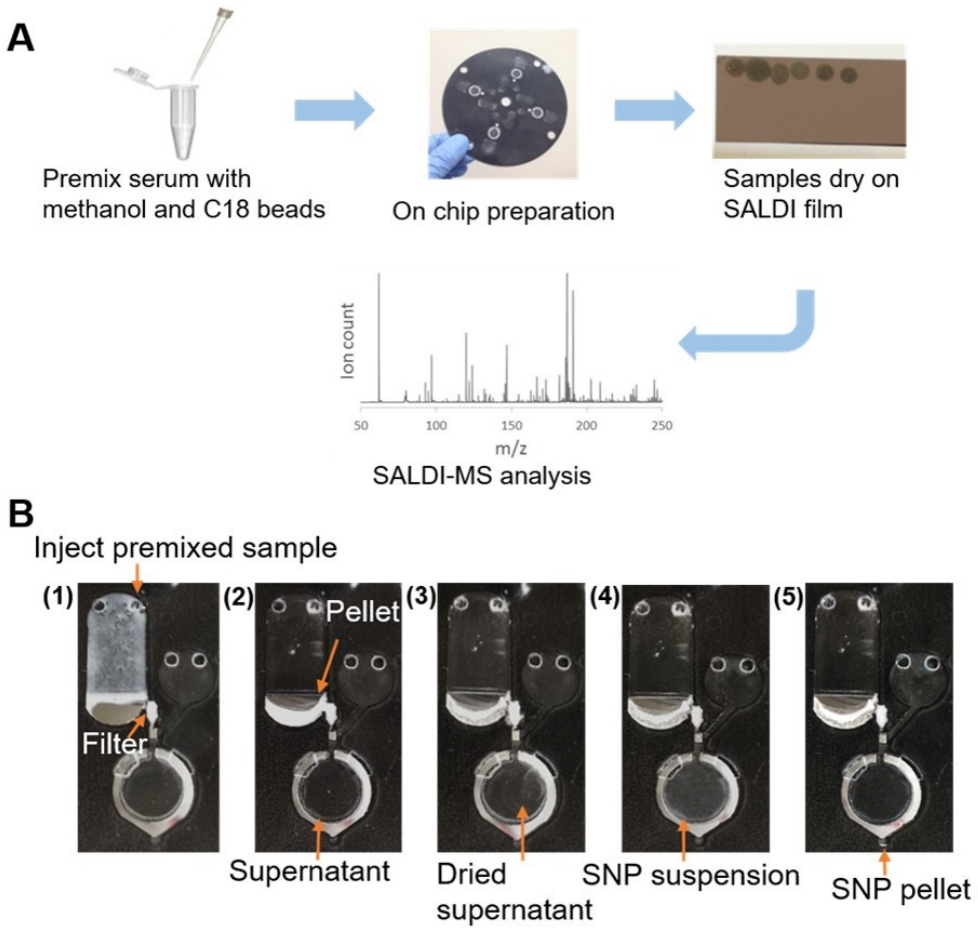

Figure 22. (A) Work flow of disc-based sample preparation and analysis of metabolites by SALDI-MS. (B) Images of disc-based preparation steps: (1) Inject serum samples premixed with methanol and C18 beads. (2) Pellet proteins and C18 beads by centrifugation and filtration. (3) Dry the supernatant by placing the disc in a vacuum chamber. (4) Add silica nanoparticles (SNP) suspension to dissolve the dried sample and adsorb remaining proteins in the sample. (5) Remove SNP by centrifugation.

Figure 22A demonstrates the workflow of the sample preparation and detection. Pooled human serum sample (Innovative Research, MI) was first premixed with methanol (LC/MS grade, Fisher Chemical) and 10 μm C18 beads (S03207B, Silicycle) for 1 min, to precipitate proteins and extract lipids, respectively. C18 beads were suspended in methanol at a density of 0-10% (weight/volume) and a volume ratio of serum to C18 suspended methanol of 1:3. A 25 μL premixed sample was then prepared with the disc (Figure 22B). The precipitated proteins and C18 beads were separated

from the liquid phase by the filter at 1500 rpm for 2 min. The supernatant containing the analytes was transferred into the two-level Chamber 3. The disc was then removed from the spinner and placed in a vacuum chamber to dry the supernatant for 20 min. After the sample was dried, 15 μL aqueous suspensions of 235 nm silica nanoparticles (microParticles GmbH, Germany), whose density was varied from 0 to 0.25% (weight/volume) during optimization, was added through chamber 2 to re-dissolve the dried sample, then mixed by spin-stop cycles for 3 min. The silica nanoparticles adsorbed the remaining proteins in the sample and were separated from the solution by 2000 rpm centrifugation for 5 min, pelleted in the small collection region. The cleaned sample was pipetted out and acidified with 2 M HCl to reach a final concentration of 0.18 M HCl. A 1.8 μL sample was then spotted onto a SALDI-chip in a petri dish and dried at 4 C overnight for salt crystallization.

The SALDI-chip with dried sample spots was attached to a customized MALDI plate with a double-sided conductive carbon tape (Electron Microscopy Sciences). The MALDI plate was inserted into an AB Sciex Voyager Elite MALDI-TOF mass spectrometer for analysis. A pulsed nitrogen laser (337 nm, 3 ns pulse) was employed for desorption and ionization. Mass spectra were acquired in negative ion mode and the signals were averaged for 100 laser shots, while rastering the beam to fresh locations within the spot. For sample preparation assay development and analyte quantification, at least four replicate spots were measured to calculate the average value and standard deviation for each sample. The laser intensity for desorption and ionization was set to 2200 (a.u.) for C18 optimization and 2100 for other measurements. Other detailed instrument settings are employed using previously optimized conditions.[188] Data Explorer 4.0 was used for MS data processing to calculate ion count intensity and signal to noise ratio.

Six metabolites, including taurine, aspartic acid, malic acid, glutamic acid, histidine and citric acid, and two isotope labeled metabolites, L-Glutamic acid-^{15}N and Citric acid-1,5-$^{13}C_2$, were purchased from Sigma-Aldrich and prepared in deionized water (18.2 MΩ) as standard solutions. Metabolites were quantified using the standard addition method. Briefly, serum samples were spiked with various volumes of standard solutions of analytes, followed by disc-based preparation and SALDI-MS detection. Isotope labeled or endogenous metabolites were selected as internal standards.

2.2.5. Clean sample recovery test

The disc-based preparation was divided into two steps, methanol/C18 treatment and silica nanoparticle treatment, for recovery evaluation of each step. Standard solutions were prepared containing fixed concentration of isotope labeled internal standards (200 μM glutamic acid and 200 μM citric acid) and various concentrations of non-isotope labeled metabolites (0-500 μM glutamic acid and 0-800 μM citric acid). TBS buffer was run through the disc for preparation, 1:1 mixed with standards, acidified with HCl and measured by SALDI for calibration curves. A clean sample with known concentrations of glutamic acid and citric acid in TBS buffer was prepared with the disc, using either the methanol/C18 or the silica nanoparticle extraction steps. The disc-prepared sample was mixed 1:1 with isotope labeled internal standard solution, acidified with HCl to 0.18 M, measured by SALDI and quantified according to calibration curves.

2.2.6. Sample preparation by ultrafiltration

Ultrafiltration of human serum samples was performed using centrifugal ultrafiltration tubes (Amicon Ultra-4, 3K Da cut-off) and the protocol described previously. The ultrafiltered sample was acidified with HCl to reach a final concentration of 0.18 M HCl and then spotted on a SALDI-

chip for drying and MS analysis. A standard addition method was employed for quantification with isotope labeled internal standards.

2.2.7. Hydrophilic Interaction Chromatography (HILIC) with MS

A hydrophilic interaction chromatography column (Agilent InfinityLab Poroshell 120 HILIC-Z phase) was used to separate the amino acids, coupled with a positive ion mode operated Single Quadrupole MS (Agilent Technologies 1100 HPLC with G1946A MSD) for detection. Isotope-labeled glutamic acid served as internal standard, and was spiked into serum samples before disc processing for glutamic acid quantification. All reagents were HPLC grade or higher. Water was purified using an EMD Millipore Milli-Q Integral System (Darmstadt, Germany). HPLC Mobile phase A was 25 mM ammonium formate in water at pH = 7.5, Mobile phase B was 25 mM aqueous ammonium formate in 9:1 acetonitrile/water, the flow rate 0.50 mL/min with an injection volume of 1 μL, at a 25 °C column temperature. Quantitation of glutamic acid in serum was accomplished with four-point calibration curve using ratios of peak areas at times of 6.56 min, for isotope labeled Glu (147 Da) and native Glu (146 Da).

2.3. Results and Discussion

2.3.1. Sample preparation assay development for serum clean-up

To identify a sample clean up process that can be realized on a centrifugal disc (CD), we first considered existing sample preparation methods that remove proteins and lipids from serum samples. A widely used clean-up method for metabolomics in serum uses methanol precipitation of protein[258], followed by liquid-liquid extraction with chloroform to extract hydrophobic

molecules from the sample. The aqueous phase is then analyzed. Another common approach is to use ultrafiltration, which we employed for SALDI-MS previously, with acidification by HCl.

Methanol precipitation and supernatant collection is readily accomplished on a CD. However, chloroform can cause severe damage to the disc by dissolving the toners, so we replaced liquid-liquid extraction with solid phase extraction. As a first stage extraction, C18 beads suspended in methanol were mixed with serum with a volume ratio of 3:1 for protein precipitation and extraction. The supernatant, after mixing of serum, methanol and C18 beads, was collected, dried under vacuum and re-dissolved with the same volume of water for SALDI-MS detection. Particle densities of 1.7, 3.3, 6.6 and 10 % were tested, the sample spots on SALDI-chips were observed under microscope, and the signal to noise ratio (S/N) of six different metabolites were evaluated. Figure 23A shows spots from sample preparation with 0 and 1.7% C18 beads (wt/vol % in methanol) are larger than sample spots prepared with higher density C18. For densities of 3.3 % or higher, the contact angle of the spotted droplets is higher, which means the dried spots are cleaner, and background electrolyte crystallization is localized in larger crystals, allowing better mass spectrometry of the metabolites. Treating samples with 3.3 % C18 beads improved the SNR of aspartic acid, glutamic acid, and histidine by a factor of 2 compared to methanol alone. A two-tailed t-test shows that the SNR for these three components, prepared with 3.3% C18, are improved from samples prepared with 1.7% C18 ($p < 0.05$), but the SNR decreased again at higher particle density. Taurine and citric acid showed their best results at 1.7 %, with a small decline at 3.3 %. Malic acid showed the same response at 0 and 3.3% particle density. Based on this study, 3.3% C18 particle density was selected for the solid phase extraction step.

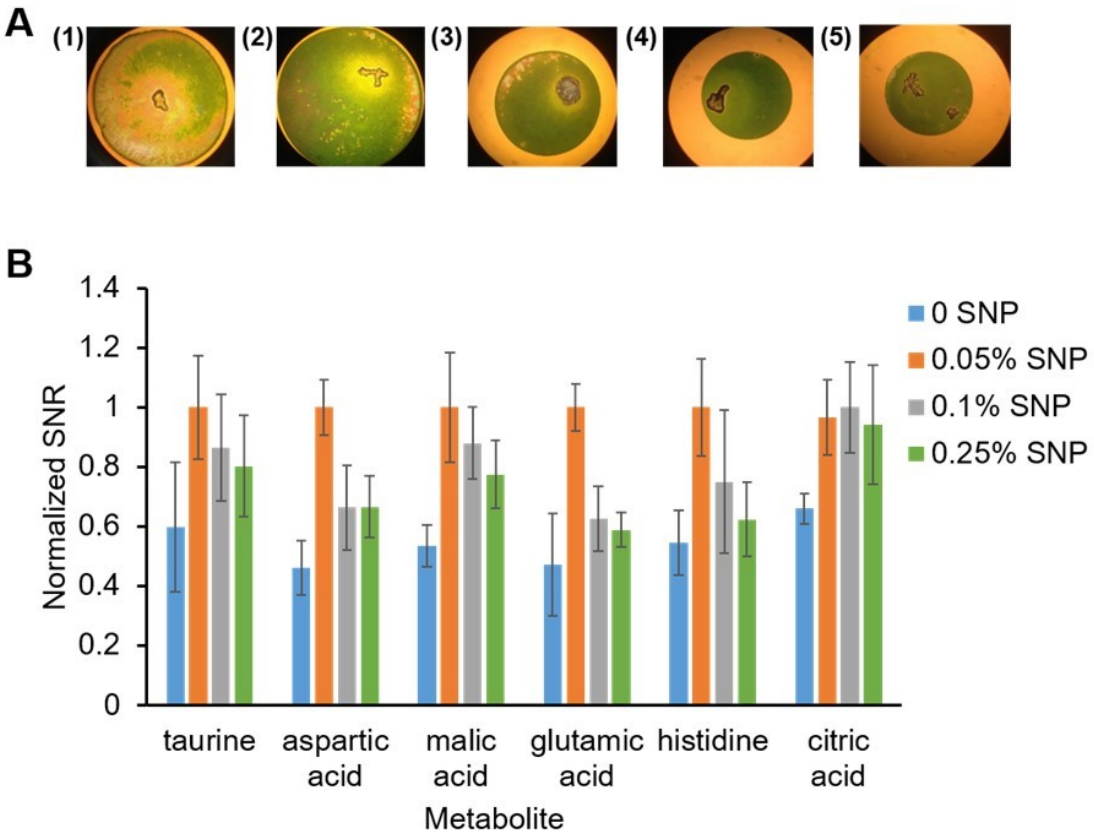

Figure 23. (A) Microscopic photos of serum samples prepared with methanol precipitation and solid phase extraction with different densities of C18 beads: (1) 0%; (2) 1.7%; (3) 3.3%; (4) 6.6%; (5) 10%. (B) Normalized signal to noise ratio of metabolites from serum samples prepared disc-based with different densities of silica nanoparticles (SNP) to remove proteins after disc-based methanol precipitation and C18 beads extraction. Error bars represent standard deviations of average.

Additional steps may be required to further clean serum samples, as methanol precipitation cannot completely remove the proteins in serum.[259, 260] Silica nanoparticles were selected for a second extraction stage, since they adsorb proteins in serum samples[261-264]. Mixing and separation of the nanoparticles was not difficult to realize on a centrifugal microfluidic platform. The effect of the size of the silica nanoparticles on protein adsorption has been studied previously, showing that smaller size nanoparticles with larger surface area adsorb more proteins.[261] In our microfluidic device, particles with a diameter less than 200 nm took too long to remove by centrifugation, while particles with a diameter larger than 500 nm were difficult to mix in the spin-stop cycles, leading

us to select 235 nm silica nanoparticles. Figure 23B illustrates the SNR of six metabolites in serum samples prepared with different densities (wt/vol % in methanol) of nanoparticles. Compared to preparation with methanol and C18 beads alone, 0.05% silica nanoparticles increase the SNR of all six metabolites by a factor of ~2, as confirmed by $p < 0.05$ for the six metabolites. However, a higher density of silica nanoparticles leads to lower SNR. The net increase in SNR from the two optimized stages of C18 and silica extraction versus using methanol alone is ~4.

2.3.2. Mass spectra of disc-based sample preparations

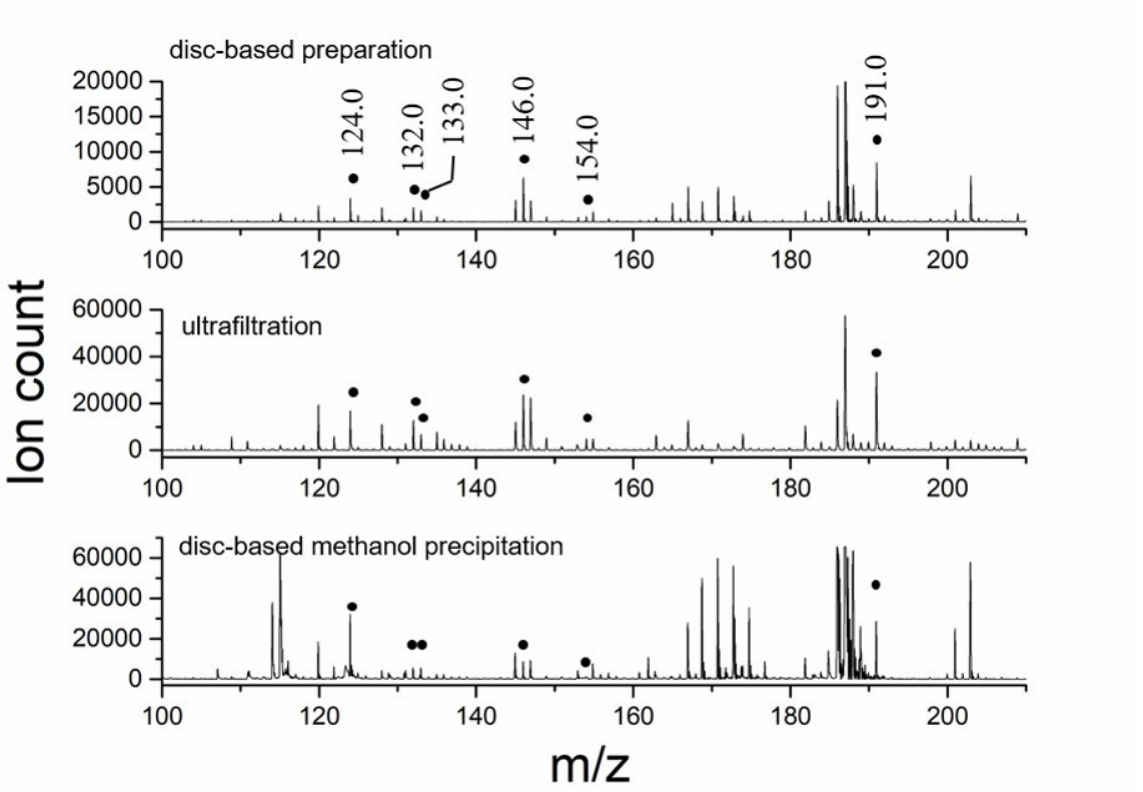

Figure 24. SALDI Mass spectrum (negative mode) of serum sample after disc-based preparation with labeled peaks (taurine: 124.0; aspartic acid: 132.0; malic acid: 133.0: glutamic acid: 146.0; histidine 154.0; citric acid: 191.0), off-chip ultrafiltration and disc- based methanol precipitation in the mass range of 100-210.

Figure 24 illustrates the mass spectra of serum samples after disc-based preparation with the optimized methanol precipitation, C18 and silica particle cleanup method, versus laboratory-based

ultrafiltration and acidification. The identified metabolite [M-H] peaks are labeled with their m/z values. The mass spectrum of the disc-based sample preparation (Figure 24 upper trace) gives a flat baseline, little noise and tens of metabolite peaks, which is similar to the spectrum of the ultrafiltered sample (Figure 24 middle trace). The lower intensities of the metabolites for disc-based sample preparation compared to the ultrafiltered sample is mainly attributed to dilution in the disc-based preparation. The SNR of the six metabolites in on-chip prepared samples shows is ~2 times lower when compared to samples prepared by ultrafiltration. However, after methanol precipitation and C18 extraction, the sample is about four times diluted and not concentrated again in the following steps. This dilution impacts the signal, but can be readily overcome by evaporation of the solvent, and reconstitution in a smaller volume. The results establish that a useful mass spectrum can be obtained using the disc-based preparation, comparable to commonly employed laboratory-based methods.

To further evaluate the role of the C18 and silica treatment, a negative control was performed using disc-based methanol precipitation alone, followed by SALDI of the aqueous reconstituted serum sample. The lower trace in Figure 24 shows a poor baseline, large background peaks and low SNR for analytes, presumably due to incomplete removal of proteins and lipids. There are clusters of background peaks with strong intensities in several m/z regions, such as 170-175 and 185-190, which could be identified as false positive metabolite peaks, or could result in false negatives for metabolites in this region due to the chemical noise. Figure 24 shows the C18 and silica extraction steps greatly reduce the background peaks seen when using methanol alone, providing a spectrum that is much more similar to the ultrafiltration preparation. It is clear that the C18 and silica particle treatment contribute substantially to improved analytical performance.

2.3.3. Quantification using isotope labeled internal standard

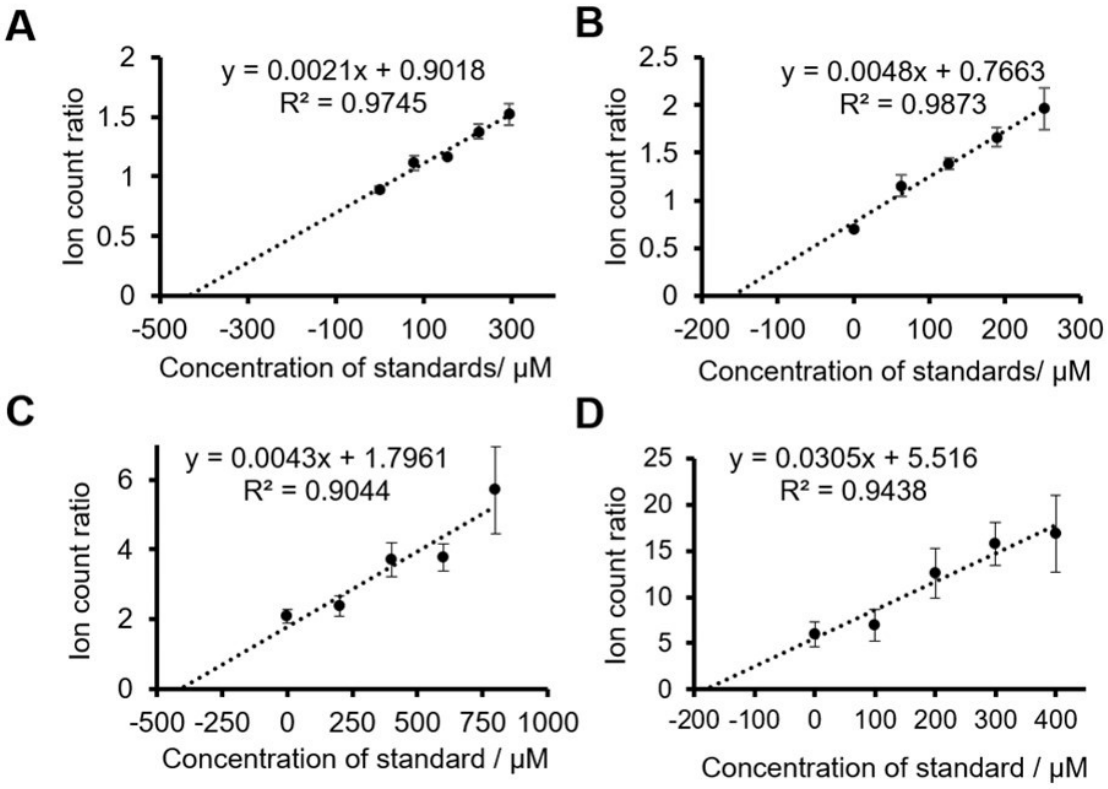

Figure 25. Calibration curves of glutamic acid (A, C) and citric acid (B, D) in serum samples prepared by centrifugal microfluidic disc and detected on SALDI-chip with isotope labeled (A, B) or endogenous (C, D) internal standards. Standard addition method was employed for quantitative analysis. Ion count ratio (analyte/internal standard) in each calibration curve is 14N glutamic acid/15N glutamic acid (A), 12C citric acid and 13C citric acid(B), glutamic acid/glutamine(C), or citric acid/malic acid(D). Error bars represent the standard deviations of average.

Two metabolites, glutamic acid and citric acid, were selected for quantification by the standard addition method with isotope labelled internal standards (^{15}N glutamic acid and ^{13}C citric acid), as illustrated in Figure 25A and 25B. The SALDI-MS results from disc-based serum sample preparations were 430 μM for glutamic acid and 160 μM for citric acid (Table 1). The same serum sample prepared by ultrafiltration and detected by SALDI-MS shows consistent results, 463 μM and 157 μM for glutamic acid and citric acid, respectively (Table 1). The serum samples were also assayed by HILIC-MS, following disc-based sample preparation, and the result for glutamic acid

was 405 μM. The RSD is ~ 10% in these analyses, meaning the concentrations observed by the three approaches are in reasonable agreement. (Citric acid interacts too strongly with the HILIC column to useful quantitative LC-MS results.)

Table 1. Comparison of the quantitative results for metabolites in human serum samples[a]

	Concentration in original serum sample /μM		
	Centrifugal disc-SALDI-MS	Ultrafiltration-SALDI-MS	Database[4]
Taurine	70[1]	72[3]	45-130
Aspartic acid	43[1]	53[3]	<25
Malic acid	23[1]	18[3]	3-21
Glutamic acid	430[2]	463[2]	<100
histidine	108[1]	88[3]	26-120
Citric acid	160[2]	157[2]	30-400

a) Prepared and quantified by centrifugal microfluidic disc-SALDI-MS with endogenous or isotope labeled internal standards and by ultrafiltration-SALDI-MS.

1 Data quantified with endogenous internal standards, as shown in Fig 6.

2 Data quantified with isotope labeled internal standards, as shown in Fig 5.

3 Data from reference22

4 Data from Human Metabolome database (HMDB, www.hmdb.ca).

2.3.4. Analysis with endogenous internal standard

While isotope labelled chemicals are ideal internal standards for mass spectrometry based metabolite analysis, the limited availability and relatively high cost of these chemicals provide

challenges for analyzing large varieties of metabolites. Biological samples usually contain numerous endogenous small molecules with various physical and chemical properties, which hold great potential for serving as internal standards. And unlike in LC-MS, where using the same chemical with a different isotope is required to ensure the same elution time, in SALDI-MS all masses are ionized simultaneously. We evaluated several endogenous internal standards for the metabolites we have studied, for both reproducibility and quantitative precision.

Table 2. Assessment of reproducibility of disc-prepared serum samples

Metabolite (m/z)	RSD		
	Ion count	Relative intensity[1] (reference metabolite)	Relative intensity (malic acid)
Taurine (124.0)	40%	18% (citric acid)	30%
Aspartic acid (132.0)	11%	4% (glutamine[2])	9%
Malic acid (133.0)	12%	9% (aspartic acid)	-
Glutamic acid (146.0)	5%	7% (glutamine)	18%
Histidine (154.0)	17%	11% (aspartic acid)	17%
Citric acid (191.0)	26%	15% (malic acid)	15%

[1] Relative intensity is the intensity ratio of metabolite and reference metabolite (internal standard)

[2] m/z of glutamine is 147.0

The reproducibility of the disc-based sample preparation method was assessed, with six parallel sample preparation experiments, performed in separate microfluidic units on two discs. The relative standard deviations in ion counts for six metabolites are summarized in Table 2. When referenced to endogenous internal standards, the ratio of intensities showed substantially improved RSD. Given their chemical differences, there is no single metabolite that is a satisfactory internal standard for all six metabolites, as shown in Table 2 when malic acid is used as the reference for

all. The optimal choices observed are given in the table, where it can also be seen that taurine and citric acid show higher RSD relative to the other compounds.

Figure 25 shows a comparison of the standard addition calibration curves obtained with isotope labeled internal standards, versus alternate endogenous internal standards (Figure 25A vs. 25C, and 25B vs. 25D). The extrapolated concentration values for glutamic acid and citric acid are in good agreement for both types of internal standard. The higher R^2 values in the curve fits do indicate greater precision when using isotope labeled internal standards, as expected with the isotope standards, but the performance of endogenous internal standards is nearly comparable.

Four additional metabolites in serum samples prepared with the disc were quantified by standard addition. Endogenous metabolites in serum were selected as internal standards for those analytes. The calibration curve for each metabolite was plotted as intensity ratio *vs.* concentration of standard (Figure 26). The results of quantification are summarized in Table 1, together with results obtained from a metabolite database, as well as those from previous analysis of serum prepared by ultrafiltration then quantified by SALDI-MS[188]. The results of all six metabolites were consistent with those from the other preparation and quantification methods. The limit of quantitation for the compounds evaluated here in serum were in the range of 0.5-5 μM, similar to our previous reports for GLAD films used for amino acid analysis.[188]

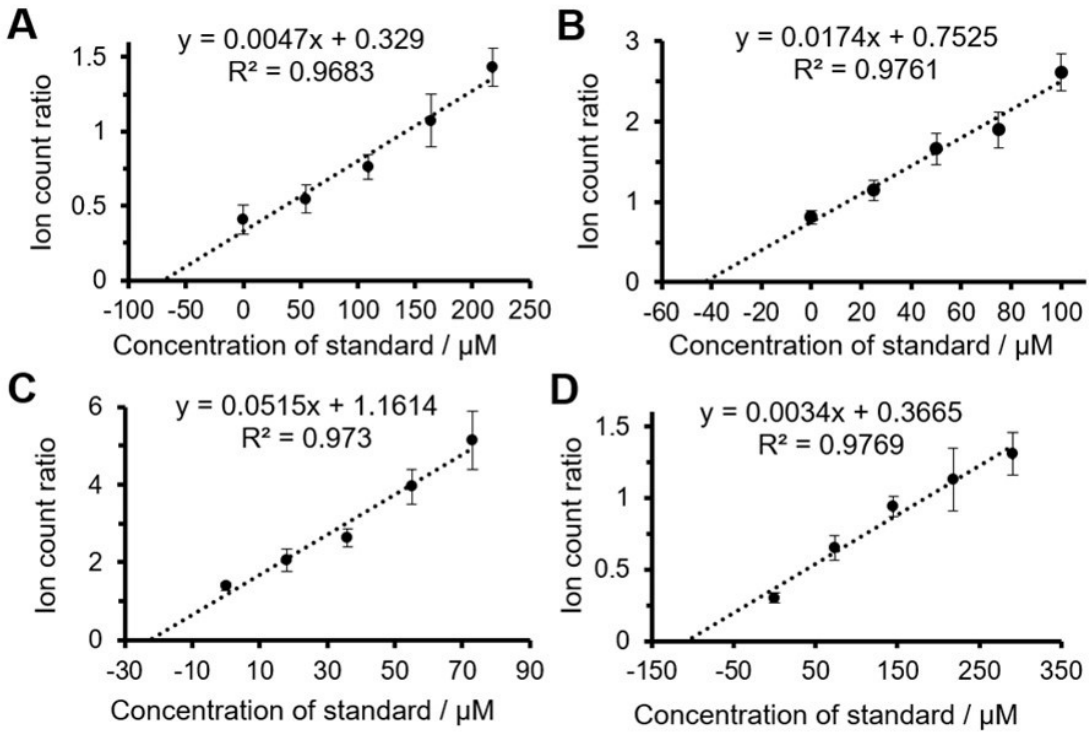

Figure 26. Calibration curves of taurine (A), aspartic acid(B), malic acid(C), and histidine(D) in serum samples prepared by centrifugal microfluidic disc and detected on SALDI-chip with endogenous internal standards. Standard addition method was employed for quantitative analysis. Ion count ratio (analyte/internal standard) in each calibration curve is taurine/citric acid (A), aspartic acid/glutamine(B), malic acid/aspartic acid(C), or histidine/aspartic acid(D). Error bars represent standard deviations of average.

To evaluate the recovery of the six metabolites in the process of disc-based preparation, we analyzed and compared two groups of samples spiked with standards, either before or after preparation with a disc. Standards spiked in serum samples before preparation (Group 1) may suffer from losses during preparation, whereas standards spiked in the samples after preparation (Group 2) do not. Recovery was calculated as in equation 7, assuming a linear relation between signal and concentration. S_1 and S_2 are the signals of a spiked metabolite from Group 1 and Group 2, respectively. S_0 is the signal of a metabolite from a disc-prepared sample without spiking.

$$Recovery = \frac{S1-S0}{S2-S0} \times 100\% \quad (7)$$

The recovery of each metabolite is summarized in Table 3. The recovery of malic acid and citric acid are significantly lower than those of the other four metabolites. Malic acid and citric acid have analogous chemical structures, containing one hydroxyl group and multiple carboxyl groups, which lead to different interactions with the beads in the preparation step.

Table 3. Metabolite recovery from disc-prepared serum with endogenous internal standards

metabolite	Taurine	Aspartic acid	Malic acid	Glutamic acid	Histidine	Citric acid
Recovery/%	105±16[1]	87±14	38±3	101±7	103±26	28±6

[1]Error represents the standard deviation of average.

To further understand the recovery observed, two isotope labeled chemicals (^{15}N glutamic acid and ^{13}C citric acid) were used to test recovery of the two non-isotope labeled metabolites in "clean" buffer samples (analyte in pH 7.4 tris buffer). The two individual sample preparation steps, methanol precipitation with C18 treatment, or silica nanoparticle treatments, were assessed separately. The results (Table 4) are in good agreement with the serum recovery experiments, and show the absence of protein did not change the observed recoveries. Glutamic acid shows no obvious loss from either of the sample preparation steps, while citric acid suffers from low recovery in the methanol/C18 step.

Table 4. Recovery of metabolites for each individual disc-prepared step

	Methanol/C18	Silica nanoparticles
Glutamic acid	101±2%[1]	101±5%
Citric acid	27%±5%	99±10%

1) Determined in buffer, "clean samples" with isotope labeled internal standards

2) Error represents the standard deviation of average value.

In using two solid phase extraction steps, there can be concern about a bias in the final concentration due to selective extraction. It is known that silica nanoparticles can adsorb some metabolites when protein is absent,[265] but in the presence of proteins, silica is not likely to adsorb metabolites, due to stronger interactions with proteins compared to metabolites.[262] The C18 phase may also result in some bias, and this is illustrated in the case of the citric acid. Given the use of standard addition and an internal standard as an approach, the impact of such bias can be reduced.

2.3.5. Centrifugal disc preparation coupled with LC-MS

To explore the versatility of our disc preparation for different analytical methods, we combined the disc-based sample preparation of serum with HILIC-MS, using an isotope-labeled internal standard. As indicated above, the result for glutamic acid using disc-LC-MS was 405 μM, which is in agreement within experimental error of the results from disc-SALDI. The standard addition curve had an R^2 of 0.943, similar to the plots for SALDI-MS, indicating a similar level of precision. (Interactions with the HILIC phase for citric and malic acids were very strong, showing strong tailing in the chromatograms, so an equivalent study with labelled citric acid was not performed.)

The HILIC-MS study was also used to establish that the m/z peaks assigned to various metabolites in the SALDI-MS data were correctly assigned, and did not include other chemicals of a similar mass. HILIC-MS of metabolite standards established the elution times, while extracted ion chromatograms of disc-prepared serum samples showed only a single peak, at the same elution time.

2.4. **Conclusion**

This work realizes the goal of producing sufficient processed sample volume from a microfluidic device for sample recovery and subsequent external laboratory measurement of the cleaned up sample. The strategy separates the low-cost, disposable, microfluidic device for sample preparation, from the detection elements, which can be costly or impossible to fabricate in a microfluidic system. The centrifugal disc device demonstrates sufficient removal of proteins, lipids and other biomolecules for effective mass spectrometry of multiple small-ion metabolites in human serum samples. Disc-prepared serum samples were analyzed by both SALDI-MS and HILIC-MS, with similar performance characteristics. The results illustrate the potential usefulness of the centrifugal disc in sample preparation for more than one type of analytical measurement, with the target of specific metabolite assays, or panels of metabolites for a specific disease.

Chapter 3. An automated centrifugal microfluidic for efficient multistep blood sample preparation and clean-up towards mass spectrometry

3.1. Introduction

In Chapter 3, efforts are described to increase the level of automation of sample preparation on a disc, compared to the proof of concept disc described in Chapter 2. All sample preparation steps, beginning with whole blood, are integrated into the disc operations, without a need for external delivery of reagents during the analysis.

Blood is one of the most informative samples for bioanalysis,[266] and can accurately reflect the state and progression of many diseases.[238] Target molecules within blood samples are encompassed by the various "ohmics", including genomics, transcriptomic, proteomics, and metabolomics.[267] However, the biological sample matrix is extremely complex in blood, so extraction of the target molecule from the biological sample, along with purification, is required for analysis. At the same time, most often sample preparation procedures for blood analysis requires skilled technicians and well-equipped, expensive laboratories. Microfluidics and related technologies are being explored to create automated, cost-effective and rapid solutions for a wide variety of blood analyses. For example, Kitamori's group have combined axial migration effect and filtration to obtain blood-cell-free plasma in a microfluidic chip.[268] And Wheeler's group developed a total automated blood-plasma separation on a digital microfluidic device.[269] But since most blood-related microfluidic devices are developed for blood to plasma separation, the chemical complexity of the sample matrix in plasma remains high, and further processing is often necessary.

As illustrated in the previous chapter centrifugal microfluidic devices, also known as lab-on-disc, employs centrifugal force to realize on-disc flow control. Many functional valves have been developed and can be applied on the centrifugal disc including metering, mixing and switching build on the centrifugal force field.[20] Centrifugal microfluidic discs able to perform multiple steps are utilized in clinical chemistry, immunodiagnostics, cell handling, molecular diagnostics, as well as in food, water, and soil analysis. It is anticipated there will be a high potential for commercialization.[10, 270] However, as for a lab-on-chip, most blood-related lab-on-disc devices are developed for preparing cell-free plasma.[271] A blood sample preparation involving further protein cleanup, to allow small, polar molecule extraction is an undeveloped area. Herein, we aim to design a centrifugal chip that could complete sample preparation during a quick sequence of uninterrupted spinning cycles, further automating the concept developed in Chapter 2.

Mass spectrometry (MS) based methods are excellent approaches, in terms of high sensitivity and specificity, high throughput and high accuracy for small molecule detection.[272] Amino acids are essential nutrients that also play an important role in revealing the metabolic pathway of many major diseases like Alzheimer and Parkinson, and early detection of these diseases as well as different types of cancers.[273, 274] So we chose to analyze unlabeled free amino acids in the on-disc processed sample by both LC-MS and SALDI-MS to verify the performance of our on-disc blood sample processing. The goal is to create a device that we can put sample in, and obtain a cleaned up, prepared sample back out again for subsequent MS analysis. This differs from the typical concept of a microchip device with a sample in, answer out concept, which has been the typical goal in microfluidics. We anticipate our strategy will be more general, more flexible and more useful commercial deployment of microfluidics technology.

Chapter 2 reported a modified GLAD thin film for SALDI-MS that offers a rapid detection of several amino acids and organic acids with a high tolerance of salts.[188] In this chapter, glutamic acid and citric acid are used for quick SALDI-MS quantitative estimation with easy available isotope internal standards on modified GLAD film. The results are compared with the more traditional hydrophilic interaction chromatography in low pH with positive mode LC/MS.

3.2. Experimental section

3.2.1. GLAD film preparation for SALDI-MS

The SALDI chips were prepared as described previously.[188] Briefly, vertical silicon nano-posts were deposited on a silicon wafer substrate by glancing angle deposition (GLAD), followed by oxidation in an air environment and surface derivatization with (1H, 1H, 2H, 2H-perfluorooctyl) dimethylchlorosilane (pFMe2SiCl, Gelest). 60 ul (1H, 1H, 2H, 2H-perfluorooctyl) dimethylchlorosilane was diluted by 5 ml methanol in a glass Petri dish. By soaking the film in that diluted solution for 30 min at ambient temperature, silanol groups on the surface could be covalently fluorinated. Then the GLAD film was laid flatly in a Petri dish for air drying and stored overnight for polymerization at room temperature.

3.2.2. Design and fabrication of the centrifugal disc

Figure 27 shows the 15 cm diameter centrifugal microfluidic device consists of four layers of 1.5 mm-thick poly(methyl methacrylate) (PMMA)(Acrylite FF, Johnston plastics) and four layers of 127 μm-thick pressure sensitive adhesive (PSA)(Adhesives Research) which serves as the bonding layer to accomplish disc assembling avoiding wet chemical procedures (Figure 27a). Features are

cut by CO_2 laser ablation (Epilog Zing Laser Series) and aligned layers are laminated by laminator (Cheminstruments HL-100 rolling laminator) with 100 psi. PSA layers serve as bonding layers between PMMA layers. One disc contained three processing units for sample preparation, as seen in Figure 27b. The assembled disc is fixed on a centrifuge (Eppendorf 5415C centrifuge) by a custom-made adaptor (Figure 27c) for spinning.

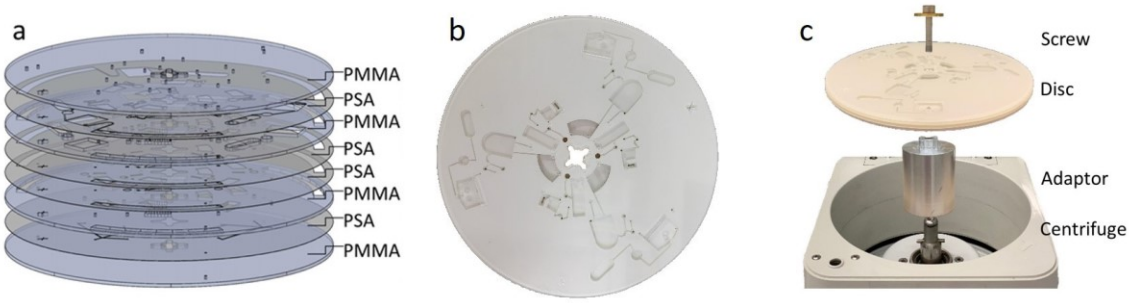

Figure 27. (a) The disk's components: four layers of 126 μm PSA and four layers of 1.5 mm PMMA. (b) Photo of the assembled disc. (c) Disk fits into centrifuge by the adaptor.

3.2.3. Analysis of processed Sample by offline LC-MS

Separation of different amino acids is performed by hydrophilic interaction chromatography column (Agilent InfinityLab Poroshell 120 HILIC-Z phase), while detection uses a Single Quadrupole MS (Agilent Technologies 1100 HPLC with G1946A MSD) in positive ion mode. All reagents were HPLC grade or higher. Water was purified using an EMD Millipore Milli-Q Integral System (Darmstadt, Germany). For the separation of 16 free, underivatized amino acids including Phenylalanine (F), Leucine (L), Isoleucine (I), Methionine (M), Tyrosine (Y), Valine (V), Proline (P), Alanine (A), Threonine (T), Glycine (G), Serine (S), Glutamic acid (E), Aspartic acid (D), Histidine (H), Arginine (R) and Lysine (K), we followed the method from Agilent to prepare mobile phase and set instrument conditions.[275] Mobile phase A was 20 mM ammonium formate in water at pH = 3.1, Mobile phase B was 20 mM aqueous ammonium formate in 9:1

acetonitrile/water, the flow rate was 0.50 mL/min with an injection volume of 0.2 µL, at a 30 °C column temperature.

3.2.4. Analysis of processed sample by SALDI-MS

A 5 µL sample is pipetted out of a disc after sample cleanup, then acidified with 2 M HCl to a final concentration of 0.18 M HCl. A 1.3 µL sample was then spotted onto a GLAD chip in a petri dish and dried at 4°C for salt crystallization. All chemicals including amino acids, organic acids and isotope standards were purchased from Sigma and were prepared as high concentration stock solution in DI water. A customized MALDI plate was made to fit the MS inlet, adapting to the thickness of the GLAD chip. Double-sided conductive carbon tape (Electron Microscopy Sciences) attached the GLAD film, with dried sample spots, to the MALDI plate. The MALDI plate was inserted into to AB Sciex Voyager Elite MALDI-TOF mass spectrometer for analysis. The nitrogen laser (337 nm, 3 ns pulse) pulse provides energy for both desorption and ionization. The carboxyl group in AAs and organic acids could be easily ionized under negative ion mode. Mass spectrum reflects averaged ion counts for 100 laser shots while moving the beam to new locations in the spot. Each data point stands for the average value of ion count or ion count to noise ratio of 3 replicate spots. Standard deviation is calculated the same way for sample preparation assay development and quantification. The laser intensity was set to 1850 (a.u.) for C18 and silica particle optimization, 2100 (a.u.) was used for real sample measurements. All other information about instrumental settings is listed in our previous work.[188] For rapid quantitative estimation, fresh blood samples were spiked with isotope standard stock solutions before loading the blood sample to the disc, followed by MS detection after on-disc cleanup. Ion counts were read from the MS spectrum by inputting the certain m/z value in the data analysis software Data Explorer 4.0.

3.3. Results and discussion

3.3.1. Workflow of on-disc blood sample preparation and optimization

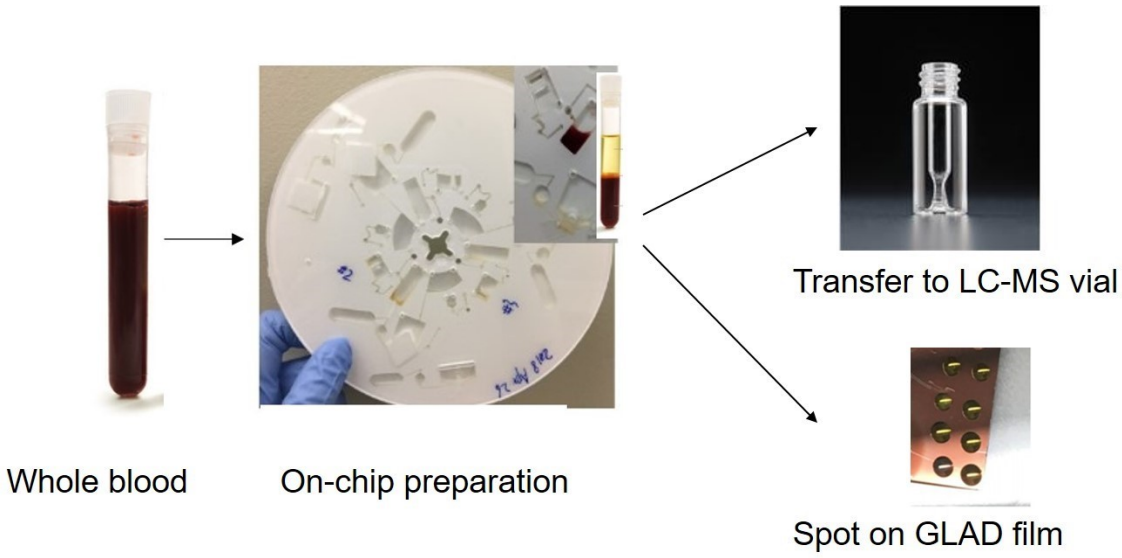

Figure 28. Workflow of on-chip sample preparation, followed by LC-MS and SMALDI-MS.

Figure 28 illustrates the intended workflow for sample preparation using the lab on a disc device. The goal is to introduce a whole blood sample, perform all processing steps within the device without further manual intervention except for rotational speed variations, and then extract a 5 µL sample for instrumental analysis of small, polar metabolites. In this study, the two methods employed for analysis are SALDI-MS utilizing porous silicon films fabricated using the glancing angle deposition (GLAD) process, or HILIC-MS.

We have previously established a sample cleanup procedure that could be used on a disc, but the procedures on-disc were not fully automated. Plasma, methanol, and C18 beads were mixed in a vial to precipitate protein and remove lipids, then introduced on-disc, filtered and mixed with silica to remove remaining chemical interferences that were apparent in the mass spectrometry (assumed

to be hydrophilic proteins or protein fragments). The disc operation then separated supernatant from the silica, allowed the silica to be removed from the disc manually. Then the sample was dried on-disc, reconstituted with aqueous buffer manually (0.18 M HCl) and pipetted to a SALDI-MS device for analysis.

Fully integrating and automating all of the sample preparation steps on disc, starting from whole blood, necessitated some modifications in the previous procedure, requiring validation of the revised process. The work flow for the revised disc, and optimization of the revised procedures is discussed below.

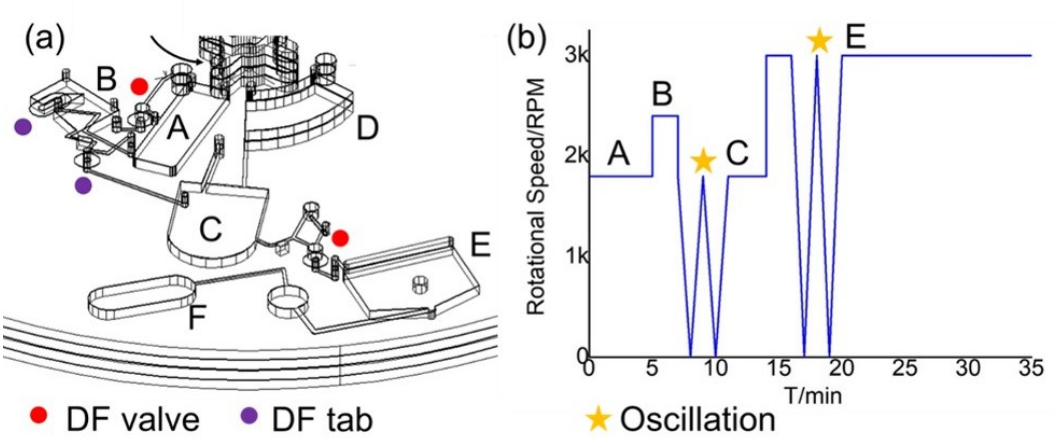

Figure 29. (a) 3D view and design for one unit. The on-disc DF valves only burst at a specific spinning speed while DF tabs will open once be dampened. (b) The spinning operation procedure. The oscillation part is only for schematic purposes; the actual oscillation frequency and acceleration are not labeled.

Table 5. List of the function of each chamber and the releasing frequency of each subsequent valve.

Chamber	Function	Release rotational speed/rpm
A	Blood cell separation	2400Hz
B	Serum metering	Once the DF tab is dampened
C	Protein precipitation by MeOH	3000Hz
D	Preload MeOH	NA
E	C18/Silica particle clean up and sample drying	NA
F	Facilitate pneumatic mixing	NA

Figure 29 illustrates the various chambers on the disc, used to stage the sequential processing of a blood sample for ultimate delivery to a SALDI-MS surface, or a HILIC-MS assay. The timing, and rotational speeds in RPM, are shown in Table 5. Integrated dissolvable film (DF) burst valves are used to stage each step. A 190 μL blood sample, collected from a healthy female volunteer in an ethylenediaminetetraacetic acid (EDTA) coated tube was loaded into plasma preparation chamber A. A suitable spin time to separate the cells from the plasma was easily determined by running the experiment under a video camera.[130] After 5 min of on-chip blood cell separation in chamber A at 30 Hz, 50 μL of separated plasma is metered by chamber B, using the first DF-burst valve at 2400 rpm. We designed the decanting DF valve to lie much higher than the 45% volume line of the blood loading chamber, to avoid transferring any blood cells after the separation.[276]

The metered plasma is then diluted 3:1 (v/v) with preloaded methanol (LC/MS grade, Fisher Chemical) in reservoir C, for protein precipitation. The spinning speed was oscillated between 0 to 30 Hz for 3 mins to realize thorough mixing below the DF valve burst frequency. Spinning the disc for 3 mins at 1800 rpm then precipitates the aggregated proteins to the chamber bottom, so that a filtration process was not required, in contrast to the previous design. Avoiding filtration simplifies the disc fabrication process. The supernatant was transferred to chamber E by increasing the spinning speed to the DF valve burst frequency 50 Hz. Removal of remaining lipid and protein contaminants is then effected in the next step, by mixing with 10 μm C18 beads (S03207B, Silicycle) and 235 nm silica nanoparticles (microParticles GmbH, Germany) preloaded in chamber E. The optimum dose of C18 beads and silica nanoparticles was determined by comparing the signal-to-noise (S/N) value in the MS spectrum, as described below. Repeating the 3 min oscillating spinning speeds between 0 and 50 Hz helps to achieve rapid mixing. Methanol was then rapidly evaporated away by spinning at constantly at 50 Hz for 15 mins. The particles settle to the

chamber bottom in this step. The methanol needed to be removed, to increase the surface tension of the supernatant enough that very small spots are formed transferred to the hydrophobic SALDI plates. The supernatant is then ready to be pipetted out for subsequent analysis.

3.3.2. Sample preparation assay optimization for blood sample preparation

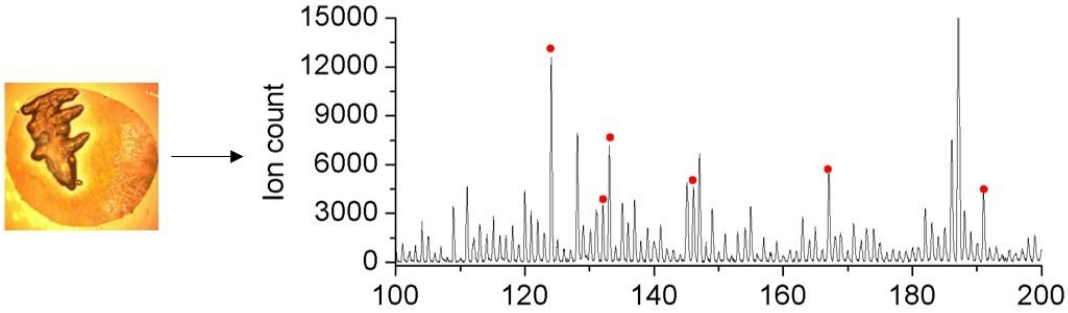

Figure 30. Mass spectrum for desalted sample spot, m/z peaks of the six analytes are labeled.

Methanol precipitation was used as the primary method for protein removal from the metered plasma delivered by chamber A on the disc.[258] Lipid interferences were again removed with C18 coated silica particles, and any remaining proteins were removed with bare silica particles. These particles were preloaded into chamber E. They were then were co-mixed with the methanol treated plasma, and both particle types were pelleted by on-disc centrifugation.

Different amounts of C18 coated silica particles and bare silica particles were added to determine the optimum dose. The signal to noise ratio (S/N) of six amino acids and organic acids from the SALDI-MS spectrum were compared, and the conditions that gave the best SNR were selected. Figure 30 gives a typical SALDI-MS spectrum observed. Peaks of the six analytes are labeled by red dots in the SALDI-MS spectrum.

Figure 31A shows that the sample prepared with 5.3% (m/v) C18 yields higher S/N than samples prepared with less C18, so this loading of C18 beads was utilized in subsequent studies. Figure 31B compares S/N values of the sample prepared with different doses of silica particles. Using 0.05% bare silica particles gives higher S/N values than other amounts. It is likely that an excess of silica nanoparticles adsorbs analytes, but the small amount that is required is sufficient to remove trace remaining protein. To summarize, densities of 5.3% (m/v) C18 coated silica particles and 0.05% （m/v） bare silica particles achieved the most effective sample cleanup.

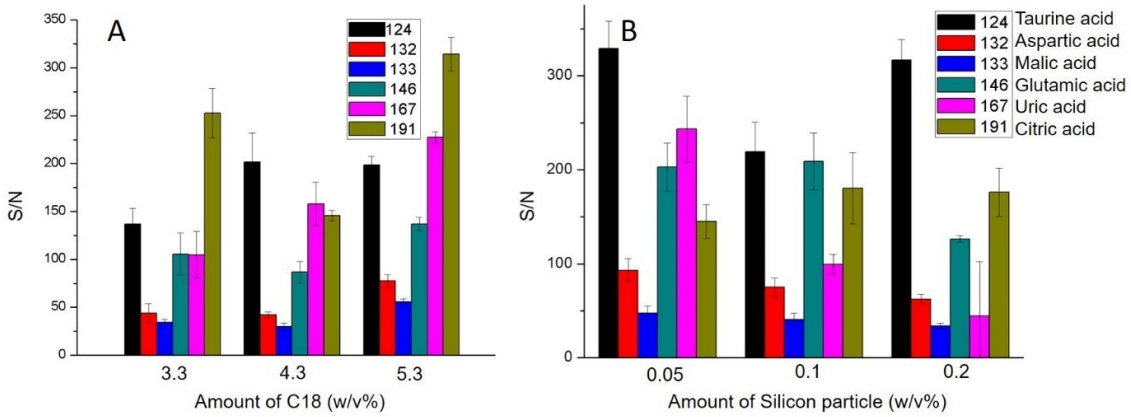

Figure 31. Signal to noise ratio of different metabolites in blood samples prepared on-chip with different densities of C18 beads (A) and silica nanoparticles (B).

3.3.3. Centrifugal disc preparation coupled with LC-MS

Table 6. The retention time of amino acids elute by HILIC column.

Analyte	tR /min	m/z	Analyte	tR /min	m/z
Phenylalanine(F)	2.62	166.1	Threonine(T)	6.61	120.0
Leucine(L)	3.70	132.1	Glycine(G)	6.68	76.0
Isoleucine(I)	3.21	132.1	Serine(S)	6.87	106.1
Methionine(M)	4.28	150.0	Glutamic acid(E)	7.62	148.1
Tyrosine(Y)	5.14	182.1	Aspartic acid(D)	8.08	134.0
Valine(V)	5.08	118.1	Histidine(H)	7.99	156.1
Proline(P)	5.10	116.1	Arginine(R)	8.70	175.1
Alanine(A)	6.54	90.1	Lysine(K)	9.15	147.1

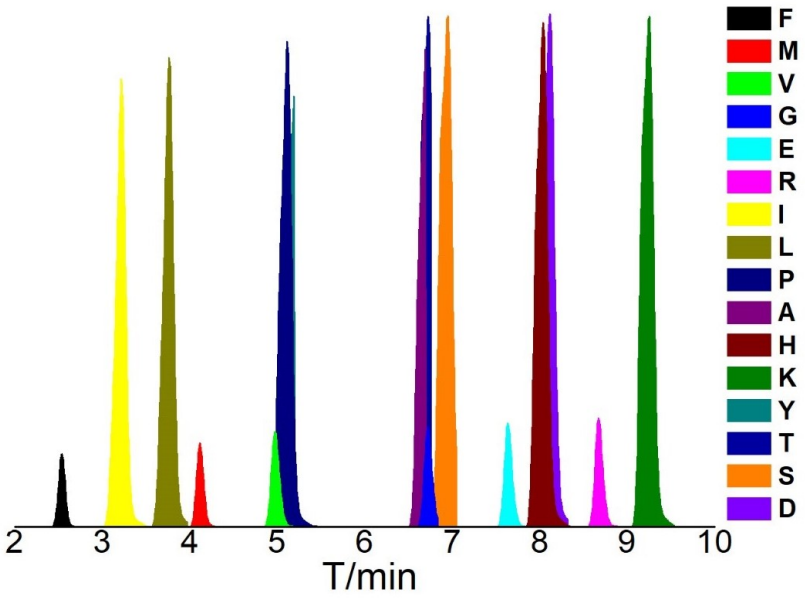

Figure 32. Separation of 16 amino acids in the disc processed blood sample using the HILIC-Z column.

To verify the coupling of disc processed samples, two different kinds of MS detection methods were utilized. HILIC LC-MS has become a standard method, and was employed to demonstrate the coverage of 16 underivatized Amino Acids (AA) in a blood sample, following Agilent's protocol for these 16 AA. Initial studies were performed on the 16 AAs in buffer using the HILIC LC-MS method, following preparation with the disc protocol. As Figure 32 displays, AAs in the disc-processed blood sample were successfully analyzed by LC/MS under positive mode with combination of HILIC, which means only one analyte is eluted at each specific retention time and m/z (Table 6). A standard mix of amino acids was prepared according to the Agilent protocol. Similar ion counts were observed for the blood sample and for the standard mix, indicating major ion suppression problems present in a whole blood or plasma sample were removed by the disc preparation procedure. Other than leucine/isoleucine no two m/z values obtained from extracted ion chromatograms were observed to be the same. Consequently, the HILIC-MS study also verifies that m/z peaks in SMALDI-MS data can be correctly matched to the expected target amino acids.

So even though SALDI-MS/MS fragment data was not obtained, we still could confirm that there is no other chemical with a similar mass sharing one m/z peak when using SALDI MS for quantification, other than Leucine/Isoleucine.

3.3.4. Fast estimation of target molecules by SALDI-MS Analysis

Table 7.SALDI-MS quantitative results for glutamic acid and citric acid in the human blood sample.

Analyte	Internal standard	[s] /μM	Ix /Is	[x] /μM	C in HMDB /μM
L-Glutamic acid	L-Glutamic acid-^{15}N	50.01	0.82	41.01	65.19 +/- 48.71 [277]
Citric acid	Citric acid-1,5-$^{13}C_2$	100.04	1.26	126.05	80.2 +/- 44.9 [244]

[s] is the concentration of the internal standard, [x] concentration of the analyte;

Is is ion counts of the internal standard, Ix is ion counts of the standard.

Using the perfluoro-coated silicon GLAD films for SALDI-MS allows study of a large range of both amino acids, small organic acids and other low molecular weight metabolites, as we have demonstrated previously. In contrast, HILIC LC-MS is good at analyzing small polar molecules like amino acids, but eluting strong polarity acids with amino acids under the same setting and column is still challenging. As a trial to our previous work has established the range, detection limits and capabilities of the SALDI-MS method once sample cleanup is completed. In this report we have focused on rapid analysis of one amino acid and one acid with easily available isotope internal standards, by SALDI-MS, utilizing the integrated, automated disc procedure described here to perform single point calibration assays. The isotope standard is added before the blood sample is processed by the microfluidic device, so any matrix effects and impact of selective adsorption is substantially compensated. We have previously shown that the SALDI-MS method gives quantitative results in agreement with more complex, multi-step standard addition calibration curve-based HILIC-MS method.[189] Therefore, the SLADI-MS quantitative results were not

compared with results from other detection approaches again. To align with the simplicity of the centrifugal microfluidic device, one point isotope standard addition method was adopted for rapid SALDI-MS semi-quantification. Which means the concentration results were read by comparing ion counts of the isotope standard (*Is*) and the corresponding analyte (*Ix*). Table. 7 shows that the concentration results for glutamic acid and citric acid in a fresh blood sample agree with concentration data from the human metabolites database (HMDB) for healthy adults.

3.4. **Conclusion**

The centrifugal fluid device provides an integrated, automated and effective method for sample preparation starting from whole blood, facilitating all steps of sample preparation for downstream small molecule analysis. With an output of ~ 5µL of sample from 190 µL blood sample input, it is a clear demonstration of the sample in to sample out concept for a chip-in-a-lab application. The device, when coupled with the LC-MS, shows a wide range of coverage of amino acids. The convenient desalting function of nanoporous perfluoro coated Si-GLAD thin films provides sensitive, quantitative analysis when coupled with the integrated sample processing on disc. SALDI-MS measurements also allow simultaneous organic acid determination along with amino acids. The successfully coupling of the blood sample preparation disc with both LC-MS and SALDI-MS shows great potential for this device in metabolite analysis. This device fills a void in centrifugal device application to small, polar molecule extraction in blood samples, which have previously been shown to be effective for DNA/RNA[278] and proteins[279] assays from blood samples. The device is well suited to batch, clinical analysis of samples given it can be operated with a conventional benchtop centrifuge, and does not require operator intervention or significant skill in

sample preparation on the part of a technician, providing potential usefulness as routine research and clinical analysis assay.

Chapter 4. An automated centrifugal microfluidic system integrated with etalon sensor films for rapid image analysis based detection of progesterone

4.1. Introduction

Progesterone (P4) (pregn-4-ene-3, 20-dione) is a steroid hormone with α, β unsaturated ketone structure, which plays an important role in the maintenance of female reproductive tissues.[280, 281] The uterus secretes P4 to prepare for pregnancy as well as maintain the pregnancy in the period after conception.[282] In clinic diagnosis, a well-established method for measuring ovulation is to measure serum progesterone concentration in the middle-luteal phase. In the livestock industry, changes in progesterone levels are employed to predict estrus. Both naturally excreted P4, including its metabolites, along with artificial progestins that are broadly used as growth promoters for domestic animals and in human pharmaceuticals, contaminate the aquatic environment via agricultural run-offs and wastewater.[283] In this report, when present a centrifugal microfluidic system, combined with etalon-based biochemical sensors, that establishes a pathway towards a system for point of care (or point of sampling) devices, that can rapidly report on concentration of this steroid, using relatively unsophisticated equipment that could be transported to the field.

Progesterone levels can be measured in blood plasma or milk.[284] Svennersten-Sjaunja[285] emphasized the importance of quick and effective cow-side methods in the future. Consequently, biosensors for online progesterone measurements have been presented in recent studies.[286, 287] Some studies have claimed that their biosensor could directly detect Progesterone concentrations in whole blood.[282] However, results in detection finished in unprocessed whole blood results cannot reflect the actual concentrations considering the status of P4. Because only a tiny

percentage of P4 are free to distribute, and most of P4 is bound with proteins in the blood.[288] [289] Progesterone in milk samples depends on the amount of milk fat because progesterone is present in the milk fat globule and bound to proteins present in the aqueous phase as a true solution. As a result, steroid displacement and lipid extraction are performed to release bound progesterone before either enzyme linked immunosorbent assays (ELISA)[290] or liquid chromatography- mass spectrometry (LC-MS) analysis.[291]

Most peptide hormones in wastes are rapidly degraded, however steroid hormones such as progesterone are chemically stable and are excreted in the free form, or as conjugates which bio-transform to the free form quite easily.[292, 293] Besides the use of contraceptives, humans are exposed to either natural or synthetic progestins through contaminated water, seafood and milk products.[294, 295] Excessive consumption of milk with a high P4 content can lead to breast and lung cancer.[296] Fatigue, fluid retention, lipid level changes, dysphoria, hypercoagulant states, and increased androgenicity are all potential side effects of high levels of P4 in women.[297] P4 is described as a female hormone in most encyclopedias and textbooks, however, there are no significant differences in progesterone secretion or serum progesterone levels between men and women. The role of progesterone as a modulator of the male endocrine system has become increasingly evident.[298] Even constant exposure to a very low concentration of endogenous or exogenous hormone could lead to health issues in human beings and animals. The animal model experiment shows developmental exposure to progestins causes male bias and precocious puberty[298]. Not only can constant exposure to P4 cause sexual precocity in females and male feminization, but it is also proven to be a potential carcinogen.[299] Consider that each pregnant cow releases 4400 mg gestagen through urinary/fecal excretion averagely per year.[300] With the growing size of the global livestock industry, more and more steroid hormone will enter the environment

through sewage and livestock excreta. Hence, the need for an easy, fast, and sensitive system to detect steroid hormones like P4 in environmental, food and clinical samples,[301] although the instrumentation required will differ in some aspects due to the significantly different sample matrices.

Due to its potential to incorporate and automate multiple sample-handling steps, minimize reagent and sample consumption, provide short reaction times and enable multiplexed analyses, lab-on-chip technology attracts great interest for on-site analysis.[14, 302] Microfluidic devices have demonstrated their potential for a broad range of applications in environmental monitoring[303], food safety[304] and clinic diagnostics.[305, 306] Micro-devices for detection of hormones by immunoassay have been reported, avoiding the need for sophisticated lab-based methods, such as high-performance liquid chromatography (HPLC),[307] LC-MS and gas chromatography-mass spectrometry (GC-MS).[308] However, immunoassays still require development of specific and sensitive capture moieties, multiple incubation/washing steps and may use radioactive or fluorescent tagging materials.[309, 310,311]

In this report we adapt etalon-bead technology, for specific chemical identification with an aptamer, within a centrifugal microfluidic device format. The device provides simple user-operation, including a sample clean-up, single step-incubation, followed by delivery of wash and stimulus reagents, to give an on-device display that can be read by a simple, cell phone grade, camera arrangement. Centrifugal microfluidic platforms are actuated using a spindle motor as the driving force for microfluidic flow, thus eliminating the need for pumps, making the systems particularly suitable for applications where low grade instrumentation is a key, such as in point-of-care or point of analysis deployment of bioanalytical assays. These so called Lab-on-a-disc systems have been

previously shown to be effective in deployment of various assays and detection platforms.[312] The DNA aptamer modified etalon is a novel sensor surface that enables colorimetric detection of the target molecule from complex matrices with a cell phone camera level readout design. To further enable the deployment of this etalon technology, its integration into a microfluidic platform offers considerable opportunity for on-device sensing without a complicated optical readout in an on-site setting.[313]

Etalon Background

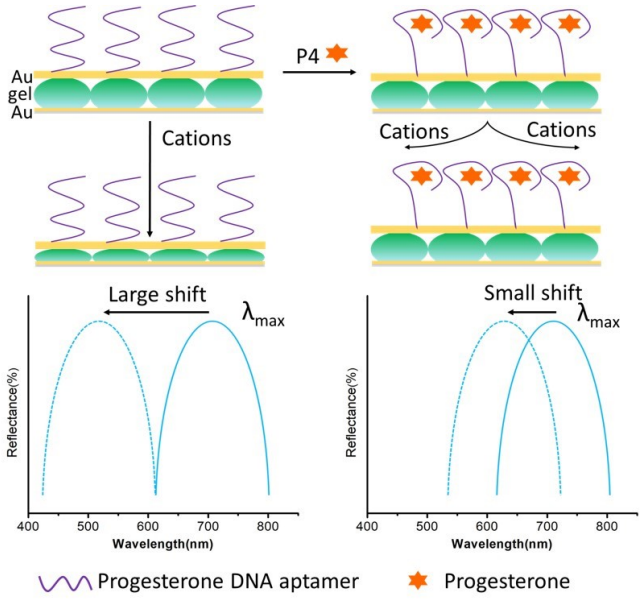

Figure 33. Schematic of an etalon sensing process. The etalon sensor is fabricated on a glass substrate, which having two 15nm Au layers sandwiching a microgel layer. With the DNA aptamer engaging P4 and producing a specific secondary structure that prevents Na^+ from entering the etalons' microgel layer (right); the degree of blockage is proportional to the amount of P4 in the sample.

Etalons are optical devices fabricated by sandwiching poly(N-isopropylacrylamide)-co-acrylic acid microgels (pNIPAm) between two thin gold layers that act as mirrors.[314, 315] When light strikes

the etalon sensor, it undergoes constructive and destructive interference[316] within the etalon's microgel-based cavity that results in a visual color due to selective reflectance of certain wavelengths of light. This easy-to-operate trait of etalons makes them a promising sensor for integration into a centrifugal microfluidic system. The principle of an etalon for P4 detection is that Na^+ ions can change the solvation state of the gel, changing its thickness and optical characteristics by changing the distance between two Au layers (Figure 33).

In this work, the top layer Au of the etalon is modified with anti-P4 DNA aptamer that is reported to show high selectivity in milk sample contains 17β-estradiol, estrone, estriol, cortisol, norethisterone and quinolones.[317, 318] P4 in a sample binds to a DNA aptamer modified etalon, and so blocks Na^+ from entering the microgel layer.[319] As a result, the concentration of P4 is inversely related to reflectance peak shifts. The etalon's selectivity and ability to quantify P4 have been previously demonstrated in off-chip work, by directly measuring peak shifts in the reflectance spectrum. However, to further simplify the on-chip readout process, this work will employ image color analysis to monitor the reflected light color change.

4.2. **Experimental section**

4.2.1. Materials

N-Isopropylacrylamide (NIPAm) was purchased from TCI (Portland, OR, USA) and purified by recrystallization from hexanes (ACS reagent grade, EMD, Gibbstown, NJ, USA) prior to use. N, N-methylenebisacrylamide (BIS) (99%), acrylic acid (AAc) (99%), ammonium persulfate (APS) (> 98%), Tris (2-carboxyethyl) phosphine hydrochloride (TCEP), dextran-coated charcoal and P4

were purchased from Sigma-Aldrich (Oakville, ON, Canada) and used as received. All tests used de-ionized (DI) water with a resistivity of 18.2 M·cm. The 10 × 10 × 0.16 mm glass coverslips were obtained from Fisher Scientific. Au (99.99%) was provided by MRCS (Edmonton, AB, Canada). Cr (99.999%) was purchased from ESPI (Ashland, OR, USA). Disulfide-modified P4 DNA aptamers were obtained from IDT (Toronto, ON, Canada). All dairy products were bought from local grocery store and kept in 4°C fridge until use. All experiments were carried out at room temperature (21 ± 1 °C), if not specifically stated.

4.2.2. Microgel synthesis and Etalon fabrication

Poly (N-isopropylacrylamide-co-acrylic acid) (pNIPAm-co- AAc) microgels were synthesized via surfactant-free, free radical precipitation polymerization as described previously. Briefly, NIPAm (11.9 mmol) and BIS (0.7 mmol) were dissolved in 99 mL DI water with stirring in a beaker followed by filtration through a 0.2-μm filter into a 200-mL 3-neck round bottom flask. The solution was bubbled with N_2 gas for 1.5 hours while heating to 70 °C. AAc (1.4 mmol) and a 1-mL aqueous solution of 0.2 M APS were added to the heated mixture, respectively. The reaction was allowed to proceed for 4 h at 70 °C followed by cooling to room temperature and stirring overnight. The mixture was then filtered through glass wool to remove any large aggregates, then polymer was pelleted by centrifugation (~8500 rcf), washed to remove unreacted monomer and resuspended in DI water, for 6 wash cycles.

A “paint-on” protocol was used to fabricate microgel-based etalons. Au-coated glass surfaces were generated by thermally evaporating 2 nm of Cr (for adhesion) followed by 15 nm of Au onto 10 × 10 × 0.16 mm precleaned glass coverslips at a rate of ~ 0.1 and ~ 0.15 Å s−1, respectively, using

a model THEUPG thermal evaporation system (Torr International Inc., New Windsor, NY). Custom-made metal masks with 4 open windows 2.5×2.5 mm were applied to create 4 small squares on each glass coverslip during thermal evaporation coating. 10 microliters of concentrated pNIPAm-co-AAc microgels (obtained by centrifugation) was then spread on the Au/Cr-coated substrate and the microgel solution was allowed to dry completely on the substrate for 2 h at 35 °C. The resultant substrate was then rinsed copiously with DI water to remove any excess microgels not bound directly to the Au and allowed to soak in DI water overnight at 30 °C. Following this step, the substrate was rinsed again with DI water, dried with N_2 gas, and an additional layer of 2 nm Cr and 15 nm Au was deposited.

4.2.3. Reflectance spectroscopy and optical microscopy

Previously reported methods were used to collect the reflectance spectra from the etalons, and measure the size of microgels.[320] Reflectance spectroscopy measurements were performed using a USB2000+ spectrophotometer, a HL-2000-FHSA tungsten light source, and an R400-7-VIS-NIR optical fiber reflectance probe from Ocean Optics (Dunedin, FL, USA). The spectra were collected using OceanView Spectroscopy Software from 350–1000 nm. Optical microscopy images of the pNIPAm-co-AAc microgels were obtained using an Olympus IX71 inverted microscope (Markham, ON, Canada) fitted with a 100X oil-immersion objective, an Andor Technology iXon camera (Belfast, Ireland). Andor SOLIS v4.15.3000.0 software was used to record microscopy images of the microgels.

4.2.4. Etalon surface modification of DNA aptamers

Thiol-modified anti-P4 DNA aptamer (HO-(CH_2)6-S-S-(CH2)6-5'-GCATCACACACCGATAC-TCACCCGCCTGATTAACATTAGCCCACCGCCCACCCCCGCTGC 3')[321] was purchased from IDT (Toronto, ON, Canada). The DNA aptamer was coupled to freshly prepared etalon devices via S-Au binding. Monolayer surfaces were prepared by immersing the clean gold substrate in a 1.0 µM solution of anti-P4 DNA aptamer in 1M KH_2PO_4 for 2 hours, followed by a 1h exposure of the sample to an aqueous solution of 1.0 mM 6-mercapto-1-hexanol (MCH). Before analysis or hybridization, each etalon slide was rinsed thoroughly with the binding buffer.

4.2.5. Design and fabrication of the centrifugal disc

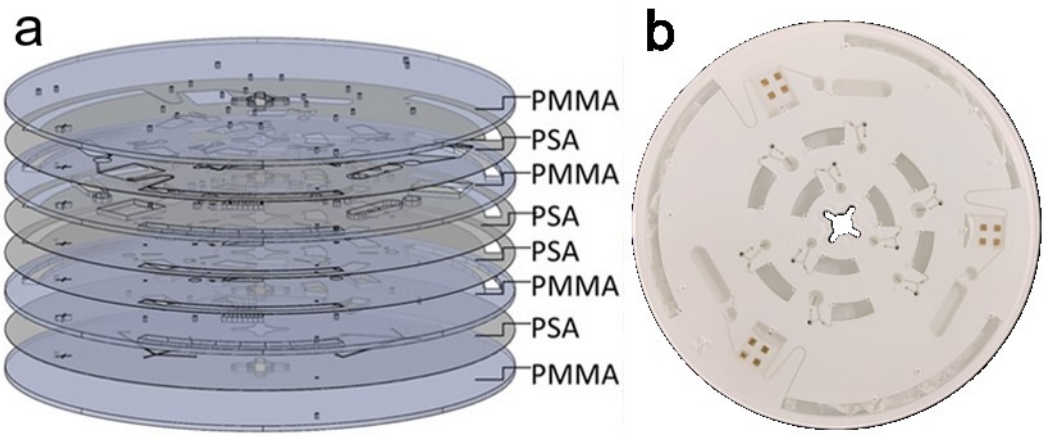

Figure 34. Microfluidic disk's components: 4 layers of 126 µm PSA and 4 layers of 1.5 mm PMMA(a). Photo of the assembled disc with embedded etalons (b)Each disc includes three individual reaction units.

This device consists of four layers of PMMA-poly (methyl methacrylate) and four layers of PSA-pressure sensitive adhesive (Figure 34). Features are cut out by laser cutter and layers are then laminated. Chambers are created by cutting through PMMA sheets. The double sided PSA bonds layers together with pressure from the laminator. Most of the channels were fabricated on PSA.

The thin PSA layers make these channels small enough to neatly fluids transfer as well as realizing a siphon effect. Dissolvable film (DF) tabs carried by PSA were inserted between two adjacent PSA layers to create DF pneumatic valves.[30] The small glass slides on which etalons are fabricated, were embedded during lamination. Each glass slide was fixed by PSA, and aligned to ensure the same location in each reaction unit. The glass slide was aligned by the left side and left bottom corner of the incubation chamber. Once the top layer was assembled, the buffer solution could be pipetted into the etalon chamber for the storage of modified etalons. Strips of non-woven fabrics were paved onto the PSA of the waste chamber, to prevent reverse siphoning from the waste storage chamber to the etalon incubation chamber.

4.2.6. Photo taken and RGB extraction

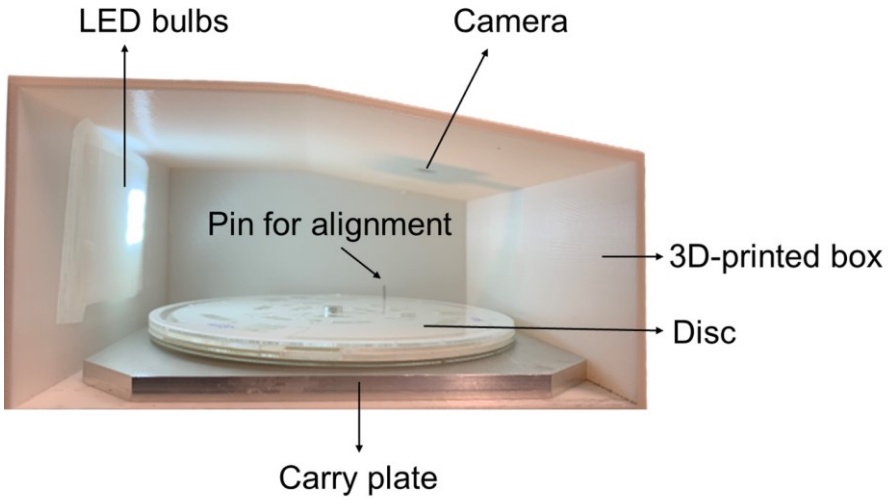

Figure 35. The photo of the 3D-printed camera box with labels of each element.

All photos of etalons were taken inside an imaging box in a darkroom. The imaging box was rapid-prototyped by using a 3D printer after designing according to well-established principles[322]. Three parameters were considered for controlling the image capturing conditions which included light level, distance and the angle between the etalon and the camera. The light level was easy to control

with a specific light source and background elimination by working in a darkroom. Constant distance and angle from the camera to the etalon were realized by establishing the camera and the etalon (Figure 35) in fixed locations.

The 3D-printed box was designed with two small open holes and one door to avoid any drilling or polishing work after printing. The one on the back wall was provided for the power cable of the LED array, which gave a constant light level. The LED array was attached on the back wall by double side tape. The power cable hole could be fully covered by the LED array which furtherly decreases light noise from the environment. The other small hole was for the camera to look through. The camera was fixed on a roof tilted 10 degrees, to enable the collection of reflectance color. The camera was fixed on the sloping roof of the box, which was 3D- printed with Polylactic Acid (PLA) filament. A custom metal plate with 90-degree edges which fit the right-angle corner of the box was used to carry the disc to the same position under the camera for photo shooting. There are three pinholes fabricated on the metal plate to accommodate pins, which correspond to pin holes on the disc. Therefore, etalons in each unit operator on the disc will be exposed to the same view under the camera. All photos were taken in the box, so the LED bulb fixed inside the box was the only light source. As a proof-of-concept, a Raspberry Pi Camera Module (V2-8 Megapixel,1080p (RPI-CAM-V2)), CanaKit Raspberry Pi 3 B+ (B Plus) Starter Kit (32 GB EVO+ Edition, Premium Black Case) and Raspberry Pi Touch Screen (5 Inch TFT LCD Display HDMI Module) are all purchased from Amazon to use as a substitute model of a cell phone. A desktop button was written to take a photo with one click of the symbol on a touch screen. Central 85 pixels area in each etalon square were cropped by Macromedia Fireworks MX 2004. All RGB (red, green and blue) data was read from copped images by MathWorks R2021a.

4.3. Results and discussion

4.3.1. Developing a milk processing platform for optical readout on-disc

The first round of a point-of need measurement system design was focussed on demonstrating the ability to prepare a P4-spiked milk sample for analysis, using integrated etalon-sensors for detection and quantification of the spiked P4. Anyone who has rinsed and cleaned a glass of milk knows the film it leaves on glass is tenacious, and so rinsing for optical measurements within a lab-on-a disc was the first challenge approached. A subsequent sample preparation step, in which P4 is separated from protein carries in the milk, by a method such as methanol precipitation and/or denaturing of the protein carrier, is to be part of subsequent efforts, outside the scope of this thesis. The performance of etalon sensors for determining P4, their integration within the device for sensing purposes, and readout by colorimetric methods with a camera represent another key aspect of the project that required development.

A number of functions must be accomplished on disc to utilize etalons for P4 sensing: these include

1) Deliver the sample to P4-selective etalon in a specific chamber on the disc, allow incubation and enhance mass transport,

2) Wash the etalon with buffer, removing milk residue from the etalons and the optical window on the disc.

3) Introduce the salt solution required to trigger a color change of the etalon.

The on-disc processing steps can be performed with three primary chambers, with additional valves, detection and waste chambers. The three large grey circles in Figure 36 isolate the solution loading zone at the top of the figure, an incubation zone with a feature, E, to aid in mixing to enhance mass transport to the lower left, and a waste storage zone to the bottom right. These functional modules are connected by channels and valves.

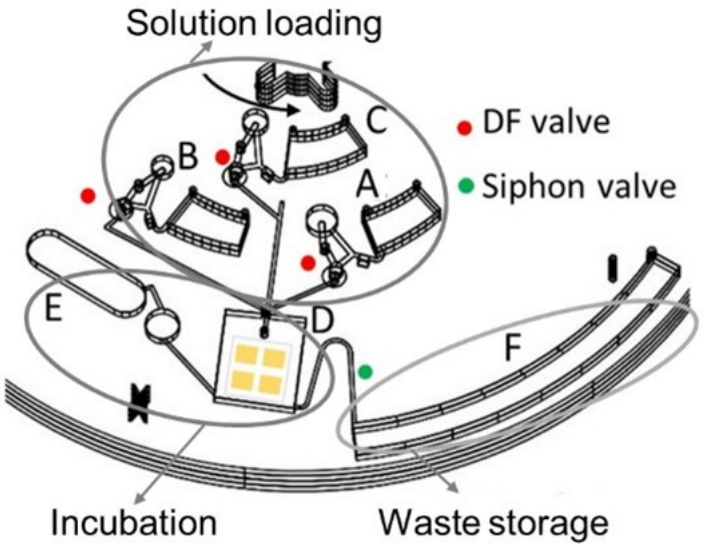

Figure 36. 3D view of the design details for each unit. Chambers are labeled by capital letters, valves are labeled by dots, and functional modules are circled

Table 8. List of the function of each chamber and the releasing frequency of the following valves.

Chamber	Function	Release speed/rpm
A	Sample loading	2100
B	Wash buffer loading	2700
C	Salt solution loading	3300
D	Incubation	300
E	Pneumatic mixing	NA
F	On-disc waste storage	NA

In the solution loading zone, chambers A, B, and C are fabricated with the same volume to store the preloaded sample solution, wash buffer, and salt solution separately. Three DF valves are assigned to control solution release from each of these three chambers (Table 8). These DF valves

are designed to burst at different spinning frequencies to realizing sequential releasing of the different solutions in the required order.

The incubation function is realized in chamber D, where a set of 4 etalons are embedded, with solution agitation facilitated by Chamber E. Etalons in chamber D react with the sample, then wash buffer, then salt solution as controlled by the design of burst speed for each DF valve. The pneumatic chamber E is able to push the air in and out chamber D during an oscillated rotation mode to enhance the reaction exchange rate in chamber D, and to enhance rinsing of the surfaces in the device.

Once incubation is completed, the sample solution is transferred to waste chamber F for on-disc waste storage by a siphon channel. The siphon valve only primes in a stationary state or low spinning rate. Which means the siphon channel is closed during sample loading and incubation. This property of the siphon valve provides a simple procedure for sequential transfer of sample and rinse buffer to waste, before delivery of the salt development solution.

The disk design was optimized by running the disk on a visualization platform equipped with a camera and synchronized strobe light.[130] The preloaded sample aliquots are selected as 200 μL, to guarantee the immersion of etalons during oscillation rotation mode, which pumps the air pressure in and out of chamber E to allow movement of the solvent in chamber D. The height of the siphon bridge is also adjusted according to this sample volume to ensure opening during low spinning speed. By incorporating fabrics in chamber F, no liquid suck back from the waste chamber is observed.

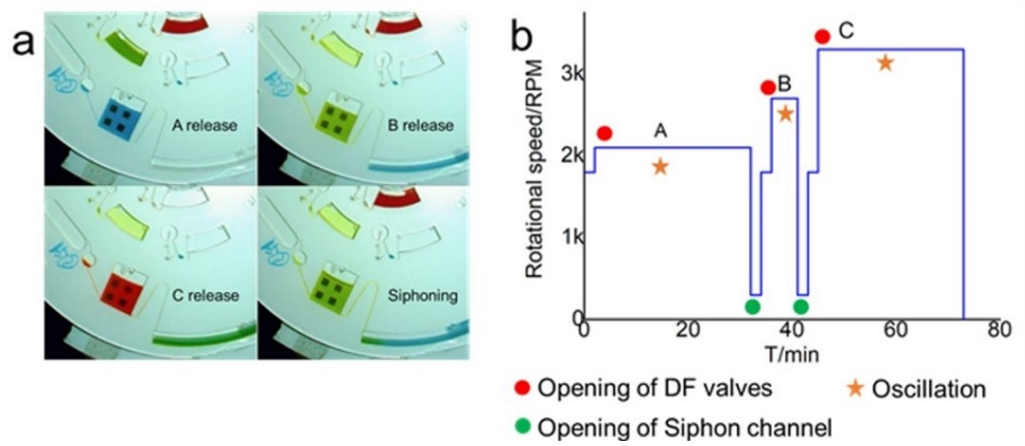

Figure 37. (a) Images from on-disc procedure video. Different dye solutions are used to demonstrate the sequential transfer of solutions in chambers A, B, and C. (b) Diagram of the operational spinning speed with a timeline. Opening of DF valves and the siphon channel.

As both the diagram and photos in Figure 37 show, the disk is first spun at 1800 rpm to transfer the buffer used during etalon storage to the waste chamber. The spinning speed then increases to 2100 rpm to burst the first DF valve, which releases the sample solution from chamber A to the incubation Chamber D. Incubation is conducted with oscillation between 900 rpm to 1500 rpm, with an acceleration of 300 rpm/sec. The exchange between solution in the incubation chamber and the etalon is facilitated by the side chamber, which is a reservoir for pressurized air during oscillation, creating constant motion of the solvent to aid in mass transport. After 30 minutes of incubation, the sample solution is transferred to the waste chamber by the siphon channel, which opens at 300 rpm. Once chamber D is emptied, the spinning speed is increased to 2700 rpm which releases the wash buffer from chamber B. The wash step takes five minutes under programmed oscillation. Then the wash buffer is transferred to the waste chamber in the same way as the previous sample solution. The last 1M NaCl developing solution, that triggers the etalon color change, is released at the highest spinning frequency of 3300 rpm. Incubation is again conducted with oscillating speed to agitate the solvent. Finally, the disc is transferred to the camera box for photo shoots after 30 minutes reaction. Video in SI confirms the automated running of all on-disc

assay procedures. By programming the spinning speed with DF valve burst frequencies and siphon primary frequency, we achieve a sample-to-answer etalon-based sensor system on the disc.

4.3.2. Microgel characterization and etalon fabrication

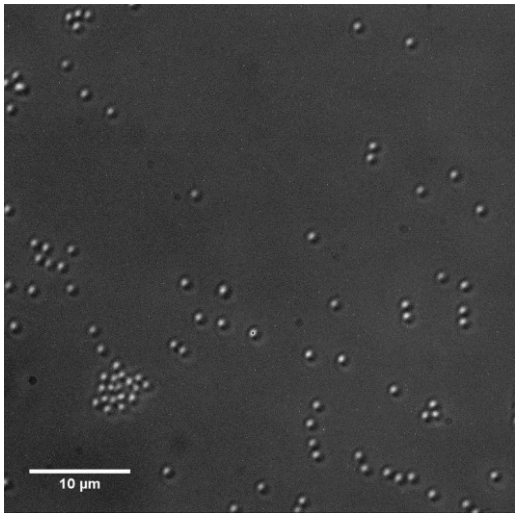

Figure 38. DIC optical microscopy image of diluted pNIPAm-co-AAc microgels on a glass slide, the scale bar is 10 µm.

Figure 38 shows an image of pNIPAm-co-AAc microgels under differential interference contrast (DIC) microscopy. Compared to the 10 µm scale bar, the microgels show a diameter of about 1 µm. More detailed analysis of these micrographs shows the size ranges from 1.0-1.2 µm. To image individual microgel particles 20 µL of concentrated microgel solution was diluted in 1 mL of DI water before spreading on a slide. Assembled etalon arrays were prepared by painting the concentrated microgel solution on glass slides, to form a monolayer and create the middle layer of the etalon sandwich structure. Salts like NaCl cause desolvation of the microgel reflected by a change in the microgel layer thickness. A previous study showed that microgel particle diameter decreases with the increasing concentration of NaCl.

To verify the performance of the sandwich structured etalon sensor, the response of fabricated etalons to salt solution was studied by reflectance spectroscopy. Figure 39 shows that the microgel

layer responded to salt with a shift in the reflectance spectrum to longer wavelength. The decrease of the distance between the top and bottom Au layer triggered the reflectance peak to move toward longer wavelength range. Obviously, this will also cause a change in the observed color of the etalon.

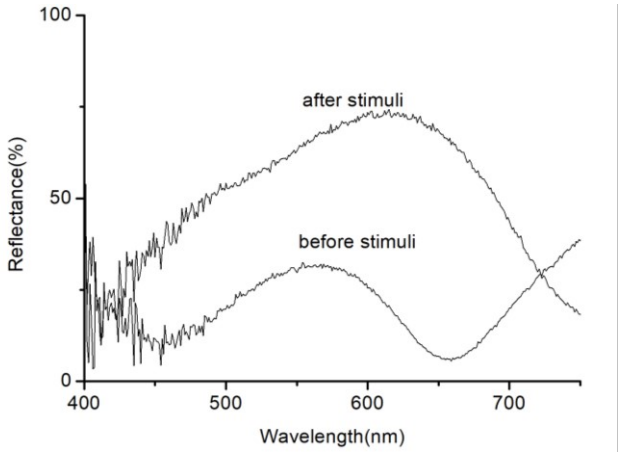

Figure 39. The reflectance spectrum obtained from an etalon used in this study. The reflectance peak moves toward longer wavelength (red) when the microgel layer shrinks in salt solution.

4.3.3. P4-DNA aptamer modification

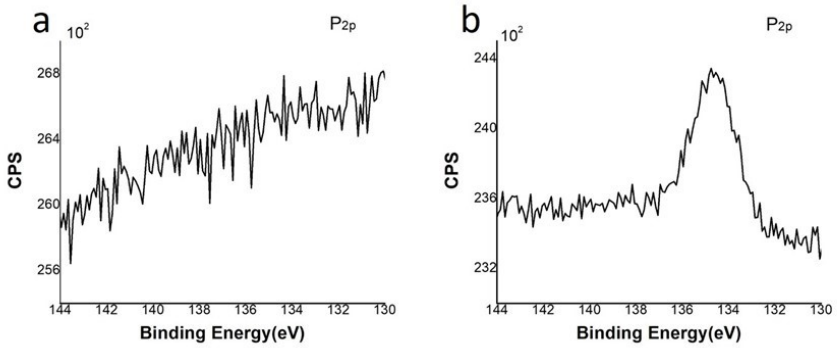

Figure 40. XPS spectrum of the (a) bare etalon and (b) the P4 aptamer-modified etalon. The peak of element P in (b) suggests that the aptamer was successfully modified on the etalon surface.

A single-strand DNA aptamer was used to modify the bare gold surface of the etalon, through a thiol group on the aptamer. Presence of the aptamer after modification was determined using XPS

to detect P present as PO_4^{3-} in the backbone of the DNA helix.[323] Figure 40 shows the XPS spectra for P on the surface of the etalon before (a) and after (b) DNA aptamer modification. There is no P peak on the bare Au etalon surface, while after modification with DNA aptamers, an obvious P peak with a binding energy of 130-132 eV[324] was present. Successful modification of DNA aptamer on the etalon's top Au surface was confirmed by the observed P_{2p} binding peak.

4.3.4. P4 detection in a sample

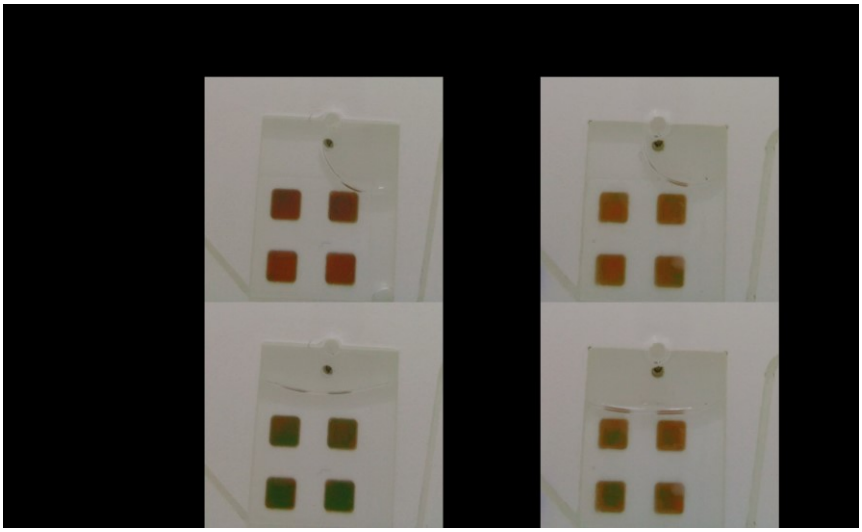

Figure 41. Real color changes of etalons in NaCl solution incubated without P4 (a)and with P4(b).

To simplify the on-chip readout process, this work employs image color analysis to monitor change in the reflected light of the modified etalon. Compared to monitoring reflectance spectra, image analysis avoids the employment of specialized equipment such as fiber optic probes and spectrometers. Figure 41 shows photos of an etalon film (a) incubated with 40 pg/ml P4 for 30 mins, and (b) an etalon film incubated with buffer solution for 30 mins for a control. Both etalons were then exposed to the salt developing solution, for microgel dehydration. The bottom images show that the etalon incubated with P4 exhibited a smaller colour change, because of the blockage caused by the DNA aptamer binding to P4. Based on a previous study, 500 mM NaCl gives the

maximum change of the microgel diameter and the largest change in the reflectance of the etalon. Herein, we directly adopted 1 M NaCl solution as the stimuli, which is a higher concentration than the optimal concentration, to guarantee the fast and maximum microgel response. Several concentrations of P4 were studied by extracting the RGB data from the corresponding etalon photographs. The results are shown in Figure 42 as a G channel-based calibration curve for different concentrations of P4 in delivered samples. The linear plot equation is Y= (6.5890±0.15274) - (8.118 ±0.34) %X with regression coefficient R2=0.9930. The LOD is estimated to be 5.64pg/mL with a linear range from 0 to 81.17 pg/mL.

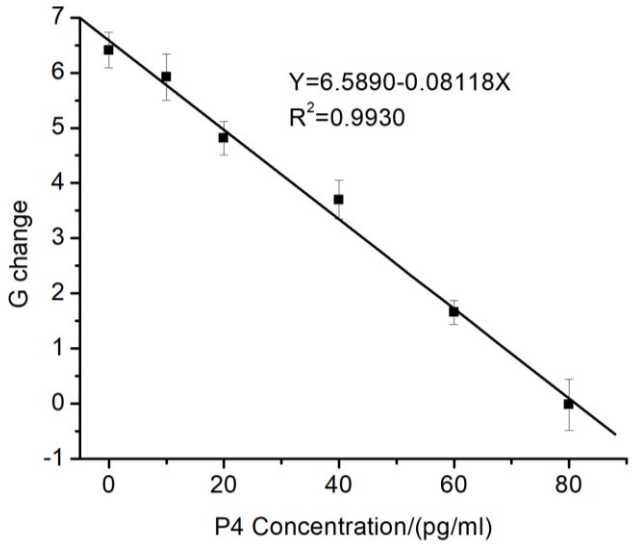

Figure 42. Green color changes of the P4 modified etalons in response to 1M NaCl as a function of P4 concentration.

To verify the etalon performance in milk, we compared the G changes of etalon incubate with 0% fat milk and charcoal processed 0% fat milk separately. The etalon incubated with charcoal processed milk shows a larger green color change as progesterone is removed by charcoal adsorption.[325] Furthermore, P4 detection results of 0%, 2% fat milk and cream imply the same increasing P4 concentration tendency as results from literature.[326]

4.4. **Conclusion**

With the integration of modified Etalon, this disc realized automated P4 detection in 3 unit steps within 1 hour and 10 mins, which is much faster than existing technology like HPLC or ELISA. P4 can be quantified in aqueous solution via the modification of the etalon surface with anti-P4 DNA aptamers. The sensor's ability to detect different P4 concentrations was determined by image analysis of the etalon's color changes in 1 M NaCl. The LOD was estimated to be 5.64 pg/mL, with good linearity with a R^2 value of 0.9930. The LOD is much lower than the P4 concentration range in milk(0.1 to 18 ng/ml)[327]. The maximum P4 concentration that could be detected is 81.17pg/ml, which is near to the mean value of P4 level in river water.[328] This is the first time that P4 DNA aptamer detection has been demonstrated on an on-site deployable microfluidic automatic system for rapid detection in the field. Also, this is the first time that a simple and convenient color image colour analysis other than reflectance spectrum was adopted to read the etalon's response to stimuli. The device is very compact and low cost, at the same time, the detection sensitivity is relatively high. All these above features of this system indicate the potential use of the sensor as an on-site P4 testing method for aqueous samples. Furthermore, these four etalons on each glass cover slide can enable multiplexed analyte analysis using specific DNA aptamer probes. For instance, different etalons on one glass slide could be modified by anti-Estradiol, anti-Progesterone, anti-Testosterone DNA aptamer[329] and anti-cortisol[330] DAN aptamer separately to realize steroid hormones detection routinely undergoing in clinics. The etalons modification is flexible with the target molecule on demand thus opening up possibilities for on-site detection of various targets in a simple point of use device. Our demonstrator here provides a foundation of an easy-to-use and versatile device for hormone detection in an aqueous sample which exhibits potential applications in environmental monitoring, food regulation and clinical diagnostics.

Chapter 5. Concluding Remarks and Future Work

5.1. Concluding remarks

In this thesis, three different centrifugal microfluidic devices have been explored for bio-chemical application. The key link between the three devices is integration of the processing steps required to determine small, polar or non-polar biomarkers in complex sample matrices, specifically plasma, blood and milk.

Chapter 2 lays out a strategy to develop the chip-in-a-lab concept to a deliverable approach. Since the spread of this technology has been limited by the perceived need to integrate all processing steps, up to and including analytical readout of the device, the effort in this chapter and Chapter 3 signals success in using a microfluidic system to deliver sample back into a laboratory stream. The disc fabrication technique used in Chapter 2 is simple, inexpensive, and rapid, but it has limitations in terms of solvents that can be used for sample preparation, the types of valves that can be utilized, and the rotational speeds that can be attained. Nevertheless, the project illustrates that rapid sample preparation of plasma on a disk can then be integrated into downstream laboratory methods that ultimately lead to mass spectrometric analysis of small, polar metabolites of relevance for disease diagnostics. The results compare favourably with HILIC-MS, which tends to be regarded as a gold standard for small polar metabolite analysis.

To more fully automate blood sample preparation for small molecules, a more sophisticated device fabrication technology was employed, through collaboration with the lab of Jens Ducrée of Dublin City University. Chapter 3 describes an automatic sample processing disc using preloaded reagent and functional particles, in which blood is directly introduced, then plasma is generated by

centrifugal precipitation. The supernatant plasma is then transferred and metered by a pneumatic valve. Plasma is mixed with methanol (3:1 v/v) in a disc shaking mode to denature proteins. C18 and silica particles further clean up lipids released by organic solvent denaturation, and remaining proteins, in a very similar clean up procedure to that used in Chapter 2, again using pneumatic mixing. The optimization of on-disc procedures is performed by observing the sample spot crystallization and S/N ratio of target analytes of MALDI-MS. The powerful tool for small polar molecule analysis, HILIC-MS, is employed to verify the sample was processed correctly by the disc. All expected 16 amino acids were successfully eluted and detected with excellent peak shape. The disc can be run by regular centrifuges using a simple adaptor without any additional instrument. This work demonstrates the prototype disc can be a practical tool in the labs, preparing samples for a variety of analytical techniques. Further improvements to meet the challenges in a laboratory environment are proposed in chapter 5.2.1.

Chapter 4 explored another type of application of centrifugal microfluidic, which is suitable for point-of-care and on-site use. Usually, data readout is integrated on a disc without any other extraordinary instrument. Optical techniques are the most commonly used detection approaches, not only for centrifugal systems but also for bioassays in general. Absorbance and fluorescence readouts are common, but they do require some sophistication in the instrumentation. In this chapter we have collaborated with Mike Serpe's group at the University of Alberta, to embed their etalon sensor into the centrifugal microfluidic system, allowing a simple cell-phone camera like readout. A hormone detection etalon was developed for farmers to schedule artificial insemination by estimating cow's estrus, although the final step of P4 release from milk protein has not yet been developed within the project. Nevertheless, the device demonstrates the ability to deliver, and then rinse away the milk matrix, and give a readout based upon the etalon and camera concepts. As we

pushed the conventional reflectance detection to a more convenient alternative image color analysis, we aimed the protocol for the device for a general point of care and on-site use, including diagnosis, food, and environment monitoring. All steps required for DNA aptamer modified etalon censoring such as incubation, wash, and stimulating are automated with sequential bursting pneumatic valves and siphon valves. The G channel image color shows a good linearity relationship with P4 concentrations in the clean sample. Strategies to use the methanol precipitation steps described in Chapters 2 and 3 to release P4, and other sample handling steps are discussed in Chapter 5.2.2.

5.2. Future work

5.2.1. Improving blood processing disc towards central lab use

We aim to develop the blood processing disc as a practical tool that could replace the routine bench-top blood preparation and save both time and labour in central labs. Therefore, future work will be focused on improving the user experience. The current blood sample load used could be fully met by the volume that is yielded by lancing the fingertip.[331] However, efforts would still be required to minimize the sample load to reduce the pain of punctures, considering the blood volume and finger prick pain level increase with lancet diameter and penetration depth.[332] Also, a lower loading volume could make the device easier to use for challenging patients such as children and dehydrated patients. To achieve this goal, we would keep current on-disc procedures the same, but down-scale the size of each chamber, including the sample loading chamber, and change the corresponding setting of valves to ensure the sequential releasing.

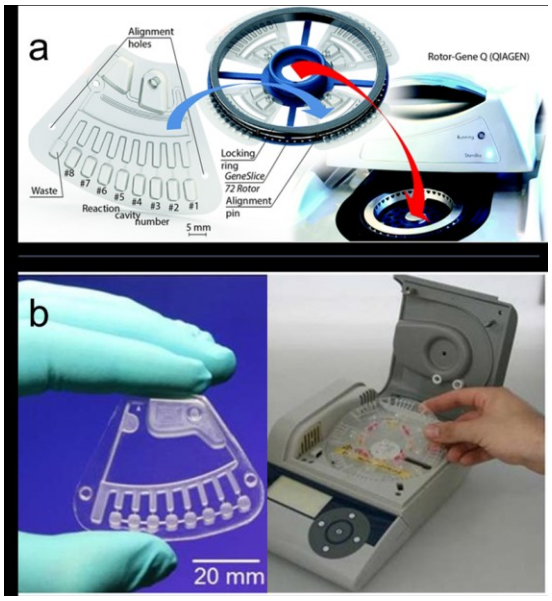

Figure 43. Insertion of disk segment into a custom rotor(a) and disc player(b). a: © The Royal Society of Chemistry 2015. b: © PLOS 2014.

Furthermore, the disc will redesign to enable direct capillary blood sampling. Usually, parallel reaction units are fabricated on an integral disc which is convenient and straightforward. However, segment each unit is already well studied in commercial products, making the disc operation more flexible. Figure 43 shows how disc segments fit into a spin platform in two ways, and individual segments could be carried by either a disc[333](Figure 43. a) or a rotor holder[334] (Figure 43. b). The flexibility of disc slice makes it easier to accomplish fingertip capillary blood sampling illustrated in Figure 44 without contaminating other units.[335]

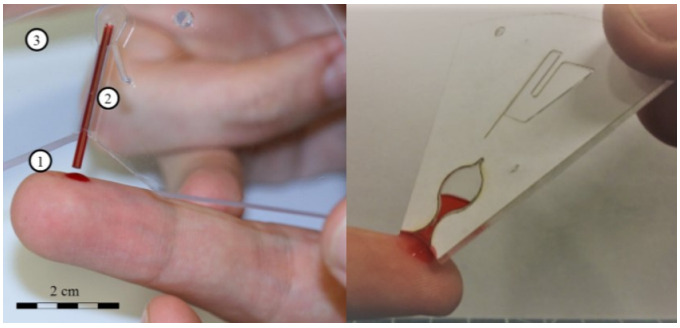

Figure 44. Different designs for capillary finger-prick blood loading performance. Left: © CBMS 2012. Right: with permission from the author- Joao Pedro Barreira.

5.2.2. Combined disc design for testing P4 in bio-samples.

Methanol is known to be an effective progesterone extraction solvent.[336] This fact provides the possibility of a combination of the disc designs in chapters 3 and 4. The methanol procedure employed for protein precipitation in the blood sample preparation disc could also be adapted to extract progesterone for the etalon sensor disk. The only change required, other than an added solvent chamber, is rearranging the burst frequencies of the blood cell separation chamber, the ethanol mixing chamber, and the three reagent-releasing valves in the P4 detection disc by a sequential way in one disc. Currently, the methanol rinse is not compatible with the etalon sensor design. The etalon edges are sealed with nail polish which cannot withstand an organic solvent like methanol. Sealing the edge by Au edges using masks is predicted to yield better etalon reproducibility than manually applied nail polish, and would make the system methanol compatible.

Overall, we demonstrate protocols for one sample-in-clean-sample-out and one sample-to-answer centrifugal device to develop practical centrifugal devices for both sample processing and detection. Before putting these designs into practical use, efforts still need to be involved in quality control. The commercial Piccolo Xpress® device has a comprehensive quality control system built in its disc spinner/analyzer. The so-called INTELLIGENT QUALITY CONTROL (IQC®) covering checks for preloaded reagents, reactions on disc, fluidics, and detection signal adjustment.[337] This thorough IQC® ensures the output result is accurate and reliable for each fully automated on-disc test. A similar approach could be applied to our system to ensure each on-disc performance is reliable. Also, customized quality control approaches will be developed to meet specific tasks for our discs. For example, on-disc color calibration could be added into the P4

detection device by introducing a built-in reflective color card to calibrate the camera system[338, 339] or a separate assay channel with an embedded unmodified etalon to calibrate the response of etalon to salt.[270] Also, a sensor embedded in the spinner helping read the real-time status of valves could give feedback for automatically adjusting the spinner, which avoids failure in disc operations caused by the opening frequency variance of the DF valves. There are likely other, more sophisticated approaches to further validate each operation on disc, but these ones are key to confidence in their operation.

5.2.3. Embedding P4 detection sensor on digital microfluidic platform

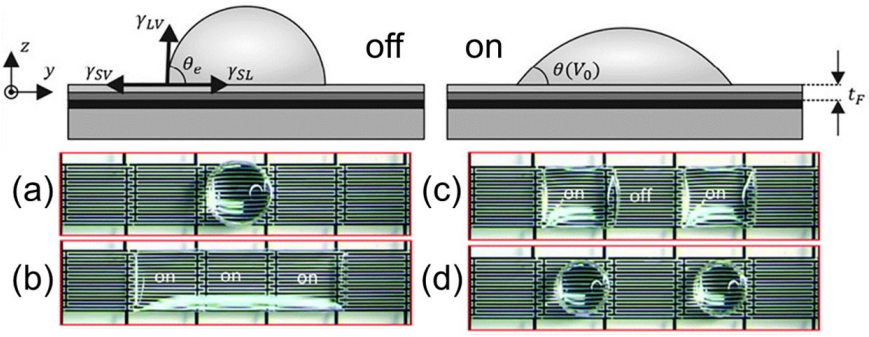

Figure 45. Schematic (top) of the contact angle change before and after applying voltage. Droplet wetting and splitting by powering on/off three pads (a)-(d). © Royal Society of Chemistry 2017. © Elsevier 2018.

Digital microfluidics (DMF) involves the operation of tiny, discrete droplets on a microlitre or smaller scale. Dispensing droplets, transferring droplets, joining droplets, and combining contents within a droplet are the critical tasks of DMF. Electrowetting-on-dielectric is one of the most common DMF techniques (EWOD).[340] A droplet is positioned between two plates, one of which has a dielectric layer. A voltage difference around the droplet causes asymmetric contact angles between the droplets, resulting in a driving force (Figure 45). The droplet is moved by switching the voltage difference promptly. Improved versions of the EWOD model, such as optoelectro-

wetting[341] and dielectro-wetting,[342] and a variety of techniques for DMF fluid/droplet handling have been developed.[343, 344]

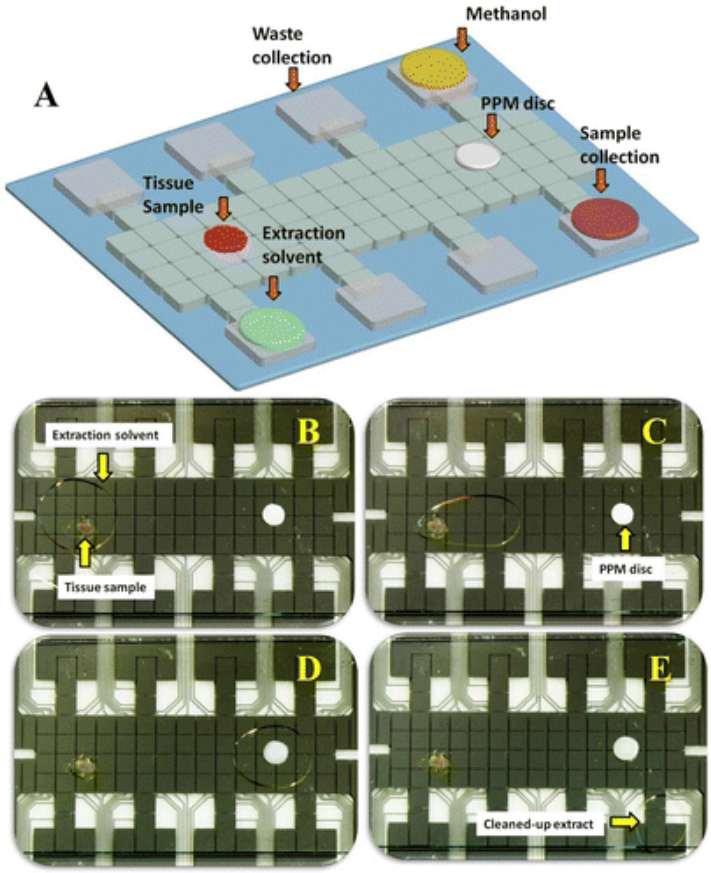

Figure 46. (A)Schematic of the digital microfluidics for steroid extraction from a tissue sample. (B - C) Images from a video recording liquid-phase extraction. (D - E) Solid-phase extraction on porous polymer disc. © American Chemical Society 2015.

Preparing the analyte for integration to the on-chip detection system is crucial in most diagnostic and chemical detection applications, especially for complicated biosamples.[345] DMF is already applied to blood cell separation,[269] protein extraction,[249] steroid extraction[346] and small molecules extraction.[347] Furthermore, miniaturized and automated systems for hormone analysis in blood[346] and tissue samples[348] are well developed (Figure 46). All typical assay steps, including sample lysing, estradiol extraction by methanol, nonpolar solvent extraction of unwanted components, and

separation of the two phases after liquid-liquid extraction, are integrated into one DMF platform. So DMF might be regarded as a mature and reliable technology for bio-sample preparation.

Besides significant progress in fabrication, miniaturization, and programming of DMF operations, the ability to couple with detection approaches is another crucial factor strengthening the device's competition for biochemical applications.[349] Optical, mass spectrometry and electrochemical detection are already used in combination with EWOD devices for biochemical applications. Optical and electrochemical "online" detection methods are more prevalent than MS detection as online mass spectrometry is reported mainly by employing MALDI-MS.[350] Optical detection has been extensively used in miniaturized biochemical analysis systems because of multiple advantages, such as a non-invasive mode of operation, the ability to perform multiple sensing, and the fast readout.[351]

Investigation of integrating Etalon sensors in the DMF platform has not been reported yet. After communication with research groups focusing on developing DMF devices, we found it is accessible to apply etalon sensors on DMF plates. Etalon sensors are usually fabrication on slide glasses, which could be easily taped on the DMF platform. On the other hand, the camera used for monitoring the droplet movement in a conventional DMF setting is also useful in monitoring the etalon color changes without additional optical detection equipment. Therefore, we would like to explore the possibility of etalon sensors integrated DMF systems providing both bio-sample processing and quick steroid detection in the future.

References

1. R. P. Feynman, 1959.
2. A. Manz, N. Graber and H. á. Widmer, *Sensors and actuators B: Chemical*, 1990, **1**, 244-248.
3. C. D. Chin, V. Linder and S. K. Sia, *Lab on a Chip*, 2012, **12**, 2118-2134.
4. P. Cui and S. Wang, *Journal of Pharmaceutical Analysis*, 2019, **9**, 238-247.
5. M. Gustafsson, D. Hirschberg, C. Palmberg, H. Jörnvall and T. Bergman, *Analytical chemistry*, 2004, **76**, 345-350.
6. S. Haeberle, N. Schmitt, R. Zengerle and J. Ducrée, *Sensors and Actuators A: Physical*, 2007, **135**, 28-33.
7. O. Strohmeier, M. Keller, F. Schwemmer, S. Zehnle, D. Mark, F. von Stetten, R. Zengerle and N. Paust, *Chemical Society Reviews*, 2015, **44**, 6187-6229.
8. C. Burtis, J. Mailen, W. Johnson, C. Scott, T. Tiffany and N. Anderson, *Clinical chemistry*, 1972, **18**, 753-761.
9. M. J. Madou and G. J. Kellogg, 1998.
10. R. Gorkin, J. Park, J. Siegrist, M. Amasia, B. S. Lee, J.-M. Park, J. Kim, H. Kim, M. Madou and Y.-K. Cho, *Lab on a Chip*, 2010, **10**, 1758-1773.
11. D. C. Duffy, H. L. Gillis, J. Lin, N. F. Sheppard and G. J. Kellogg, *Analytical Chemistry*, 1999, **71**, 4669-4678.
12. R. D. Johnson, I. H. Badr, G. Barrett, S. Lai, Y. Lu, M. J. Madou and L. G. Bachas, *Analytical chemistry*, 2001, **73**, 3940-3946.
13. S. Lai, S. Wang, J. Luo, L. J. Lee, S.-T. Yang and M. J. Madou, *Analytical Chemistry*, 2004, **76**, 1832-1837.
14. I. J. Michael, T.-H. Kim, V. Sunkara and Y.-K. Cho, *Micromachines*, 2016, **7**, 32.
15. J. M. Onorato, R. Langish, A. Bellamine and P. Shipkova, *Journal of separation science*, 2010, **33**, 923-929.
16. Q. Wang, T. R. Slaney, W. Wu, R. Ludwig, L. Tao and A. Leone, *Analytical Chemistry*, 2020, **92**, 10327-10335.

17. J. Ducrée, in *Encyclopedia of Microfluidics and Nanofluidics*, ed. D. Li, Springer US, Boston, MA, 2008, DOI: 10.1007/978-0-387-48998-8_203, pp. 234-245.
18. M. Madadelahi, L. F. Acosta-Soto, S. Hosseini, S. O. Martinez-Chapa and M. J. Madou, *Lab on a Chip*, 2020, **20**, 1318-1357.
19. M. C. Kong and E. D. Salin, *Analytical Chemistry*, 2010, **82**, 8039-8041.
20. M. Tang, G. Wang, S.-K. Kong and H.-P. Ho, *Micromachines*, 2016, **7**, 26.
21. K. Abi-Samra, R. Hanson, M. Madou and R. A. Gorkin III, *Lab on a Chip*, 2011, **11**, 723-726.
22. W. Al-Faqheri, F. Ibrahim, T. H. G. Thio, J. Moebius, K. Joseph, H. Arof and M. Madou, *PloS one*, 2013, **8**, e58523.
23. M. M. Aeinehvand, L. Weber, M. Jiménez, A. Palermo, M. Bauer, F. F. Loeffler, F. Ibrahim, F. Breitling, J. Korvink and M. Madou, *Lab on a Chip*, 2019, **19**, 1090-1100.
24. T. H. G. Thio, S. Soroori, F. Ibrahim, W. Al-Faqheri, N. Soin, L. Kulinsky and M. Madou, *Medical & biological engineering & computing*, 2013, **51**, 525-535.
25. J. M. Chen, P.-C. Huang and M.-G. Lin, *Microfluidics and Nanofluidics*, 2008, **4**, 427-437.
26. T. Thio, A. Nozari, N. Soin, M. Kahar, S. Dawal, K. Samra, M. Madou and F. Ibrahim, 2011.
27. J. Hoffmann, D. Mark, R. Zengerle and F. Von Stetten, 2009.
28. H. Hwang, H.-H. Kim and Y.-K. Cho, *Lab on a Chip*, 2011, **11**, 1434-1436.
29. D. Mark, T. Metz, S. Haeberle, S. Lutz, J. Ducrée, R. Zengerle and F. von Stetten, *Lab on a Chip*, 2009, **9**, 3599-3603.
30. R. Gorkin III, C. E. Nwankire, J. Gaughran, X. Zhang, G. G. Donohoe, M. Rook, R. O'Kennedy and J. Ducrée, *Lab on a Chip*, 2012, **12**, 2894-2902.
31. J. V. Zoval and M. J. Madou, *Proceedings of the IEEE*, 2004, **92**, 140-153.
32. J. Peyman, A. A. Nozari, N. Soin and F. Ibrahim, 2009.
33. H. He, Y. Yuan, W. Wang, N.-R. Chiou, A. J. Epstein and L. J. Lee, *Biomicrofluidics*, 2009, **3**, 022401.
34. M. Focke, R. Feuerstein, F. Stumpf, D. Mark, T. Metz, R. Zengerle and F. v. Stetten.
35. N. Honda, U. Lindberg, P. Andersson, S. Hoffmann and H. Takei, *Clinical Chemistry*, 2005, **51**, 1955-1961.

36. Y. Ouyang, S. Wang, J. Li, P. S. Riehl, M. Begley and J. P. Landers, *Lab on a Chip*, 2013, **13**, 1762-1771.
37. J. Siegrist, R. Gorkin, L. Clime, E. Roy, R. Peytavi, H. Kido, M. Bergeron, T. Veres and M. Madou, *Microfluidics and Nanofluidics*, 2010, **9**, 55-63.
38. H. Kido, M. Micic, D. Smith, J. Zoval, J. Norton and M. Madou, *Colloids and Surfaces B: Biointerfaces*, 2007, **58**, 44-51.
39. I. Beaulieu, M. Geissler and J. Mauzeroll, *Langmuir*, 2009, **25**, 7169-7176.
40. A. Larsson and H. Dérand, *Journal of colloid and interface science*, 2002, **246**, 214-221.
41. J. Steigert, T. Brenner, M. Grumann, L. Riegger, S. Lutz, R. Zengerle and J. Ducrée, *Biomedical Microdevices*, 2007, **9**, 675-679.
42. F. Schwemmer, S. Zehnle, D. Mark, F. von Stetten, R. Zengerle and N. Paust, *Lab on a Chip*, 2015, **15**, 1545-1553.
43. D. J. Kinahan, S. M. Kearney, O. P. Faneuil, M. T. Glynn, N. Dimov and J. Ducrée, *RSC advances*, 2015, **5**, 1818-1826.
44. Y. Ukita, M. Ishizawa, Y. Takamura and Y. Utsumi, 2012.
45. H. Eral and J. Oh, *Colloid and polymer science*, 2013, **291**, 247-260.
46. S. Okamoto and Y. Ukita, *Sensors and Actuators B: Chemical*, 2018, **261**, 264-270.
47. J.-M. Park, Y.-K. Cho, B.-S. Lee, J.-G. Lee and C. Ko, *Lab on a Chip*, 2007, **7**, 557-564.
48. Z. Cai, J. Xiang and W. Wang, *Sensors and Actuators B: Chemical*, 2015, **221**, 257-264.
49. U. Y. Schaff and G. J. Sommer, *Clinical Chemistry*, 2011, **57**, 753-761.
50. M. Amasia, M. Cozzens and M. J. Madou, *Sensors and Actuators B: Chemical*, 2012, **161**, 1191-1197.
51. Y.-K. Cho, J.-G. Lee, J.-M. Park, B.-S. Lee, Y. Lee and C. Ko, *Lab on a Chip*, 2007, **7**, 565-573.
52. D. J. Kinahan, P. L. Early, A. Vembadi, E. MacNamara, N. A. Kilcawley, T. Glennon, D. Diamond, D. Brabazon and J. Ducrée, *Lab on a Chip*, 2016, **16**, 3454-3459.
53. D. Mark, P. Weber, S. Lutz, M. Focke, R. Zengerle and F. von Stetten, *Microfluidics and Nanofluidics*, 2011, **10**, 1279-1288.
54. P. Andersson, G. Jesson, G. Kylberg, G. Ekstrand and G. Thorsén, *Analytical Chemistry*, 2007, **79**, 4022-4030.

55. J. Steigert, M. Grumann, T. Brenner, L. Riegger, J. Harter, R. Zengerle and J. Ducrée, *Lab on a Chip*, 2006, **6**, 1040-1044.
56. L. Clime, D. Brassard, M. Geissler and T. Veres, *Lab on a Chip*, 2015, **15**, 2400-2411.
57. B. H. Park, J. H. Jung, H. Zhang, N. Y. Lee and T. S. Seo, *Lab on a Chip*, 2012, **12**, 3875-3881.
58. Y. Ukita, Y. Takamura and Y. Utsumi, *Sensors and Actuators B: Chemical*, 2015, **220**, 180-183.
59. M. Grumann, A. Geipel, L. Riegger, R. Zengerle and J. Ducrée, *Lab on a Chip*, 2005, **5**, 560-565.
60. Y. Ren and W. W.-F. Leung, *International Journal of Heat and Mass Transfer*, 2013, **60**, 95-104.
61. J. Steigert, M. Grumann, T. Brenner, K. Mittenbühler, T. Nann, J. Rühe, I. Moser, S. Haeberle, L. Riegger and J. Riegler, *JALA: Journal of the Association for Laboratory Automation*, 2005, **10**, 331-341.
62. J. Ducrée, S. Haeberle, T. Brenner, T. Glatzel and R. Zengerle, *Microfluidics and Nanofluidics*, 2006, **2**, 97-105.
63. J.-N. Kuo and L.-R. Jiang, *Microsystem technologies*, 2014, **20**, 91-99.
64. Y. Ukita and Y. Takamura, *Microfluidics and Nanofluidics*, 2013, **15**, 829-837.
65. R. Burger, N. Reis, J. Fonseca and J. Ducree, 2009.
66. M. C. Kong and E. D. Salin, *Microfluidics and Nanofluidics*, 2012, **13**, 519-525.
67. A. LaCroix-Fralish, E. J. Templeton, E. D. Salin and C. D. Skinner, *Lab on a Chip*, 2009, **9**, 3151-3154.
68. H. Naito, S. Okamoto and Y. Ukita, *Electronics and Communications in Japan*, 2020, **103**, 29-35.
69. C. E. Nwankire, I. Maguire, D. Kernan, M. Glynn, D. Kirby and J. Ducrée, 2015.
70. E. J. Templeton and E. D. Salin, *Microfluidics and Nanofluidics*, 2014, **17**, 245-251.
71. A. Lee, J. Park, M. Lim, V. Sunkara, S. Y. Kim, G. H. Kim, M.-H. Kim and Y.-K. Cho, *Analytical chemistry*, 2014, **86**, 11349-11356.
72. R. Martinez-Duarte, R. A. Gorkin III, K. Abi-Samra and M. J. Madou, *Lab on a Chip*, 2010, **10**, 1030-1043.

73. M. Boettcher, M. S. Jaeger, L. Riegger, J. Ducrée, R. Zengerle and C. Duschl, *Biophysical Reviews and Letters*, 2006, **1**, 443-451.
74. H. Hwang, Y. Kim, J. Cho, J.-y. Lee, M.-S. Choi and Y.-K. Cho, *Analytical Chemistry*, 2013, **85**, 2954-2960.
75. S. Haeberle, T. Brenner, R. Zengerle and J. Ducrée, *Lab on a Chip*, 2006, **6**, 776-781.
76. B.-S. Li and J.-N. Kuo, 2013.
77. M. Müller, D. Mark, M. Rombach, G. Roth, J. Hoffmann, R. Zengerle and F. von Stetten, 2010.
78. J. H. Jung, B. H. Park, Y. K. Choi and T. S. Seo, *Lab on a Chip*, 2013, **13**, 3383-3388.
79. G. Jia, K.-S. Ma, J. Kim, J. V. Zoval, R. Peytavi, M. G. Bergeron and M. J. Madou, *Sensors and Actuators B: Chemical*, 2006, **114**, 173-181.
80. R. Peytavi, F. R. Raymond, D. Gagné, F. J. Picard, G. Jia, J. Zoval, M. Madou, K. Boissinot, M. Boissinot and L. Bissonnette, *Clinical Chemistry*, 2005, **51**, 1836-1844.
81. B. S. Lee, J.-N. Lee, J.-M. Park, J.-G. Lee, S. Kim, Y.-K. Cho and C. Ko, *Lab on a Chip*, 2009, **9**, 1548-1555.
82. B. S. Lee, Y. U. Lee, H.-S. Kim, T.-H. Kim, J. Park, J.-G. Lee, J. Kim, H. Kim, W. G. Lee and Y.-K. Cho, *Lab on a Chip*, 2011, **11**, 70-78.
83. H. Nagai, Y. Narita, M. Ohtaki, K. Saito and S.-i. Wakida, *Analytical Sciences*, 2007, **23**, 975-979.
84. Z. Noroozi, H. Kido, R. Peytavi, R. Nakajima-Sasaki, A. Jasinskas, M. Micic, P. L. Felgner and M. J. Madou, *Review of Scientific Instruments*, 2011, **82**, 064303.
85. O. Strohmeier, A. Emperle, G. Roth, D. Mark, R. Zengerle and F. von Stetten, *Lab on a Chip*, 2013, **13**, 146-155.
86. M. J. Madou, Y. Lu, S. Lai, C. G. Koh, L. J. Lee and B. R. Wenner, *Sensors and Actuators A: Physical*, 2001, **91**, 301-306.
87. A. B. Azouz, S. Murphy, S. Karazi, M. Vázquez and D. Brabazon, *Materials and Manufacturing Processes*, 2014, **29**, 93-99.
88. Y. Zhang, J. Xiang, Y. Wang, Z. Qiao and W. Wang, 2019.
89. B. K. Gale, A. R. Jafek, C. J. Lambert, B. L. Goenner, H. Moghimifam, U. C. Nze and S. K. Kamarapu, *Inventions*, 2018, **3**, 60.
90. Y. Xi, D. A. Duford and E. D. Salin, *Talanta*, 2010, **82**, 1072-1076.

91. P. Nath, D. Fung, Y. A. Kunde, A. Zeytun, B. Branch and G. Goddard, *Lab on a Chip*, 2010, **10**, 2286-2291.
92. N. Godino, R. Gorkin III, A. V. Linares, R. Burger and J. Ducrée, *Lab on a Chip*, 2013, **13**, 685-694.
93. D. J. Kinahan, L. A. Julius, C. Schoen, T. Dreo and J. Ducrée, 2018.
94. M. Mahmud, E. J. Blondeel, M. Kaddoura and B. D. MacDonald, *Micromachines*, 2018, **9**, 220.
95. D. I. Walsh III, D. S. Kong, S. K. Murthy and P. A. Carr, *Trends in biotechnology*, 2017, **35**, 383-392.
96. M. Focke, D. Kosse, C. Müller, H. Reinecke, R. Zengerle and F. von Stetten, *Lab on a Chip*, 2010, **10**, 1365-1386.
97. J. S. Mecomber, A. M. Stalcup, D. Hurd, H. B. Halsall, W. R. Heineman, C. J. Seliskar, K. R. Wehmeyer and P. A. Limbach, *Analytical Chemistry*, 2006, **78**, 936-941.
98. J. S. Mecomber, D. Hurd and P. A. Limbach, *International Journal of Machine Tools and Manufacture*, 2005, **45**, 1542-1550.
99. M. Galloway, W. Stryjewski, A. Henry, S. M. Ford, S. Llopis, R. L. McCarley and S. A. Soper, *Analytical Chemistry*, 2002, **74**, 2407-2415.
100. K. M. Weerakoon-Ratnayake, C. E. O'Neil, F. I. Uba and S. A. Soper, *Lab on a Chip*, 2017, **17**, 362-381.
101. J. Wu and M. Gu, *Journal of biomedical optics*, 2011, **16**, 080901.
102. L. Riegger, O. Strohmeier, B. Faltin, R. Zengerle and P. Koltay, *Journal of Micromechanics and Microengineering*, 2010, **20**, 087003.
103. X. Zhu, G. Liu, Y. Guo and Y. Tian, *Microsystem Technologies*, 2007, **13**, 403-407.
104. D. Ogończyk, J. Węgrzyn, P. Jankowski, B. Dąbrowski and P. Garstecki, *Lab on a Chip*, 2010, **10**, 1324-1327.
105. A. E. Ongaro, D. Di Giuseppe, A. Kermanizadeh, A. M. Crespo, A. Mencatti, L. Ghibelli, V. Mancini, K. L. Wlodarczyk, D. P. Hand and E. Martinelli, *bioRxiv*, 2019, 647347.
106. L. Martynova, L. E. Locascio, M. Gaitan, G. W. Kramer, R. G. Christensen and W. A. MacCrehan, *Analytical Chemistry*, 1997, **69**, 4783-4789.
107. R. T. Kelly and A. T. Woolley, *Analytical Chemistry*, 2003, **75**, 1941-1945.

108. S. Li, J. Xu, Y. Wang, Y. Lu and G. Luo, *Journal of Micromechanics and Microengineering*, 2008, **19**, 015035.
109. P. Salvo, R. Verplancke, F. Bossuyt, D. Latta, B. Vandecasteele, C. Liu and J. Vanfleteren, *Microfluidics and Nanofluidics*, 2012, **13**, 987-991.
110. M. Diaz-Gonzalez and A. Baldi, *Analytical Chemistry*, 2012, **84**, 7838-7844.
111. P.-C. Chen and C.-C. Chen, *Sensors and Actuators A: Physical*, 2017, **258**, 105-114.
112. C. Matellan and E. Armando, *Scientific reports*, 2018, **8**, 1-13.
113. C.-W. Tsao, *Micromachines*, 2016, **7**, 225.
114. J. Kim, R. Surapaneni and B. K. Gale, *Lab on a Chip*, 2009, **9**, 1290-1293.
115. H. Y. Tan, W. K. Loke and N.-T. Nguyen, *Sensors and Actuators B: Chemical*, 2010, **151**, 133-139.
116. J. Kim, Y. Shin, S. Song, J. Lee and J. Kim, *Sensors and Actuators B: Chemical*, 2014, **202**, 60-66.
117. D. Patko, Z. Mártonfalvi, B. Kovacs, F. Vonderviszt, M. Kellermayer and R. Horvath, *Sensors and Actuators B: Chemical*, 2014, **196**, 352-356.
118. S. E. Weigum, P. N. Floriano, N. Christodoulides and J. T. McDevitt, *Lab on a Chip*, 2007, **7**, 995-1003.
119. Y. Liu, C. B. Rauch, R. L. Stevens, R. Lenigk, J. Yang, D. B. Rhine and P. Grodzinski, *Analytical Chemistry*, 2002, **74**, 3063-3070.
120. M. Serra, I. Pereiro, A. Yamada, J.-L. Viovy, S. Descroix and D. Ferraro, *Lab on a Chip*, 2017, **17**, 629-634.
121. G. S. Fiorini and D. T. Chiu, *BioTechniques*, 2005, **38**, 429-446.
122. R. Burger, L. Amato and A. Boisen, *Biosensors and Bioelectronics*, 2016, **76**, 54-67.
123. H. Zhu, S. O. Isikman, O. Mudanyali, A. Greenbaum and A. Ozcan, *Lab on a Chip*, 2013, **13**, 51-67.
124. M. Grumann, J. Steigert, L. Riegger, I. Moser, B. Enderle, K. Riebeseel, G. Urban, R. Zengerle and J. Ducrée, *Biomedical microdevices*, 2006, **8**, 209-214.
125. J. Steigert, M. Grumann, M. Dube, W. Streule, L. Riegger, T. Brenner, P. Koltay, K. Mittmann, R. Zengerle and J. Ducrée, *Sensors and Actuators A: Physical*, 2006, **130**, 228-233.

126. L. Riegger, M. Grumann, T. Nann, J. Riegler, O. Ehlert, W. Bessler, K. Mittenbuehler, G. Urban, L. Pastewka and T. Brenner, *Sensors and Actuators A: Physical*, 2006, **126**, 455-462.
127. T. Hillig, A. B. Nygaard, L. Nekiunaite, J. Klingelhöfer and G. Sölétormos, *Apmis*, 2014, **122**, 545-551.
128. I. Kubo, T. Kanamatsu and S. Furutani, *Sens. Mater*, 2014, **26**, 615-621.
129. K.-C. Chen, T.-P. Lee, Y.-C. Pan, C.-L. Chiang, C.-L. Chen, Y.-H. Yang, B.-L. Chiang, H. Lee and A. M. Wo, *Clinical chemistry*, 2011, **57**, 586-592.
130. M. Grumann, T. Brenner, C. Beer, R. Zengerle and J. Ducrée, *Review of scientific instruments*, 2005, **76**, 025101.
131. T.-H. Kim, J. Park, C.-J. Kim and Y.-K. Cho, *Analytical Chemistry*, 2014, **86**, 3841-3848.
132. E. Bakker and M. Telting-Diaz, *Analytical Chemistry*, 2002, **74**, 2781-2800.
133. J. D. Newman and A. P. Turner, *Biosensors and bioelectronics*, 2005, **20**, 2435-2453.
134. T. Li, Y. Fan, Y. Cheng and J. Yang, *Lab on a Chip*, 2013, **13**, 2634-2640.
135. S. Z. Andreasen, D. Kwasny, L. Amato, A. L. Brøgger, F. G. Bosco, K. B. Andersen, W. E. Svendsen and A. Boisen, *RSC Advances*, 2015, **5**, 17187-17193.
136. C. E. Nwankire, A. Venkatanarayanan, T. Glennon, T. E. Keyes, R. J. Forster and J. Ducree, *Biosensors and Bioelectronics*, 2015, **68**, 382-389.
137. N. Lion, T. C. Rohner, L. Dayon, I. L. Arnaud, E. Damoc, N. Youhnovski, Z. Y. Wu, C. Roussel, J. Josserand and H. Jensen, *Electrophoresis*, 2003, **24**, 3533-3562.
138. D. L. DeVoe and C. S. Lee, *Electrophoresis*, 2006, **27**, 3559-3568.
139. D. Hirschberg, T. Jägerbrink, J. Samskog, M. Gustafsson, M. Ståhlberg, G. Alvelius, B. Husman, M. Carlquist, H. Jörnvall and T. Bergman, *Analytical Chemistry*, 2004, **76**, 5864-5871.
140. W. A. Korfmacher, *Using mass spectrometry for drug metabolism studies*, CRC Press, 2009.
141. W. C. Cho, *Genomics, proteomics & bioinformatics*, 2007, **5**, 77-85.
142. W. Henderson and J. S. McIndoe, *Mass Spectrometry of Inorganic and Organometallic Compounds: Tools-Techniques-Tips*, John Wiley & Sons, 2005.
143. F. W. Aston, *Proceedings of the Royal Society of London. Series A-Mathematical and Physical Sciences*, 1935, **149**, 396-405.

144. M. Karas and F. Hillenkamp, *Analytical Chemistry*, 1988, **60**, 2299-2301.
145. J. B. Fenn, M. Mann, C. K. Meng, S. F. Wong and C. M. Whitehouse, *Science*, 1989, **246**, 64-71.
146. C. Seger, S. Sturm and H. Stuppner, *Natural product reports*, 2013, **30**, 970-987.
147. E. de Hoffmann, *Journal of mass spectrometry*, 1996, **31**, 129-137.
148. K. Gulyuz, C. N. Stedwell, D. Wang and N. C. Polfer, *Review of Scientific Instruments*, 2011, **82**, 054101.
149. P. A. Limbach, *Spectroscopy*, 1998, **13**, 16-+.
150. J. Banoub, A. Cohen, A. Mansour and P. Thibault, *European Journal of Mass Spectrometry*, 2004, **10**, 121-134.
151. I. G. Gut, *Human mutation*, 2004, **23**, 437-441.
152. M. Balazy, *Prostaglandins & other lipid mediators*, 2004, **73**, 173-180.
153. D. J. Harvey, *International Journal of Mass Spectrometry*, 2003, **226**, 1-35.
154. S. F. Macha and P. A. Limbach, *Current Opinion in Solid State and Materials Science*, 2002, **6**, 213-220.
155. O. Vorm, P. Roepstorff and M. Mann, *Analytical Chemistry*, 1994, **66**, 3281-3287.
156. Y. Dai, R. M. Whittal and L. Li, *Analytical Chemistry*, 1999, **71**, 1087-1091.
157. S. Trimpin, A. Rouhanipour, R. Az, H. J. Räder and K. Müllen, *Rapid Communications in Mass Spectrometry*, 2001, **15**, 1364-1373.
158. A. I. Gusev, W. R. Wilkinson, A. Proctor and D. M. Hercules, *Analytical Chemistry*, 1995, **67**, 1034-1041.
159. S. Urwyler and J. Glaubitz, *Letters in applied microbiology*, 2016, **62**, 130-137.
160. R. S. Brown and J. J. Lennon, *Analytical Chemistry*, 1995, **67**, 1998-2003.
161. M. Vestal, P. Juhasz and S. Martin, *Rapid Communications in Mass Spectrometry*, 1995, **9**, 1044-1050.
162. R. Krüger, A. Pfenninger, I. Fournier, M. Glückmann and M. Karas, *Analytical Chemistry*, 2001, **73**, 5812-5821.
163. S. Hosseini and S. O. Martinez-Chapa, *Fundamentals of MALDI-ToF-MS Analysis*, 2017, 1-19.
164. N. Bergman, D. Shevchenko and J. Bergquist, *Analytical and bioanalytical chemistry*, 2014, **406**, 49-61.

165. S. Chen, L. Chen, J. Wang, J. Hou, Q. He, J. a. Liu, J. Wang, S. Xiong, G. Yang and Z. Nie, *Analytical Chemistry*, 2012, **84**, 10291-10297.
166. T. Porta, C. Grivet, R. Knochenmuss, E. Varesio and G. Hopfgartner, *Journal of mass spectrometry*, 2011, **46**, 144-152.
167. S. Guo, Y. Wang, D. Zhou and Z. Li, *Analytical Chemistry*, 2015, **87**, 5860-5865.
168. E. D. Raczyńska, J.-F. Gal and P.-C. Maria, *International Journal of Mass Spectrometry*, 2017, **418**, 130-139.
169. A. R. Korte and Y. J. Lee, *Journal of Mass Spectrometry*, 2014, **49**, 737-741.
170. Y. Fukuyama, R. Tanimura, K. Maeda, M. Watanabe, S.-I. Kawabata, S. Iwamoto, S. Izumi and K. Tanaka, *Analytical Chemistry*, 2012, **84**, 4237-4243.
171. X. Wang, J. Han, J. Pan and C. H. Borchers, *Analytical Chemistry*, 2014, **86**, 638-646.
172. H. N. Abdelhamid, *Microchimica Acta*, 2018, **185**, 1-16.
173. M. Lu, X. Yang, Y. Yang, P. Qin, X. Wu and Z. Cai, *Nanomaterials*, 2017, **7**, 87.
174. S. A. Trauger, E. P. Go, Z. Shen, J. V. Apon, B. J. Compton, E. S. Bouvier, M. Finn and G. Siuzdak, *Analytical chemistry*, 2004, **76**, 4484-4489.
175. L. Cohen, E. Go and G. Siuzdak, *Journal*, 2007.
176. R. A. Picca, C. D. Calvano, M. J. Lo Faro, B. Fazio, S. Trusso, P. M. Ossi, F. Neri, C. D'Andrea, A. Irrera and N. Cioffi, *Journal of Mass Spectrometry*, 2016, **51**, 849-856.
177. H. Z. Alhmoud, T. M. Guinan, R. Elnathan, H. Kobus and N. H. Voelcker, *Analyst*, 2014, **139**, 5999-6009.
178. A. Kundt, *Annalen der Physik*, 1886, **263**, 59-71.
179. Y. Zhao, D. Ye, G.-C. Wang and T.-M. Lu, 2003.
180. M. Jensen and M. Brett, *Applied Physics A*, 2005, **80**, 763-768.
181. D. Deniz and R. J. Lad, *Journal of Vacuum Science & Technology A: Vacuum, Surfaces, and Films*, 2011, **29**, 011020.
182. J. Wei, J. M. Buriak and G. Siuzdak, *Nature*, 1999, **399**, 243-246.
183. D. A. Gish, F. Nsiah, M. T. McDermott and M. J. Brett, *Analytical Chemistry*, 2007, **79**, 4228-4232.
184. H. Chu, S. Song, D. Gibson and L. Porteous, 2015.
185. R. De, S. M. Haque, M. Sikdar, P. Sahoo, T. Som and K. D. Rao, *Journal of Physics: Condensed Matter*, 2020, **32**, 395701.

186. M. M. Hawkeye and M. J. Brett, *Journal of Vacuum Science & Technology A: Vacuum, Surfaces, and Films*, 2007, **25**, 1317-1335.
187. A. B. Jemere, L. W. Bezuidenhout, M. J. Brett and D. J. Harrison, *Rapid Communications in Mass Spectrometry*, 2010, **24**, 2305-2311.
188. Y. Zhou, C. Peng, K. D. Harris, R. Mandal and D. J. Harrison, *Analytical Chemistry*, 2017, **89**, 3362-3369.
189. Y. Zhao, Y. Hou, J. Ji, F. Khan, T. Thundat and D. J. Harrison, *Analytical Chemistry*, 2019, **91**, 7570-7577.
190. Y. Hsieh, *Journal of separation science*, 2008, **31**, 1481-1491.
191. G. Zhou, H. Pang, Y. Tang, X. Yao, X. Mo, S. Zhu, S. Guo, D. Qian, Y. Qian and S. Su, *Amino Acids*, 2013, **44**, 1293-1305.
192. A. Santos-Fandila, A. Zafra-Gomez, A. Barranco, A. Navalon, R. Rueda and M. Ramirez, *Analytical and bioanalytical chemistry*, 2014, **406**, 2863-2872.
193. P. Krumpochova, B. Bruyneel, D. Molenaar, A. Koukou, M. Wuhrer, W. Niessen and M. Giera, *Journal of pharmaceutical and biomedical analysis*, 2015, **114**, 398-407.
194. H. C. Prinsen, B. Schiebergen-Bronkhorst, M. Roeleveld, J. Jans, M. de Sain-van der Velden, G. Visser, P. Van Hasselt and N. Verhoeven-Duif, *Journal of Inherited Metabolic Disease: Official Journal of the Society for the Study of Inborn Errors of Metabolism*, 2016, **39**, 651-660.
195. X. Wang, W. Li and H. T. Rasmussen, *Journal of Chromatography A*, 2005, **1083**, 58-62.
196. Y. Liu, Q. Du, B. Yang, F. Zhang, C. Chu and X. Liang, *Analyst*, 2012, **137**, 1624-1628.
197. S. Cubbon, T. Bradbury, J. Wilson and J. Thomas-Oates, *Analytical Chemistry*, 2007, **79**, 8911-8918.
198. S. Cubbon, C. Antonio, J. Wilson and J. Thomas-Oates, *Mass spectrometry reviews*, 2010, **29**, 671-684.
199. C. Antonio, T. Larson, A. Gilday, I. Graham, E. Bergström and J. Thomas-Oates, *Rapid Communications in Mass Spectrometry: An International Journal Devoted to the Rapid Dissemination of Up-to-the-Minute Research in Mass Spectrometry*, 2008, **22**, 1399-1407.
200. K. Inoue, R. Obara, T. Hino and H. Oka, *Journal of agricultural and food chemistry*, 2010, **58**, 9918-9924.

201. T. Nemoto, X.-P. Lee, T. Kumazawa, C. Hasegawa, M. Fujishiro, A. Marumo, Y. Shouji, K. Inagaki and K. Sato, *Journal of pharmaceutical and biomedical analysis*, 2014, **88**, 71-80.
202. R. Bogue, *Assembly Automation*, 2012.
203. J. Hu and S. Liu, *Macromolecules*, 2010, **43**, 8315-8330.
204. B. Sierra-Martin, J. R. Retama, M. Laurenti, A. F. Barbero and E. L. Cabarcos, *Advances in colloid and interface science*, 2014, **205**, 113-123.
205. A. Burmistrova, M. Richter, M. Eisele, C. Üzüm and R. Von Klitzing, *Polymers*, 2011, **3**, 1575-1590.
206. H. M. Crowther, B. R. Saunders, S. J. Mears, T. Cosgrove, B. Vincent, S. M. King and G.-E. Yu, *Colloids and Surfaces A: Physicochemical and Engineering Aspects*, 1999, **152**, 327-333.
207. K. C. Johnson, F. Mendez and M. J. Serpe, *Analytica chimica acta*, 2012, **739**, 83-88.
208. C. A. Ribeiro, M. V. S. Martins, A. H. Bressiani, J. C. Bressiani, M. E. Leyva and A. A. A. de Queiroz, *Materials Science and Engineering: C*, 2017, **81**, 156-166.
209. M. Cao, Y. Wang, X. Hu, H. Gong, R. Li, H. Cox, J. Zhang, T. A. Waigh, H. Xu and J. R. Lu, *Biomacromolecules*, 2019, **20**, 3601-3610.
210. J. H. Oh, S. Y. Hong, H. Park, S. W. Jin, Y. R. Jeong, S. Y. Oh, J. Yun, H. Lee, J. W. Kim and J. S. Ha, *ACS applied materials & interfaces*, 2018, **10**, 7263-7270.
211. M. Cao, Y. Shen, Z. Yan, Q. Wei, T. Jiao, Y. Shen, Y. Han, Y. Wang, S. Wang and Y. Xia, *Chemical Engineering Journal*, 2021, **405**, 126647.
212. C. D. Sorrell and M. J. Serpe, *Analytical and bioanalytical chemistry*, 2012, **402**, 2385-2393.
213. W. S. Carvalho, C. Lee, Y. Zhang, A. Czarnecki and M. J. Serpe, *Journal of Colloid and Interface Science*, 2021, **585**, 195-204.
214. G. Hernández, *Fabry-perot interferometers*, Cambridge University Press, 1988.
215. Y. Gao, X. Li and M. J. Serpe, *RSC Advances*, 2015, **5**, 44074-44087.
216. L. Hu and M. J. Serpe, *Journal of Materials Chemistry*, 2012, **22**, 8199-8202.
217. M. R. Islam and M. J. Serpe, *Macromolecules*, 2013, **46**, 1599-1606.
218. G. Schlotterbeck, A. Ross, F. Dieterle and H. Senn, 2006.

219. X. Wang, A. Zhang, Y. Han, P. Wang, H. Sun, G. Song, T. Dong, Y. Yuan, X. Yuan and M. Zhang, *Molecular & Cellular Proteomics*, 2012, **11**, 370-380.
220. K. Kim, P. Aronov, S. O. Zakharkin, D. Anderson, B. Perroud, I. M. Thompson and R. H. Weiss, *Molecular & cellular proteomics*, 2009, **8**, 558-570.
221. W. J. Griffiths, T. Koal, Y. Wang, M. Kohl, D. P. Enot and H. P. Deigner, *Angewandte Chemie International Edition*, 2010, **49**, 5426-5445.
222. A.-H. M. Emwas, R. M. Salek, J. L. Griffin and J. Merzaban, *Metabolomics*, 2013, **9**, 1048-1072.
223. B. Mickiewicz, H. J. Vogel, H. R. Wong and B. W. Winston, *American journal of respiratory and critical care medicine*, 2013, **187**, 967-976.
224. S. Tiziani, V. Lopes and U. L. Günther, *Neoplasia*, 2009, **11**, 269-IN210.
225. H. Wen, S. S. Yoo, J. Kang, H. G. Kim, J.-S. Park, S. Jeong, J. I. Lee, H. N. Kwon, S. Kang and D.-H. Lee, *Journal of hepatology*, 2010, **52**, 228-233.
226. Y. Miyagi, M. Higashiyama, A. Gochi, M. Akaike, T. Ishikawa, T. Miura, N. Saruki, E. Bando, H. Kimura and F. Imamura, *PloS one*, 2011, **6**, e24143.
227. H. Dong, A. Zhang, H. Sun, H. Wang, X. Lu, M. Wang, B. Ni and X. Wang, *Molecular BioSystems*, 2012, **8**, 1206-1221.
228. O. A. Jones, D. J. Spurgeon, C. Svendsen and J. L. Griffin, *Chemosphere*, 2008, **71**, 601-609.
229. X. Wang, H. Wang, A. Zhang, X. Lu, H. Sun, H. Dong and P. Wang, *Journal of proteome research*, 2012, **11**, 1284-1301.
230. U. Roessner, J. H. Patterson, M. G. Forbes, G. B. Fincher, P. Langridge and A. Bacic, *Plant physiology*, 2006, **142**, 1087-1101.
231. P. R. West, A. M. Weir, A. M. Smith, E. L. Donley and G. G. Cezar, *Toxicology and applied pharmacology*, 2010, **247**, 18-27.
232. S. J. Mihalik, S. F. Michaliszyn, J. De Las Heras, F. Bacha, S. Lee, D. H. Chace, V. R. DeJesus, J. Vockley and S. A. Arslanian, *Diabetes care*, 2012, **35**, 605-611.
233. K. L. Lindsay, C. Hellmuth, O. Uhl, C. Buss, P. D. Wadhwa, B. Koletzko and S. Entringer, *PloS one*, 2015, **10**, e0145794.
234. A. R. Oliveira, I. Silva, E. LoTurco, H. Martins Jr and M. L. Chauffaille, *Journal*, 2014.
235. X. Cai and R. Li, *Scientific reports*, 2016, **6**, 1-10.

236. B. P. Sampey, A. J. Freemerman, J. Zhang, P.-F. Kuan, J. A. Galanko, T. M. O'Connell, O. R. Ilkayeva, M. J. Muehlbauer, R. D. Stevens and C. B. Newgard, *PloS one*, 2012, **7**, e38812.
237. C.-W. Lam and C.-Y. Law, *Journal of proteome research*, 2014, **13**, 4040-4046.
238. A. Zhang, H. Sun and X. Wang, *Analytical and bioanalytical chemistry*, 2012, **404**, 1239-1245.
239. B. L. Thompson, Y. Ouyang, G. R. Duarte, E. Carrilho, S. T. Krauss and J. P. Landers, *Nature protocols*, 2015, **10**, 875-886.
240. S. J. Bruce, P. Jonsson, H. Antti, O. Cloarec, J. Trygg, S. L. Marklund and T. Moritz, *Analytical biochemistry*, 2008, **372**, 237-249.
241. F. Michopoulos, L. Lai, H. Gika, G. Theodoridis and I. Wilson, *Journal of Proteome Research*, 2009, **8**, 2114-2121.
242. E. Zelena, W. B. Dunn, D. Broadhurst, S. Francis-McIntyre, K. M. Carroll, P. Begley, S. O'Hagan, J. D. Knowles, A. Halsall and HUSERMET Consortium, *Analytical chemistry*, 2009, **81**, 1357-1364.
243. H. Pereira, J.-F. Martin, C. Joly, J.-L. Sébédio and E. Pujos-Guillot, *Metabolomics*, 2010, **6**, 207-218.
244. N. Psychogios, D. D. Hau, J. Peng, A. C. Guo, R. Mandal, S. Bouatra, I. Sinelnikov, R. Krishnamurthy, R. Eisner and B. Gautam, *PloS one*, 2011, **6**, e16957.
245. R. Tharakan, D. Tao, C. Ubaida-Mohien, R. R. Dinglasan and D. R. Graham, *Journal of proteome research*, 2015, **14**, 1621-1626.
246. V. N. Luk and A. R. Wheeler, *Analytical chemistry*, 2009, **81**, 4524-4530.
247. H. Moon, A. R. Wheeler, R. L. Garrell and J. A. Loo, *Lab on a Chip*, 2006, **6**, 1213-1219.
248. A. R. Wheeler, H. Moon, C. A. Bird, R. R. Ogorzalek Loo, C.-J. C. Kim, J. A. Loo and R. L. Garrell, *Analytical chemistry*, 2005, **77**, 534-540.
249. M. J. Jebrail and A. R. Wheeler, *Analytical chemistry*, 2009, **81**, 330-335.
250. V. N. Luk, L. K. Fiddes, V. M. Luk, E. Kumacheva and A. R. Wheeler, *Proteomics*, 2012, **12**, 1310-1318.
251. M. J. Jebrail, H. Yang, J. M. Mudrik, N. M. Lafreniere, C. McRoberts, O. Y. Al-Dirbashi, L. Fisher, P. Chakraborty and A. R. Wheeler, *Lab on a Chip*, 2011, **11**, 3218-3224.
252. M. Abdelgawad, M. W. Watson and A. R. Wheeler, *Lab on a Chip*, 2009, **9**, 1046-1051.

253. J. R. Kraly, R. E. Holcomb, Q. Guan and C. S. Henry, *Analytica chimica acta*, 2009, **653**, 23-35.
254. M. Inoshita, H. Umehara, S.-y. Watanabe, M. Nakataki, M. Kinoshita, Y. Tomioka, A. Tajima, S. Numata and T. Ohmori, *Neuropsychiatric disease and treatment*, 2018, **14**, 945.
255. A. N. Fonteh, R. J. Harrington, A. Tsai, P. Liao and M. G. Harrington, *Amino Acids*, 2007, **32**, 213-224.
256. M. E. Mycielska, V. M. Milenkovic, C. H. Wetzel, P. Rümmele and E. K. Geissler, *Current Molecular Medicine*, 2015, **15**, 884-891.
257. W. Abebe and M. S. Mozaffari, *Am J Cardiovasc Dis*, 2011, **1**, 293-311.
258. G. N. Gowda and D. Raftery, *Analytical chemistry*, 2014, **86**, 5433-5440.
259. S. J. Bruce, I. Tavazzi, V. Parisod, S. Rezzi, S. Kochhar and P. A. Guy, *Analytical chemistry*, 2009, **81**, 3285-3296.
260. K. M. Crowe, *Clinical biochemistry*, 2014, **47**, 116-118.
261. K. Hata, K. Higashisaka, K. Nagano, Y. Mukai, H. Kamada, S.-i. Tsunoda, Y. Yoshioka and Y. Tsutsumi, *Nanoscale research letters*, 2014, **9**, 1-7.
262. B. Zhang, M. Xie, L. Bruschweiler-Li and R. Brüschweiler, *Analytical chemistry*, 2016, **88**, 1003-1007.
263. I. Lynch and K. A. Dawson, *Nano today*, 2008, **3**, 40-47.
264. L. Treuel and G. U. Nienhaus, *Biophysical reviews*, 2012, **4**, 137-147.
265. B. Zhang, M. Xie, L. Bruschweiler-Li, K. Bingol and R. Brüschweiler, *Analytical chemistry*, 2015, **87**, 7211-7217.
266. N. Scott Ferguson, N. Dicken Weatherby and V. M. Press, *Journal*, 2003.
267. P. Erpicum, O. Hanssen, L. Weekers, P. Lovinfosse, P. Meunier, L. Tshibanda, J.-M. Krzesinski, R. Hustinx and F. Jouret, *Clinical Kidney Journal*, 2017, **10**, 106-115.
268. A. Aota, S. Takahashi, K. Mawatari, Y. Tanaka, Y. Sugii and T. Kitamori, *Analytical Sciences*, 2011, **27**, 1173-1173.
269. C. Dixon, J. Lamanna and A. R. Wheeler, *Lab on a Chip*, 2020, **20**, 1845-1855.
270. O. Strohmeier, N. Marquart, D. Mark, G. Roth, R. Zengerle and F. von Stetten, *Analytical Methods*, 2014, **6**, 2038-2046.

271. R. Burger, D. Kirby, M. Glynn, C. Nwankire, M. O'Sullivan, J. Siegrist, D. Kinahan, G. Aguirre, G. Kijanka and R. A. Gorkin III, *Current opinion in chemical biology*, 2012, **16**, 409-414.
272. A. M. Evans, C. D. DeHaven, T. Barrett, M. Mitchell and E. Milgram, *Analytical chemistry*, 2009, **81**, 6656-6667.
273. E. G. Armitage and C. Barbas, *Journal of pharmaceutical and biomedical analysis*, 2014, **87**, 1-11.
274. K. Blennow, H. Hampel, M. Weiner and H. Zetterberg, *Nature Reviews Neurology*, 2010, **6**, 131-144.
275. J. J. H. A. P. Kennedy, G. C. Van de Bittner Ta and C. Wei, 2018.
276. S. M. T. Delgado, D. J. Kinahan, L. A. N. Julius, A. Mallette, D. S. Ardila, R. Mishra, C. M. Miyazaki, J. G. Korvink, J. Ducrée and D. Mager, *Biosensors and Bioelectronics*, 2018, **109**, 214-223.
277. S. Koike, M. Bundo, K. Iwamoto, M. Suga, H. Kuwabara, Y. Ohashi, K. Shinoda, Y. Takano, N. Iwashiro and Y. Satomura, *Translational psychiatry*, 2014, **4**, e379-e379.
278. D. Brennan, H. Coughlan, E. Clancy, N. Dimov, T. Barry, D. Kinahan, J. Ducrée, T. J. Smith and P. Galvin, *Sensors and Actuators B: Chemical*, 2017, **239**, 235-242.
279. J.-N. Klatt, M. Depke, N. Goswami, N. Paust, R. Zengerle, F. Schmidt and T. Hutzenlaub, *Lab on a Chip*, 2020.
280. M. Christian, R. Brent and P. Calda, *The Journal of Maternal-Fetal & Neonatal Medicine*, 2007, **20**, 89-112.
281. P. L. Senger, *Pathways to pregnancy and parturition*, Current Conceptions, Inc., 1615 NE Eastgate Blvd., 1997.
282. E. Ehrentreich-Förster, F. W. Scheller and F. F. Bier, *Biosensors and Bioelectronics*, 2003, **18**, 375-380.
283. P. Šauer, A. Stará, O. Golovko, O. Valentová, A. Bořík, R. Grabic and H. K. Kroupová, *Water research*, 2018, **137**, 64-71.
284. R. Firk, E. Stamer, W. Junge and J. Krieter, *Livestock Production Science*, 2002, **75**, 219-232.
285. K. Svennersten-Sjaunja, L.-O. Sjaunja, J. Bertilsson and H. Wiktorsson, *Livestock Production Science*, 1997, **48**, 167-174.

286. M. Delwiche, X. Tang, R. Bondurant and C. Munro, *Transactions of the ASAE*, 2001, **44**, 2003.
287. T. Mottram, M. Velasco-Garcia, J. Hart and R. Pemberton, 2001.
288. C. S. Negi, *Introduction to Endocrinology*, Prentice-Hall Of India Pvt. Limited, 2009.
289. L. Speroff and M. A. Fritz, *Clinical gynecologic endocrinology and infertility*, lippincott Williams & wilkins, 2005.
290. B. Wang, Y.-b. Liu, X.-f. Zhang, T.-t. Feng, W.-g. Xu and S.-q. Han, *Monoclonal antibodies in immunodiagnosis and immunotherapy*, 2014, **33**, 8-12.
291. Y. Wang, T. Zhang, H. Zhao, W. Zhou, J. Zeng, J. Zhang, C. Zhang and W. Chen, *Analytical and bioanalytical chemistry*, 2019, **411**, 2363-2371.
292. L. S. Shore and M. Shemesh, *Pure and Applied Chemistry*, 2003, **75**, 1859-1871.
293. S. K. Wasser, K. E. Hunt, J. L. Brown, K. Cooper, C. M. Crockett, U. Bechert, J. J. Millspaugh, S. Larson and S. L. Monfort, *General and comparative endocrinology*, 2000, **120**, 260-275.
294. A. S. Kolok, J. M. Ali, E. G. Rogan and S. L. Bartelt-Hunt, *Current environmental health reports*, 2018, **5**, 225-232.
295. S. Liu, H. Chen, X.-R. Xu, S.-S. Liu, K.-F. Sun, J.-L. Zhao and G.-G. Ying, *Science of the Total Environment*, 2015, **502**, 400-407.
296. D. Ganmaa and A. Sato, *Medical hypotheses*, 2005, **65**, 1028-1037.
297. N. V. Goletiani, D. R. Keith and S. J. Gorsky, *Experimental and clinical psychopharmacology*, 2007, **15**, 427.
298. M. Oettel and A. Mukhopadhyay, *The Aging Male*, 2004, **7**, 236-257.
299. T. Key and M. Pike, *British journal of cancer*, 1988, **57**, 205.
300. I. G. Lange, A. Daxenberger, B. Schiffer, H. Witters, D. Ibarreta and H. H. Meyer, *Analytica chimica acta*, 2002, **473**, 27-37.
301. M. Adeel, X. Song, Y. Wang, D. Francis and Y. Yang, *Environment international*, 2017, **99**, 107-119.
302. S. Smith, D. Mager, A. Perebikovsky, E. Shamloo, D. Kinahan, R. Mishra, S. M. Torres Delgado, H. Kido, S. Saha and J. Ducrée, *Micromachines*, 2016, **7**, 22.
303. J. C. Jokerst, J. M. Emory and C. S. Henry, *Analyst*, 2012, **137**, 24-34.
304. H. Gao, C. Yan, W. Wu and J. Li, *Sensors*, 2020, **20**, 1792.

305. J. Ozhikandathil, S. Badilescu and M. Packirisamy, *Journal of Neural Transmission*, 2017, **124**, 47-55.
306. J. R. Mejía-Salazar, K. Rodrigues Cruz and E. M. Materon Vasques, *Sensors*, 2020, **20**, 1951.
307. I. S. Levina, A. K. Nazarov, G. V. Nazarov, L. E. Kulikova, Y. V. Kuznetsov, A. S. Dmitrenok, D. V. Minin, A. V. Aksenov and I. V. Zavarzin, *The Journal of steroid biochemistry and molecular biology*, 2019, **194**, 105436.
308. M. G. Roper, J. G. Shackman, G. M. Dahlgren and R. T. Kennedy, *Analytical chemistry*, 2003, **75**, 4711-4717.
309. C. M. Miyazaki, D. J. Kinahan, R. Mishra, F. Mangwanya, N. Kilcawley, M. Ferreira and J. Ducrée, *Biosensors and Bioelectronics*, 2018, **119**, 86-93.
310. A. E. Taylor, B. Keevil and I. T. Huhtaniemi, *Eur J Endocrinol*, 2015, **173**, D1-D12.
311. S. K. Ludwig, H. Zhu, S. Phillips, A. Shiledar, S. Feng, D. Tseng, L. A. van Ginkel, M. W. Nielen and A. Ozcan, *Analytical and bioanalytical chemistry*, 2014, **406**, 6857-6866.
312. R. Mishra, J. Zapatero-Rodriguez, S. Sharma, D. Kelly, D. McAuley, S. Gilgunn, R. O'Kennedy and J. Ducree, *Sensors and Actuators B: Chemical*, 2018, **263**, 668-675.
313. Y. Hou, R. Mishra, M. Wei, N. Balasuriya, M. J. Serpe, J. Ducrée and J. Harrison, 2019.
314. M. R. Islam and M. J. Serpe, *Biosensors and Bioelectronics*, 2013, **49**, 133-138.
315. Y. Gao, M. Wei, X. Li, W. Xu, A. Ahiabu, J. Perdiz, Z. Liu and M. J. Serpe, *Macromolecular Research*, 2017, **25**, 513-527.
316. T. Dohi, K. Matsumoto and I. Shimoyama, 2004.
317. H. Li, Y. Li, J. Li, F. Yang, L. Xu, W. Wang, X. Yao and Y. Yin, *Analytical chemistry*, 2020, **92**, 4094-4100.
318. J. Velayudham, V. Magudeeswaran, S. S. Paramasivam, G. Karruppaya and P. Manickam, *Materials Letters*, 2021, 130801.
319. Y. Jiang, M. G. Colazo and M. J. Serpe, *Analytical and bioanalytical chemistry*, 2018, **410**, 4397-4407.
320. Y. Jiang, M. G. Colazo and M. J. Serpe, *Colloid and Polymer Science*, 2016, **294**, 1733-1741.
321. G. n. Contreras Jiménez, S. Eissa, A. Ng, H. Alhadrami, M. Zourob and M. Siaj, *Analytical chemistry*, 2015, **87**, 1075-1082.

322. S. C. Kim, U. M. Jalal, S. B. Im, S. Ko and J. S. Shim, *Sensors and Actuators B: Chemical*, 2017, **239**, 52-59.
323. R. R. Sinden, *DNA structure and function*, Gulf Professional Publishing, 1994.
324. F. Xiao, X. Yao, Q. Bao, D. Li and Y. Zheng, *Bioinorganic chemistry and applications*, 2012, **2012**.
325. A. Benabdelaziz, S. Boudjemai, R. Khelili, M. Besbaci and R. Kaidi, *Journal of Immunoassay and Immunochemistry*, 2020, **41**, 195-207.
326. P.-N. Jouan, Y. Pouliot, S. F. Gauthier and J.-P. Laforest, *International Dairy Journal*, 2006, **16**, 1408-1414.
327. A. A. Zaied, C. J. Bierschwal, R. G. Elmore, R. S. Youngquist, A. J. Sharp and H. A. Garverick, *Theriogenology*, 1979, **12**, 3-11.
328. H. R. Kasambala, M. J. Rwiza and R. H. Mdegela, *Water Science and Technology*, 2019, **80**, 1107-1117.
329. M. Jauset-Rubio, M. L. Botero, V. Skouridou, G. l. B. l. Aktas, M. Svobodova, A. S. Bashammakh, M. S. El-Shahawi, A. O. Alyoubi and C. K. O'Sullivan, *ACS omega*, 2019, **4**, 20188-20196.
330. S. Dalirirad and A. J. Steckl, *Sensors and Actuators B: Chemical*, 2019, **283**, 79-86.
331. A. Pfützner, C. Schipper, S. Ramljak, F. Flacke, J. Sieber, T. Forst and P. B. Musholt, *Journal of diabetes science and technology*, 2013, **7**, 1522-1529.
332. H. Fruhstorfer, G. Schmelzeisen-Redeker and T. Weiss, *European Journal of Pain*, 1999, **3**, 283-286.
333. C. Escadafal, O. Faye, O. Faye, M. Weidmann, O. Strohmeier, F. von Stetten, J. Drexler, M. Eberhard, M. Niedrig and P. Patel, *PLoS negl trop dis*, 2014, **8**, e2730.
334. M. Keller, S. Wadle, N. Paust, L. Dreesen, C. Nuese, O. Strohmeier, R. Zengerle and F. Von Stetten, *RSC advances*, 2015, **5**, 89603-89611.
335. M. Rombach, S. Lutz, D. Mark, G. Roth, R. Zengerle, C. Dumschat, A. Witt, S. Hensel, S. Frenzel and F. Aßmann, 2012.
336. D. Maliwal, P. Jain, A. Jain and V. Patidar, *Journal of young pharmacists*, 2009, **1**, 371.
337. NTELLIGENT QUALITY CONTROL (IQC®)ON THE PICCOLO XPRESS® POINT-OF-CARE CHEMISTRY ANALYZER, https://abaxis.com/sites/default/files/resource-papers/piccolo_iqc_whitepaper.pdf).

338. M. I. G. S. Almeida, B. M. Jayawardane, S. D. Kolev and I. D. McKelvie, *Talanta*, 2018, **177**, 176-190.
339. G. G. Morbioli, T. Mazzu-Nascimento, A. M. Stockton and E. Carrilho, *Analytica Chimica Acta*, 2017, **970**, 1-22.
340. M. G. Pollack, A. D. Shenderov and R. B. Fair, *Lab on a Chip*, 2002, **2**, 96-101.
341. S. N. Pei, J. K. Valley, S. L. Neale, A. Jamshidi, H.-Y. Hsu and M. C. Wu, 2010.
342. G. McHale, C. Brown, M. Newton, G. Wells and N. Sampara, *Physical review letters*, 2011, **107**, 186101.
343. S. Mashaghi, A. Abbaspourrad, D. A. Weitz and A. M. van Oijen, *TrAC Trends in Analytical Chemistry*, 2016, **82**, 118-125.
344. Y. Zhang and N.-T. Nguyen, *Lab on a Chip*, 2017, **17**, 994-1008.
345. R. B. Fair, A. Khlystov, T. D. Tailor, V. Ivanov, R. D. Evans, V. Srinivasan, V. K. Pamula, M. G. Pollack, P. B. Griffin and J. Zhou, *IEEE Design & Test of Computers*, 2007, **24**, 10-24.
346. N. A. Mousa, M. J. Jebrail, H. Yang, M. Abdelgawad, P. Metalnikov, J. Chen, A. R. Wheeler and R. F. Casper, *Science Translational Medicine*, 2009, **1**, 1ra2-1ra2.
347. S. Abdulwahab, 2017.
348. J. Kim, S. Abdulwahab, K. Choi, N. M. Lafrenière, J. M. Mudrik, H. Gomaa, H. Ahmado, L.-A. Behan, R. F. Casper and A. R. Wheeler, *Analytical chemistry*, 2015, **87**, 4688-4695.
349. L. Malic, D. Brassard, T. Veres and M. Tabrizian, *Lab on a Chip*, 2010, **10**, 418-431.
350. K. P. Nichols and J. G. Gardeniers, *Analytical chemistry*, 2007, **79**, 8699-8704.
351. C. Yi, Q. Zhang, C.-W. Li, J. Yang, J. Zhao and M. Yang, *Analytical and bioanalytical chemistry*, 2006, **384**, 1259-1268.

Appendix A. VIDEOS OF ON-DISC FLUID CONTROL

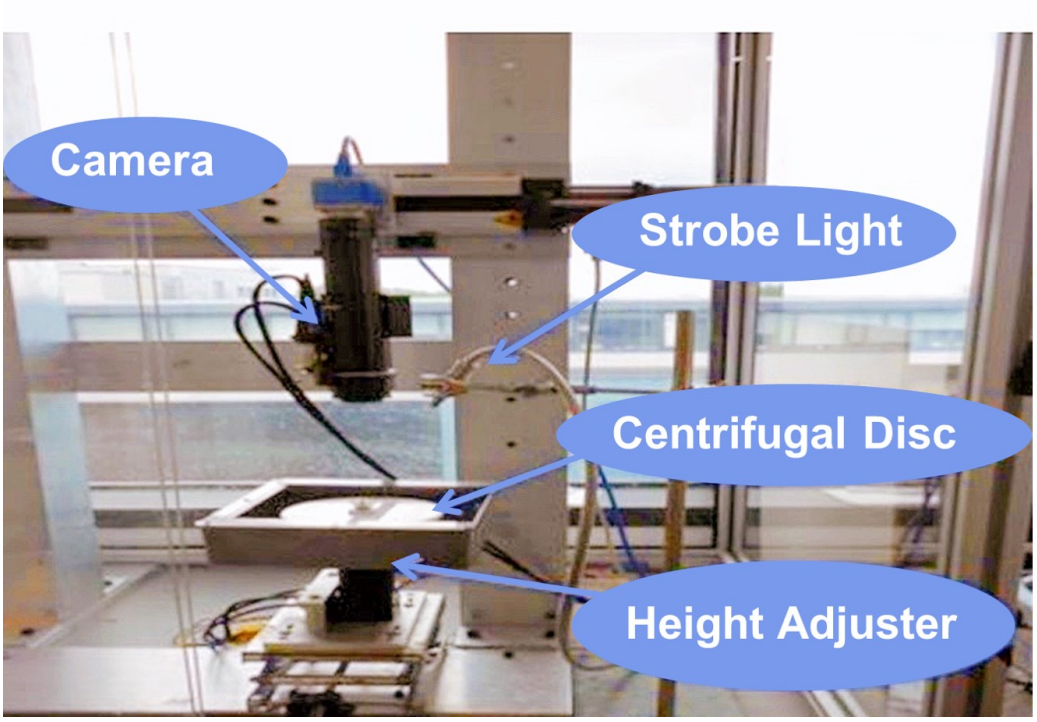

All frames in the video are captured on the spin-stand in Fraunhofer Project Centre for Embedded Bioanalytical Systems at DCU (FPC@DCU). The spin-stand is composed of a spindle motor, a synchronized camera for image acquisition during rotation coupled to a motorized zoom lens, and a strobe light unit. The image capture is operated by a real-time PC board, which receives the spinning disk's zero-crossing signal and sends delayed trigger signals to the CCD camera and stroboscopic light.

Video 3-1: On- disc blood sample preparation

https://drive.google.com/file/d/1CIH4zAB7Kjw65s9o3YAYP0dIM4R8eN-A/view?usp=sharing

Video 4-1: On -disc P4 detection

https://drive.google.com/file/d/163oziVc7nVc1OBow3lJLp7oOcRdQXi_D/view?usp=sharing